Methane and High Volume Hydraulic Fracturing: Quantifying non-point diffuse methane leakage through geochemical surface detection methods

By

Moyosore AJAYI

Thesis

Submitted to the Faculty of the

Graduate School of Vanderbilt University

in partial fulfillment of the requirements

for the degree of

MASTER OF SCIENCE

in

Earth & Environmental Sciences

August, 2016

Nashville, Tennessee

Approved:

John C. Ayers, Ph.D.

George M. Hornberger, Ph.D.

This work is dedicated to my supportive family.

"The most beautiful thing we can experience is the mysterious. It is the source of all true art and science."

Albert Einstein

Acknowledgements

This work could have not been completed without the funding from the Discovery Grant provided by Vanderbilt University and the supervision and guidance by my patient advisor, Prof. John Ayers and my second reader, Prof. George Hornberger. Thanks is also deserved for Vince Antonacci and the other geoscientists at TN Geological Survey who allowed me into their office and answered my questions and gave me plenty of advice. I owe a tremendous debt to our collaborators at the University of Tennessee: Martin Schubert, Kevin Hoyt, Sean Schaeffer, Marie English, and Julie McKnight. Finally, no measurements would have been possible without the kind landowners, Eddie Walls and Lewis Carson.

Contents

List of Tables

Table Page

List of Figures

Figures Page

List of Abbreviations

Bcf	Billion Cubic Feet
bcm	Billion Cubic Meters
EIA	Energy Information Administration
GHG	Greenhouse Gas
HVHF	High Volume Hydraulic Fracturing
MMcf	Million cubic feet
Tcf	Trillion cubic feet
TDEC	Tennessee Department of Environmental Conservation
USGS	United States Geological Survey
WS-CRDS	Wave Scanned-Cavity Ring-down Spectroscopy

Chapter 1

Motivation & Problem Statement

1.1 Motivation for this Research

The extraction of hydrocarbons around the globe, especially in the United States, has entered a new era. Unconventional sources of hydrocarbons that were previously uneconomical have become strong contributors to the hydrocarbon energy sector in the last decade due to technological advances. The most controversial technology is High Volume Hydraulic Fracturing (HVHF). HVHF is employed by many oil and gas companies for the extraction of fossil fuels from shale; this is accomplished by drilling vertically to depths on the order of hundreds of meters and then drilling horizontally parallel into a source rock layer. Once the source rock is penetrated, a slurry of highly pressurized water, chemicals, and proppants is injected to generate permeable fractures throughout the source rock. These fractures allow extraction of the previously trapped natural gas for production. Approximately 40% of all of the natural gas in the United States is acquired using HVHF methods (Beaver, 2014).

In 2013 and 2014, the United States extracted 689 and 729 billion cubic meters (bcm), of natural gas or roughly 20% of global natural gas production each respective year (Iea, 2014). The US also leads the world in the consumption of natural gas (EIA, 2016a). In 2010, the US accounted for 26% of global natural gas consumption. Both trends, leading in production and consumption of natural gas, combine to highlight the importance of natural gas in the US energy portfolio.

Natural gas is often used to heat homes and to generate electricity at power plants. One of the attractive features of using natural gas as an energy source in the generation of electricity stems from its lower impact on the environment than the commonly used alternative source, coal. In fact, natural gas-powered plants emit about half of the carbon dioxide emissions per unit energy than coal-powered plants (Beaver, 2014). However, even with this advantage in the reduction of carbon dioxide emissions, many individuals and institutions do not believe the benefits of using natural gas outweigh the risks of natural gas extraction with HVHF methods. Increased seismic activity near HVHF and wastewater injection sites has alarmed residents. This has been well documented with the increase in the frequency in low magnitude seismic events near HVHF regions (Ellsworth,

2013; Atkinson et al., 2016). Another reason for concern has been the documentation of elevated concentration of methane near drinking wells. These elevated measurements have been attributed to a variety of reasons but authors have speculated that faulty casings are an important factor (Darrah et al., 2014; Jackson et al., 2014b). These wells have been shown to leak gas into the groundwater at levels exceeding federal (EPA) and state standards (Jackson et al., 2014a). Perhaps the most severe disadvantage of HVHF is the possibility of fugitive emissions of natural gases, specifically methane. It is not possible for all of the methane that escapes from the fractured rock to be extracted for consumption , and if methane leaks to the surface it may enter groundwater as well as the atmosphere. The potential transfer of methane into the atmosphere is troubling because it is a strong greenhouse gas (GHG). Present day concentrations of methane in the atmosphere, approximately 1.90 parts per million (ppm), are greater than pre-industrial levels of 0.68-0.715 ppm (Miller et al., 2013). Methane accounts for roughly 18% of all climate warming attributed to greenhouse gases, thus motiving the need to understand escaped, or fugitive methane emissions (Denmead, 2008).

1.2 Problem Statement

Currently, several studies have begun to tackle the link between HVHF practices and point and line sources of methane contamination (e.g. faulty well casings (Jackson et al., 2013; Maher, Santos, and Tait, 2014)) and pipelines (Jackson et al., 2014a). However, there is less literature of methane emissions based on measurements of gases fluxed directly from the soil. Many of the methane emission studies are conducted at the regional level use remote sensing and top-down methods. Top-down methods start with a measurement of methane in the atmosphere and work towards producing an inventory of terrestrial sources of methane (e.g. ((Kort et al., 2014)). Conversely, bottom-up methods, or ground-based studies, collect measurements from multiple locations at the near-surface. Unfortunately, comparisons between these methods have shown poor congruency (Miller et al., 2013). Top-down studies tend to yield greater estimates of methane emissions than bottom-up measurements (Kirschke et al., 2013). Additionally, the research in this field has continued to produce wide ranging estimates for the fossil fuel contribution of methane in the atmosphere. Authors have suggested more ground-based measurements ought to be completed to validate remotely sensed reports (Kirschke et al., 2013). Therefore, the problem presented is to reduce the uncertainty in the methane emissions sourced from fossil fuel extraction.

The Marcellus and Utica shale plays have been fervently studied in the last decade to address this problem, and for good reason; the Marcellus and Utica delivered 12.19 bcm (43,000 million cubic feet, MMcf) of natural gas to consumers in 2013 (EIA, 2016b). Another play of interest is the southern extension of the Marcellus, the lesser exploited Chattanooga Shale. The Chattanooga is the most important source of shale gas in eastern Tennessee, specifically in Morgan, Anderson, Scott, and Fentress counties. Roughly 42% of the natural gas produced in Tennessee originates

from these four counties (TDEC, 2015). Additionally, the Chattanooga Shale play has been carefully eyed by many prospective oil and gas companies for expanding production (EIA, 2015).

To determine whether HVHF sites could be the missing ground source of fugitive methane, our research focused on measuring methane emissions in regions of sustained HVHF activity through a bottom-up process. More specifically, we tested the hypothesis that HVHF practices lead to enhanced fluxes of methane in areas of shale gas development against the null hypothesis that leakage is due to natural processes unassociated with HVHF.

Chapter 2

Introduction & Background Information

2.1 Geographic Setting

The study site is located in Morgan County in northeastern Tennessee, 19 km northwest of Oak Ridge, TN. The county has a rugged landscape, a product of being located at the eastern edge of the Cumberland Plateau, just west of the Appalachian Mountains. The rural nature of Morgan County and its neighboring counties makes it ideal for HVHF development.

2.2 Geologic Setting

The geologic setting of Tennessee contains a large degree of variation moving from west to east across the state. A coarse description of the geology of Tennessee begins with the western border. This region is classified as the Mississippi Embayment. Moving east to Middle Tennessee, this region is classified as the Nashville Basin, bounded on the west, south and east by the Highland Rim. East of the Highland Rim lie the Cumberland Plateau and Valley and Ridge regions. The Valley and Ridge physiographic region has been well studied by geoscientists due to its record of the Taconic, Acadian, and Alleghenian Orogenies that contributed to the formation of the Appalachian Mountains. The central location of this field site is near the Cumberland Forest (36° 2 N, 84° 28 W) in the Cumberland Plateau region.

The Cumberland Plateau is a subsection of the southern portion of the Appalachian Plateau (Hatcher, 2013; Wilson and Stearns, 1958). This region extends from Kentucky, through Tennessee, and into north central Alabama. Though Cambrian and Ordovician aged rocks surround the Plateau, the rocks of primary concern are Pennsylvanian in age. These Pennsylvanian aged rocks compose the lions share of the material that underlie the field site.

The structure of the Cumberland Plateau was organized into three sections by Wilson and Stearns (1958), presented here from northeast to southwest: 1) Pine Mountain block, 2) Wartburg Basin (Evenick and Hatcher, 2006), and 3) Cumberland Plateau overthrust sheet (Figure 2.1). The Pine

Mountain block is separated from the Wartburg Basin by the Jacksboro Fault, and is bounded to the east by the Eastern Cumberland Escarpment, which divides the region from the Valley and Ridge province. Skipping ahead to the Cumberland Plateau overthrust sheet, similarities are found with the Pine Mountain block in that there is a fault (Emory River Fault) of similar strike as the Jacksboro fault that separates the sheet from the Wartburg Basin. This area is bounded by the Sequatchie Valley Anticline to the west and the Eastern Escarpment to the east. Beds of both the Pine Mountain block and the Cumberland Plateau overthrust sheet have been disturbed by bedding thrusts that have moved underlying beds generally in a northwestward direction for 3 to 10 miles. This displacement of underlying beds is described in greater detail in Wilson and Stearns (1958). The field site is located in the undisturbed Wartburg Basin, where the underlying beds remain flat until the eastern escarpment where the beds are sharply deformed but continuous (Wilson and Stearns, 1958).

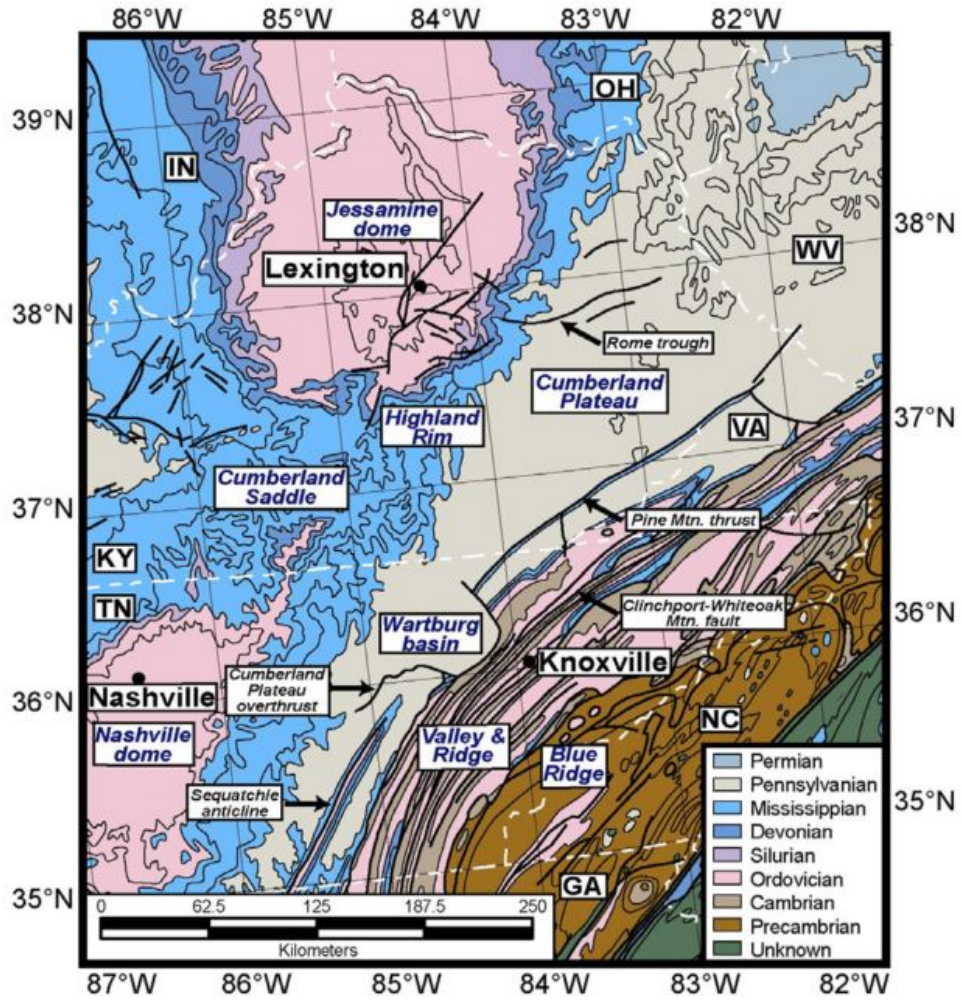

FIGURE 2.1: Geological map of eastern Tennessee (Evenick and Hatcher, 2006).

From work completed by Evenick and Hatcher [2006], we know that the Cumberland Plateau is

home to several stratigraphic groups (Appendix D). Near the surface, there are several Pennsylvanian aged layers of primarily sandstone and coal. Of these near surface layers, there are five layers exposed at the surface, all Pennsylvanian in age. Generally found closest to the surface is the Redoak Mountain (Prm) formation. This is a package of alternating sandstone and shale layers with thin coal layers interbedded in the group. Found beneath the Redoak Mountain formation is the Graves Gap formation (Pgg) that consists of shale and sandstone layers; the Indian Bluff formation (Pib) composed primarily of alternating shale sandstone and shale layers; the Slatestone (Psl) formation composed of shale and sandstone units; and the Crooked Fork (Pcf) group, which contains several sandstone and shale formations.

With regard to thicker packages deeper in the subsurface there are four groups of note above the Chattanooga Shale, the primary source rock. First, lying under the Crooked Fork group is the Crab Orchard Mountains (Pco) formation. It is roughly the same thickness as the Crooked Fork and contains sandstone, shale, thick conglomerate layers, and several coal seams (Wilson and Stearns, 1958). Underlying the Crooked Fork is the Gizzard (Pg) formation, which is thinner than the previous two groups and is comprised of shale and sandstone layers.

Beneath these Pennsylvanian aged strata are two Mississippian aged packages, the Newman Limestone (Mn) and the Fort Payne (Mfp). The Newman Limestone is a shaly limestone package with siltstone and sandstone composing a minor portion of the unit. The Fort Payne formation provides the foundation of the Mississippian aged material and it is a thick cherty layer roughly 31 to 82 m thick (USGS, 2016). The bottom of the Fort Payne is composed of green (Maury) shale.

Finally, underneath the Mississippian layers lies the source rock for the majority of the wells in Morgan Co., the Chattanooga Shale (MDc). The Chattanooga is Devonian in age, and can be characterized as a black to dark-grey thinly laminated carbonaceous shale that is roughly 5 to 8 m thick (Evenick and Hatcher, 2006).

2.3 Current Status of HVHF Activity in Tennessee and the Cumberland Plateau

2.3.1 General energy production and consumption by Tennessee

Tennessee is a moderate producer of energy and natural gas in the US. The Energy Information Agency (EIA) reported that the state produced 545 trillion BTU in 2013, which earned the state a national ranking 30^{th} in total energy production. For natural gas, Tennessee ranks slightly higher at 25^{th} in the nation with 149 MMcm (5,294 MMcf) of production. However, Tennessee and other midlevel producing states pale in comparison to leaders of US producers like Wyoming, Oklahoma, Pennsylvania, and Texas who produce roughly two orders of magnitude more natural gas

(EIA, 2016b). With regard to consumption, Tennessee consumes about 7.94 Bcm (280 Bcf) or 1.1% of the total share of US natural gas (EIA, 2015). The values for production and consumption are not impressive for several reasons that can be tied to several energy indicators. First, population tends to be an indicator of energy consumption; Tennessee, ranks near the middle of the nation at the 20^{th} position. Second, the gross domestic product (GDP) for Tennessee, ranked 19^{th}, is also near the middle of the nation. Third, Tennessee does not currently have a large capacity for downstream fossil fuel processing.

2.3.2 Current Status of Natural Gas Within Tennessee

In Tennessee, natural gas is a distant third place behind nuclear and hydroelectric generation in energy production. However, even though natural gas is not currently a dominant energy player, evidence of recently increased production suggests that Tennessee could play a larger role in natural gas development in decades to come. For instance, Figure 2.3 shows that gas production is increasing to the highest volumes it has ever been within the state. Furthermore, much of the state is currently being explored for more natural gas resources due to the fact that the eastern part of the state overlies the gas-rich Chattanooga Shale (EIA, 2015). Also, unique to Tennessee, the primary fluid used for fracturing the shale is nitrogen gas. Other chemicals and proppants are used in the slurry, but Tennessee is one of two states (the other being Kentucky) that use nitrogen gas instead of water as the primary fluid within their injection slurries (Hirji and Song, 2015). These factors combine to demonstrate the increased interest in natural gas production in Tennessee.

Morgan County is home to 432 of the 1404 active gas wells in the State of Tennessee (TDEC, 2016). Morgan Co. is home to 31% of the active wells in Tennessee, whereas 26% of active gas wells lie in eastern neighbor Anderson Co. and 19% are drilled in northern neighbor, Fentress Co (TDEC, 2016). The rest of the active wells are scattered around eastern Tennessee. Since the advent of widespread HVHF in the US, production in between 2006 through 2014 in Tennessee has increased an average of 9.88 million cubic meters (344 MMcf) per year. This may be a modest increase when compared to a top producing state like Pennsylvania (approx. 127 million cubic meters (45,000 MMcf) per year); however, the point to be underscored is that between 1991 and 2005 Tennessee averaged an annual growth in production of only 8.87 MMcf. Thus, the proliferation of HVHF activity has resulted in an increase in annual production of natural gas in the region.

2.4 Methane in the Atmosphere

Methane, being composed of a single carbon and four hydrogen atoms (CH_4), makes up 70-90% of natural gas (Natural Gas, 2013). Other major constituents include other alkanes such as ethane

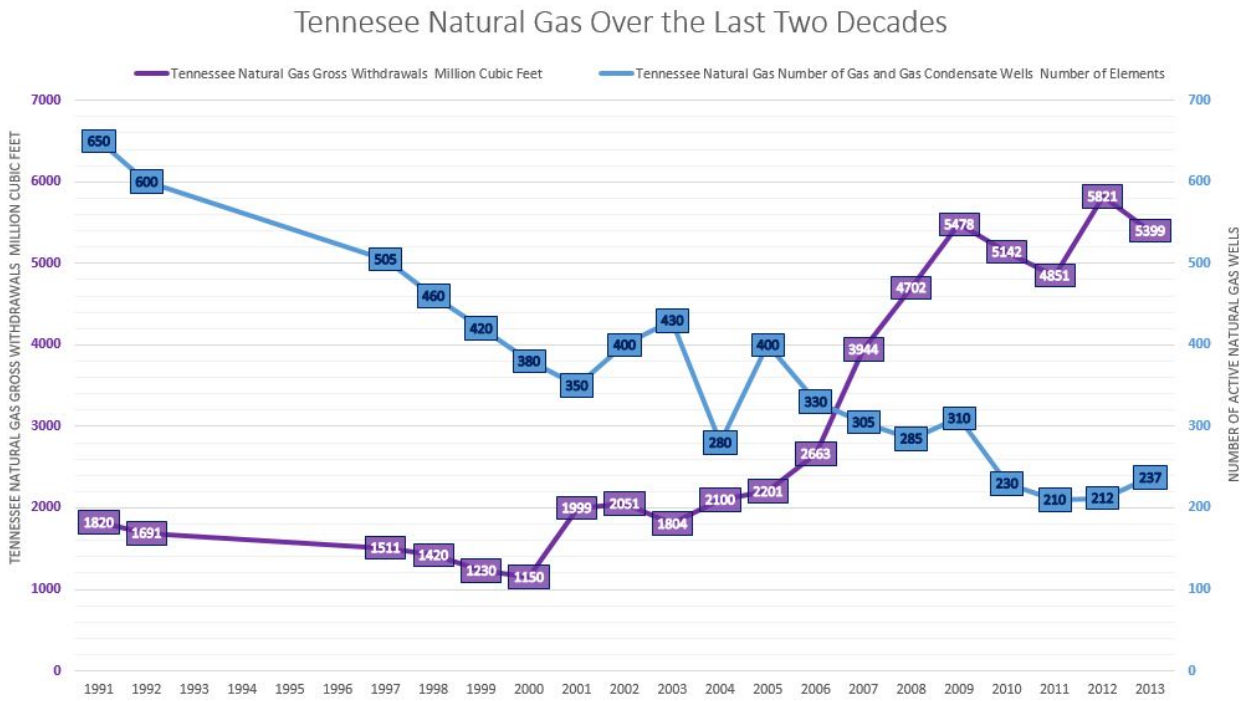

FIGURE 2.2: Withdrawls of natural gas in the state of Tennessee over the last two decades. The annual withdrawls are presented in purple using the left-sided y-axis, and the annual count of wells are presented in blue using the right-sided y-axis (EIA, 2016a).

(C_2H_6), propane (C_3H_8), and butane (C_4H_{10}). Carbon dioxide (CO_2) can also be found in small amounts (0 to 8%) as well (Natural Gas, 2013). Once methane has escaped from the subsurface and enters the atmosphere it now becomes an important contributor climate warming. The atmosphere contains roughly 4850 terragrams (Tg) of CH_4 , roughly equivalent to a concentration of 1.90 ppm. The atmospheric residence time is roughly 10 years shorter for CH_4 than CO_2, which can last in the atmosphere for a century. Though the atmospheric lifetime and concentration are far less than for carbon dioxide (CO_2), the 100-year global warming potential of CH_4 is 25 times greater than for CO_2 (EPA, 2015). The contribution of methane to global warming makes it important to understand the inventory of sources and sinks of CH_4.

Methane in the atmosphere can have terrestrial and aquatic origins; furthermore, CH_4 sources are often generalized into two categories, natural and anthropogenic. Natural sources of methane stem largely from wetlands, and the remaining portion sourced from geologic origins (e.g. mud volcanoes, gas hydrates, and macro-seeps) and termites (Dale et al., 2008; Etiope and Klusman, 2010; Kvenvolden and Rogers, 2005). Anthropogenic sources of CH4 are not limited to fossil fuels but include biomass burning, rice agriculture, enteric fermentation, and landfill emissions (Kvenvolden and Rogers, 2005).

The two major sinks for CH_4 are the atmosphere and terrestrial surface layers. Within the atmosphere, CH_4 is lost in the troposphere and the stratosphere. In the troposphere, CH_4 reacts with free hydroxyl radicals to form a methyl group and a mol of water (Ehhalt and Schmidt, 1978). Methane that escapes destruction in the troposphere will enter the troposphere where it may react with hydroxyls, free chlorine, or oxygen-deuterium (O^1D) compounds (Ehhalt and Schmidt, 1978). However, it is important to note that the troposphere, the largest sink for CH_4, transforms between 428-507 Tg of CH_4 per year, and the stratosphere 30-45 Tg of CH_4 per year (Backman, 2009). The terrestrial surface in the form of soils also contributes as sink for atmospheric CH_4. Under certain meteorological conditions (e.g. high atmospheric pressure) methane can be stored within near-surface layers, and further consumed by microbes in the soil or stored as soil gas. The amount of CH_4 stored in the soil ranges between 26-43 Tg yr^{-1}, which is just under 10% of CH_4 that is lost each year (Backman, 2009).

There are two essential points to understand regarding methane in the atmosphere: 1) the present concentration of methane in the atmosphere has reached a value that that has not been surpassed in the last 800,000 years, and 2) methane traps 25 more times more solar radiation per unit of mass than carbon dioxide (EPA, 2016). With these two points in mind, the importance in accounting for components of the methane cycle cannot be understated

2.5 Geochemistry of Methane

Methane that is extracted for commercial use is usually thermogenic methane, though biogenic sourced methane comprises roughly 20% of commercial natural gas (Martini et al., 2003). Thermogenic CH_4 is formed deep below the surface at temperatures between 160 and 220 °C (Stolper et al., 2014). Thermogenic CH_4, is formed by breaking down larger organic molecules through a process called cracking. Cracking and thermogenic methane formation in general is dependent on high temperatures and pressure.

When considering the geochemistry of CH_4, especially thermogenic CH_4, it is also important to consider methane migration. Conventional sources of thermogenic methane migrate from the source rock, a fine-grained sedimentary rock like shale that has undergone significant diagenesis, to another but more permeable sedimentary rock like sandstone known as the reservoir. The source rock is connected to the reservoir through a fault, which allows the gases and oil to migrate from source to reservoir (Chapman, 1983; Lampe et al., 2012). However, when HVHF methods are employed, the impermeable source rock can be tapped immediately by injecting a fluid at high pressure to fracture the rock. These fractures are understood as fracture networks and their properties like fracture width (aperture), length, and orientation occur probabilistically (Long and Billaux, 1987). This differs from conventional natural gas extraction in that the source rock may leak from the impermeable source rock through a fracture or set fractures, allowing methane and other

light carbon gases to be transported to the surface. Transport of natural gas from the source rock to the surface has yet to be connected to HVHF activity and is currentlt a controversial explanation (Flewelling and Sharma, 2014), but several studies have documented natural gas ebulliating from natural fractures and seeps in terrestrial and marine environments (Etiope and Klusman, 2010; Klusman, Leopold, and Leroy, 2000; Kvenvolden and Rogers, 2005; Teasdale et al., 2014).

In addition to thermogenic methane, CH_4 is formed at shallower depths (less than one kilometer) through metabolic processes of bacteria at temperatures less than 50°C (Rooney, Claypool, and Chung, 1995). These processes, collectively called methanogenesis, lead to another class of methane known as biogenic methane. Methanogenesis can be largely described as the breakdown of large high molecular weight (HMW) carbon chains of organic material. About 90% of these HMW chains are broken down into smaller low molecular weight (LMW) substrates via extracellular hydrolysis (Megonigal, Hines, and Visscher, 2003). Through aerobic and anaerobic reactions, CH_4 is formed through the consumption of monomeric LMW substrates and carbon dioxide gas such as volatile fatty acids (VFAs) (e.g. formic, humic, and acetate) methylated compounds (e.g. dimethylsulphide and trimethyl amine), and carbon dioxide (Dale et al., 2008; Stolper et al., 2014; Topp and Pattey, 1997). In anoxic and reducing marine conditions, CH_4 is formed by the reduction of CO_2 by hydrogen (H_2). This pathway is limited by the concentration of H_2, hence the name, hydrogentrophic methanogenesis and is present amongst 73% of methanogen species (Megonigal, Hines, and Visscher, 2003). Methanogens that primarily consume the LMW substrate, acetate, comprise only 10% of methanogens. But even though the distribution amongst methanogen taxa is limited, the geographic distribution of this class of methanogens is high, specifically across freshwater ecosystems (Megonigal, Hines, and Visscher, 2003; Whiticar, 1999). These acetotrophic methanogens are associated with greater production rates of methane thus making this group important to understand (Megonigal, Hines, and Visscher, 2003).

In contrast to the production of CH_4 through methanogenesis, is the consumption of CH_4 through a process known as methanotrophy (Megonigal, Hines, and Visscher, 2003). This process occurs close to the soil-atmosphere interface and in well-drained soils because the microbes, known as methanotrophs, require oxidative conditions. Apart from the presence of O_2 and CH_4, methanotrophy can also be regulated by nitrogen. For some methanotrophs, ammonium ions can outcompete CH_4 as a substrate and thus prohibit methanotrophy (Megonigal, Hines, and Visscher, 2003). Furthermore, methanotrophy can be limited in environments with high concentrations of $NO_2{}^-$. But it should also be stated that there are published instances in which methanotrophy was not depressed in nitrogen-rich environments thus increasing the difficulty of a straight-forward generalizations (Megonigal, Hines, and Visscher, 2003). However, the important aspect to understand in the context of this project is that methanotrophs consume some of the CH_4 that is being measured.

At the global scale, recent studies have shown that biogenic methane contributes between 220 and 345 Tg CH_4 yr^{-1} to the atmosphere compared to roughly 96 Tg CH_4 yr^{-1} from fossil fuels

(Kirschke et al., 2013). Though the non-anthropogenic sources of CH_4 are greater than anthropogenic emissions, it remains important to properly balance the amount of methane entering and exiting the atmosphere. Methane flux measurements are one method that assist in this accounting. However, it is not only important to understand the exact amount of methane cycling between the atmosphere and the surface but to also understand the source of the methane.

Distinguishing between natural and anthropogenic, as well as sources within their respective categories, requires an analysis of the stable carbon isotope (δ^{13}C) composition of the gas. Generally, biogenic methane has a δ^{13}C isotopic range of -110 to -55‰ and a range of -50 and -25‰ for thermogenic methane (Figure 2.4) (Kirschke et al., 2013; Martini et al., 2003; Schoell, 1988; Sharp, 2007).

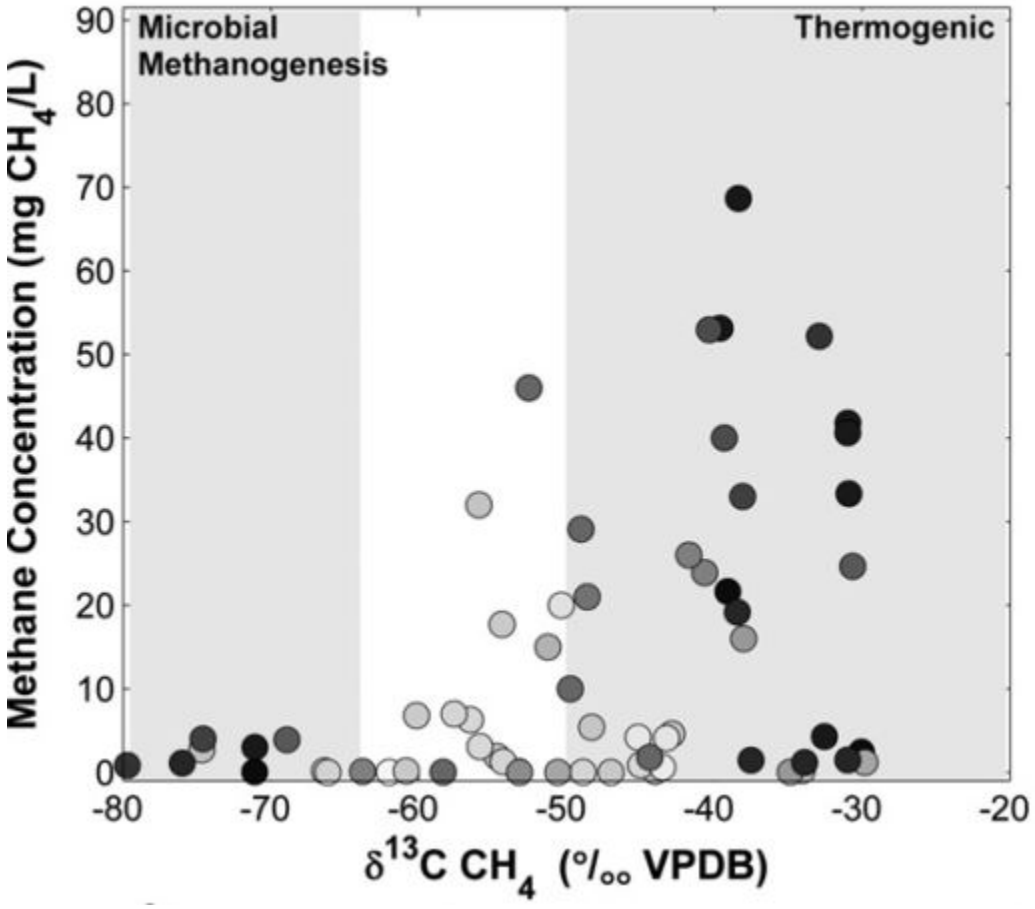

FIGURE 2.3: Results of previously conducted research illustrating the carbon isotopic value and the relation to a specific source. These aqueous samples were plotted in either the microbial, mixed, or thermogenic zones (as determined by the δ^{13}C-CH_4) as well as the concentration of CH_4 in that sample. The color of each dot pertains to the proximity to HVHF well. Taken from Jackson et al., 2013

Classifying the source of methane is not a cut-and-dried process. About 80% of methane in natural gas has a thermogenic origin (Schoell, 1988). This further demonstrates that methane migration

from the source rock, or more likely, from a leaky wellhead, to the surface is not a trivial process. The CH_4 may mix with biogenic gas along the way and therefore it is important to establish accurate endmembers using the carbon isotope composition.

HVHF methods may increase the risk of thermogenic CH_4 escaping from the source rock and into underground potable aquifers as well as the atmosphere. The destination of CH_4 flow is of primary concern for residents and legislators; understanding how CH_4, and especially, thermogenic CH_4 ends up in groundwater sources or in the atmosphere as a greenhouse gas is the focus of many environmental impact assessments of hydraulic fracturing activity.

2.6 Efforts to Quantify Methane Emissions & Isotopic Compositions

Research into quantifying methane emissions in the context of natural gas development is growing in the literature, with measurements of methane concentrations in groundwater composing a large portion of that database. For example, the Marcellus Shale is one of the largest shale gas plays in the United States, spanning from upstate New York southwards to the border between Kentucky and Tennessee. The Marcellus has drawn large interest because it is the largest known natural gas play, containing 140-1,000 trillion cubic feet (Tcf) of natural gas (Arthur, Bohm, and Layne, 2008; Wang et al., 2014; Zhang et al., 2014). Geoscientists such as Darrah et al. (2014) have attempted to identify and quantify fugitive methane leakage into groundwater associated with Marcellus shale gas development. Darrah et al. (2014) examined over 100 domestic groundwater wells located within the Marcellus Shale play in New York and Pennsylvania. Using pairings of methane isotope values and noble gases, the authors found evidence of thermogenic methane in the groundwater, which they described as most likely due to seepage through well annuli, faulty well casings, and abandoned wells (Darrah et al., 2014). One component missing from this and other Marcellus Shale studies were pre-drilling measurements of methane concentrations. Without background measurements one cannot definitively link thermogenic CH_4 in aquifers to natural gas development.

Other research conducted by Boyer *et al*. (2011) made measurements of methane concentrations in groundwater prior to and after HVHF activity occurred on the Marcellus. However, no statistically different amounts of thermogenic methane were found through the pre- and post-drilling results, although confidence in the conclusions is limited by the small number of post-drilling measurements (Boyer et al., 2011).

Additionally, other have reported measured methane concentrations in the atmosphere rather than in groundwater. Kort et al. (2014) discovered large methane out fluxes in the Four Corners region of southwestern United States using remote sensing techniques. The authors measured emissions of 0.59 Tg CH_4 yr^{-1} coming from this region, which accounts for 10% of methane emissions inventory associated with natural gas systems for the United States in 2008 (Kort et al., 2014).

Furthermore, the authors report the Four Corners region accounts for 5% of all methane emissions from US fossil fuel (petroleum, natural gas, and coal) extraction (Kort et al., 2014). However, this study used inverse techniques, and did not specify clear factors of resolving the sources of methane between the different subsectors of the fossil fuel industry. Therefore, it would behoove geoscientists to further the research by building a strong ground measurement program for validation (Kort et al., 2014) cited a ground validation component in their study).

To evaluate the potential for methane leakage induced by HVHF activity, more studies of methane emissions before and after drilling are needed (Hornberger et al., 2015). Moreover, the impact of HVHF activity on methane leakages could be better understood from the aspect of soil flux analysis. Near-surface earth material (*i.e.* soil) is a reservoir that is not highlighted in methane leakage studies. Whether the leak be a subsurface point or non-point emission, it is crucial to understand the biogeochemical cycles and rates of exchange of gases between this reservoir and the atmosphere in order to comprehensively understand HVHF impact on the environment.

2.7 Motivation for Field Site Location

The Cumberland Plateau was chosen for the field area (Figure 05) in this study primarily because of its prevalence for relatively high amount of HVHF activity and potential for increased HVHF activity in the future. Also, no previous studies have reported CH_4 surface fluxes associated with HVHF, and studies of methane leakage from HVHF wells in the Cumberland Plateau are nonexistent. If HVHF activity in the region is to increase, it will be essential to demonstrate that HVHF does not increase CH_4 emissions. Furthermore, this field area has sites that are HVHF-active (test) and -inactive (control) within close proximity (2.25 km). The similar surface and, to our knowledge, subsurface geology between test and control sites reduces the amount of confounding variables. Moreover, attempts made by the University of Tennessee to lease the Cumberland Forest for HVHF development have been met with concerns by the public regarding the potential negative impacts of HVHF activity (Fowler, 2013; Gang, 2013). Along with the combination of the close proximity between the two types of sites and the public interest in the area, this location will allow for baseline measurements in non-fractured areas to be made as well as comparisons to previously fractured areas to articulate a complete and relevant story with regard to the environmental impact of the HVHF method of natural gas extraction.

Chapter 3

Research Hypothesis & Objectives

3.1 Hypothesis

Simply stated, the objective driving this research project is as follows: to test the idea that HVHF practices lead to enhanced thermogenic CH_4 emissions in areas of shale gas development against the null hypothesis that CH_4 emissions are due to background processes unassociated with HVHF.

3.2 Research Objectives

The primary research objective is addressed by measuring fluxes and carbon isotope compositions of CH_4 and CO_2 from soil in areas in which HVHF is and is not practiced, to estimate the amount of gas being emitted and identify the source of the gas as, biogenic or thermogenic. Ancillary objectives include:

RO.01 : Compare methane emissions in geologically similar areas where fracking has yet to occur and where HVHF methods is currently being practiced.

RO.02 : Assess if there is a diurnal effect on methanotrophs

RO.03 : Measure and analyze if excavating pits (30 cm) deep has any effect on the soil fluxes and/or carbon isotope measurements. The motivation for this objective is to see how the microbial activity may vary with depth.

To assess RO.01, the null hypothesis will be that there is no statistical difference in methane flux or isotopic composition between HVHF and non-HVHF areas. If the null hypothesis is rejected, the next step will be to test whether thermogenic methane emissions increase as distance to the well head decreases. Objective RO.03 can be achieved by taking measurements during the daytime and during the nighttime at the same location and assessing for a statistical difference between the two datasets. Finally, RO.03 can be accomplished through a similar concept, where the measurements taken in the same location will be compared for a statistical difference before and after excavation.

Chapter 4

Research Methods & Materials

4.1 Closed Loop Gas Chamber and CRDS Analysis: Soil Gas Collection Method A

4.1.1 Picarro: In situ Flux and Isotopic Analysis

In this study a Picarro G2201-i wavelength-scanned cavity ring-down spectroscopy (WS-CRDS) analyzer was used to measure the concentrations and carbon isotope compositions of methane and carbon dioxide. The analyzer measures the decay rate of infrared radiation at absorption wavelengths of the molecules $^{13}CH_4$, $^{12}CH_4$, $^{13}CO_2$, and $^{12}CO_2$. An infrared laser emits light at one of these absorptive wavelengths. As the light passes through the gas-filled cavity, some of the light is absorbed by the gas, and the remaining light is reflected by a mirror and passes again through the cavity. This process is repeated thousands of times in order to increase the path-length of the laser, the amount of gas absorbed, which results in greater precision. The light intensity is continuously measured by a detector, and the intensity decay rate is used to calculate a concentration of each isotopologue and the corresponding values of δ^{13}C-CH_4 and δ^{13}C-CO_2 (Crosson, 2008). WS-CRDS technology records measurements at a high temporal frequency (approx. one measurement every second) thus providing a large data set, which is useful for calculating a flux with high precision.

The WS-CRDS analyzer is large but portable instrument; it has a length of 44.58 cm (17.55 in), a width of 43.18 cm (17.00 in), and a height of 17.78 cm (7.00 in). The WS-CRDS unit is connected to an external vacuum pump and the combined weight of the analyzer and the pump is 25.40 kg (56.00 lbs). In order to mobilize the WS-CRDS analyzer, it was placed in a wagon and powered by a deep cycle battery (12VDC).

4.1.2 Eosense Autochamber

Chamber Specs and Hardware

An Eosense autochamber (eosAC) was used to quantify soil methane and carbon dioxide fluxes. This autochamber is a dynamic closed loop chamber (also known as a non-steady-state flow through chamber). The chamber is automated in the sense that it is automated to open or close by the schedule put in place by to place by the user. A vacuum pump continuously draws soil gas from the chamber to the WS-CRDS analyzer. Once analyzed, the gas is then returned to the autochamber, completing the loop.

Deployment Procedure

The closed loop chamber method was deployed solely in the field. The collar of the chamber was inserted into the soil to a depth of 4 to 8 cm, and then the autochamber was placed on top of the collar in the open position. As soon as the temperature and pressure conditions for the cavity of the WS-CRDS analyzer stabilized, the chamber was scheduled to remain open for 5 minutes to collect ambient background measurements. Following this pre-measurement background collection, the chamber closed for 30 minutes to seal the headspace of the chamber from the ambient environment and collect only the gases escaping from the soil. After the 30-minute measuring period, the chamber reopens for another 5 minutes to collect post-measurement background data.

Data Analysis Procedure

The measured chamber concentrations of methane [CH_4] and carbon dioxide [CO_2] were plotted vs. time (t, sec). The resulting curves become approximately linear as t approaches zero. The initial flux (F_0, μg m^{-2} sec^{-1}) was estimated by choosing the linear portion of the curve in a small region of the profile near t0 (approx. t_{30} to t_{150} sec) and fitting a linear function using least squares regression to estimate the slope in the limit that $t \to 0$. The slope (S, ppm sec^{-1}) is multiplied by a conversion factor (CF) to obtain the flux F_0 (Equation 4.1).

$$F_0 = S * CF \tag{4.1}$$

Errors for reported fluxes were estimated by calculating 95% confidence limits for the slope and subsequently applying the conversion factor to match the units of the flux.

The objective of carbon isotope analysis is to identify the source of the gas being emitted from the soil. The source of the soil gas entering the chamber headspace can be identified from measurements of concentration and stable carbon isotopes ($\delta^{13}C_{mix}$). At any point in time, the chamber

headspace contains a mixture of gases sourced from the soil and atmosphere but the proportion of soil gas increases over time. Using the principle of mass balance, a linear relationship is established between the isotopic signature of the gas mixture in the headspace ($\delta^{13}C_{mix}$) and the inverse concentration of the mixture in the headspace ($\frac{1}{c_{mix}}$). By applying a least squares linear regression for this relationship, $\delta^{13}C_{mix}$ vs. $\frac{1}{[c_{mix}]}$, a Keeling plot is generated. Theoretically, the Keeling plot should present a linear mixing line, where [c_{mix}] is the measured concentration of CH_4 or CO_2, and the y-intercept, produced by the linear regression, describes the source of the soil gas $\delta^{13}C_s$ (Equation 4.2) (Krevor et al., 2010; Pataki et al., 2003).

$$\delta^{13}C_{mix} = Slope * [c_{mix}] + \delta^{13}C_s \tag{4.2}$$

The uncertainty of for the $\delta^{13}C_s$ is expressed through a margin of error analysis at 95% confidence level.

4.2 Static Gas Chamber: Soil Gas Collection Method B

As an alternative method, soil gas measurements were collected using the classic static (non-steady-state non-flow through) chamber (Denmead, 2008; Pihlatie et al., 2013). The static chamber that was used is composed of two main parts; an anchor that is pushed firmly into the ground and an endcap on top of the anchor. Both parts are constructed from 20.32 cm (8.00 in) schedule 40 PVC pipe, with the chamber being constructed using the endcap. Two holes were drilled into the top of the endcap, diametrically opposite of each other. One hole was constructed to be the sampling port; this port is filled by a butyl septum (PerkinElmer), which allows for multiple withdrawals with minimal leakage. The second hole is for essential pressure equalization (Denmead, 2008; Pihlatie et al., 2013; Pumpanen et al., 2004); this hole is filled by a threaded pipe adapter and a 0.635cm (0.25 in) diameter stainless steel pipe. The anchor serves as a base for the cap to rest on and as a place holder so that the same area can be measured repeatedly. The cap is placed on top of the anchor only while samples are being collected. Similar to the autochamber, the static chamber creates a headspace that allows for gases sourced from the soil to accumulate. Samples of these headspace gases are drawn using a 10 mL syringe and are immediately injected into a separate evacuated 10 mL vial for storage and transport.

The static chambers were not used to make flux measurements, but were used to measure saturation concentrations of methane, ethane, and propane. The static chambers were set out at two pairs of control and test sites for 48 to 72 hours. The sampled gas (two samples per chamber) was transported back to laboratory for gas chromatographic analysis (Shimadzu 2010Plus). The gas chromatograph (GC) with a flame ionization detector (FID). An autosampler withdrew 10 μL of each sample from the storage vial and injected into the GC. The carrier gas, helium, pushed the

sample through the mesh column towards a flame which combusts the sample. The ions of the combusted sample are picked up by the detector and concentrations of the gases are calculated and reported.

4.3 Comparing Soil Gas Collection Method A vs. Method B

Advantages of implementing Method A over Method B for flux measurements include higher temporal resolution (measurement intervals of one second vs. fifteen minutes, respectively), more precise measurements, and a greater range of detectability (Christiansen, Outhwaite, and Smukler, 2015). Additionally, Method A allows for the analysis of the isotopic composition of the gas, which is not available with the GC in Method B. Furthermore, all of the measurements using Method A can be made *in situ*, which is an advantage when considering the rapid rate of oxidation of methane in samples containing atmospheric O_2, even within a sealed and evacuated vial. Also, the autochamber allows for multiple unattended measurements so long as an adequate power source is available.

However, Method B permits the measurement of higher carbon number gases such as ethane and propane, both of which are strong indicators of the presence of thermogenic natural gas. Moreover, the static chambers are cheaper to construct and have far less restrictions on locations of deployment, thus enhancing the spatial coverage of gas collection.

The two methods therefore have complementary strengths.

4.4 Accounting for Other Factors that could Influence Soil Gas Measurements Ancillary Measurements

Apart from the differences between the two soil gas collection methods, there are several other factors that may affect soil gas measurements.

4.4.1 Wind & Atmospheric Pressure

The microclimate at the near-surface can affect soil gas collection measurements, especially for flux measurements. Wind is an important microclimatic factor. Short-term measurements have been documented as being affected by large amounts of wind (Pumpanen et al., 2004). Therefore, this study use of closed chamber systems helps to reduce the effect of wind on soil gas measurements.

Atmospheric pressure is another microclimatic component that can alter measurements at the soil-atmosphere interface. During instances of high atmospheric pressure, atmospheric gas in the

chamber headspace can be pushed into the soil, resulting in a measurement of negative fluxes. The influence of atmospheric pressure was limited by making soil gas measurements at times of low atmospheric pressure, and by making measurements at control sites immediately before or after measurements at their paired test sites. Barometric pressure was recorded at every sampling location.

4.4.2 Soil Characterization

In the ideal case earth materials at all levels from the source in the subsurface to the soil-atmosphere interface would be characterized. However, the vadose zone is the only layer that contains organisms that can both consume and produce CH_4, and thus it requires special attention. Five soil core samples were taken at all test-control pairs. Each core was roughly 3 cm in diameter and 5 cm in height.

Soil bulk carbon measurements were made via a combustion module linked to a WS-CRDS analyzer (Picarro G2201-i) in order to measure concentration and 13C of soil organic carbon. Soil organic carbon concentration provides a measure of microbial activity and amount of organic detritus. The soil $\delta^{13}C$ provides information on the source of soil carbon, and can be compared with $\delta^{13}C$-CH_4 and $\delta^{13}C$-CO_2 to see if these gases were produced in the soil.

The density of the soil was estimated by collecting a known volume of soil, drying the sample, measuring its mass, and dividing that mass by the volume. This metric can constrain physical parameters of the soil such as porosity that affect rates of diffusion and mechanisms of gas transport and therefore the magnitude of measured fluxes.

Soil moisture was measured because it can affect the redox potential in the soil. Poorly drained soils (higher soil moisture) can become anoxic, promoting the production of biogenic CH_4 through methanogenesis. In dry and well drained environments (low soil moisture), the consumption of methane through methanotrophy is greater. Thus, high temporal (approx. one measurement per second) measurements of soil moisture were taken using a pair of time domain reflectance (TDR) probes.

Finally, microbial activity, such as methanotrophy and methanogenesis, can strongly influence the concentration and surface flux of methane. To minimize this effect, chamber flux measurements were made in pits excavated to depths of 30 cm below the zone of intense near-surface microbial activity.

4.5 Project Design

The measurement sessions for this study were divided into two sessions: a fall session and a winter session. The motivation behind these two sessions was to capture any seasonal, diurnal effects (fall session only), and more HVHF wells as they became more available in the winter session. There were a total of three treatments explored in this study. The first is the aforementioned seasonality. Second, the exploration of a diurnal effect on the microbial activity and thus the soil gas measurements. Thirdly, the comparison of measurements made on the natural landscape (unexcavated) against measurements made in pits (excavated).

4.5.1 Fall

The fall measurements were gathered 10 October 2015 between the hours of 09:00 and 20:00 local time. These measurements were collected under a light rain during the early part of the measuring session and under partly cloudy conditions for the remainder of the session. The soil temperature at all sites was an average of 19°C and atmospheric pressure just below standard conditions at 97 kPa.

During the fall data collection session, two control sites and one test site were measured. The sites are listed chronologically. See Figure XX for map of sampling locations and see Table XX for specific climatic metrics for each site.

Wilson Mountain Control Site (WMCS)

Location: 36° 2 52.5 N, 84° 29 51.1 W, elevation 402 m
This control site was located on the Slatestone formation (Psl), on top of an ultisol unit (Gilpin-Petros complex). It was considered as a control for the Lewis Carson 3 Site. Measurements were conducted under a light rain and just off a spur road. For this site, only unexcavated measurements were taken and this site was not repeated in the winter measuring session.

Lewis Carson 3 Site (LC3S)

Location: 36° 2 45.8 N, 84° 28 48.3 W, elevation 415 m
This test site was located on the Psl as well, and the soil is considered an ultisol unit (Gilpin-Petros complex). Unexcavated chamber measurements were made roughly 18 m (60 feet) from the well.

Bunkhouse Control Site (BHCS)

Location: 36° 3 10.5 N, 84° 28 51.2 W, elevation 407 m
This control site was located on the Psl and measured on the ultisol unit (Gilpin-Petros complex). At this site, measurements were conducted in both daytime (16:35 to 17:15 local) as well as nighttime measurements (19:40 to 20:20 local). All measurements were unexcavated and made under partly cloudy and lightly raining conditions.

4.5.2 Winter

The winter measurements took place over the course of 29 February 2016 through 01 March 2016. These measurements were all conducted during the daytime (09:00 to 18:00 local) under clear conditions on the first day and partly cloudy conditions on the second day. The average soil temperature was 11C and atmospheric pressure was 97 kPa.

During the winter data collection session, two control and three test sites were measured. The sites are listed in chronological order. See Figure XX and Table XX for site specific locations and climatic data.

4.5.3 Lewis Carson 3 Site (LC3S)

LC3S was measured again during the winter session. However, excavated measurements were made in addition to unexcavated measurements. Due to poor weather, a control site pair was not measured during the winter session.

Eddie Walls Well 1 (EWW1)

Location: 36° 2 49.8 N, 84° 25 5.8 W, elevation 349 m
The EWW1 test site is located on the Crooked Fork formation (Pcf) and the soil is an entisol (Bethesda-mines pit complex). The site was strip mined for coal three decades ago and is now used for extracting natural gas and as land for grazing cattle. The chamber was placed 28.5 m from the well. Both unexcavated and excavated measurements were made at this location.

Eddie Walls Well 1 Control Site (EWW1 CS)

Location: 36° 2 44.7 N, 84° 24 45.4 W, elevation 351 m
This control site on the Pcf layer, over a mix of Bethesda-mines pit and Gilpin Petros soils. Both unexcavated and excavated measurements were conducted at this site.

Eddie Walls Well 3 (EWW3)

Location: 36° 3 30.5 N, 84° 25 1.5 W, elevation 599 m
This test site was located on the Indian Bluff formation (Pib), on an ultisol unit (Gilpin-Petros complex). At this site, two horizontal wells were drilled into the Chattanooga Shale. The chamber was placed 81 meters from the western wellhead. Only unexcavated measurements were made at this location.

Eddie Walls Well 3 Control Site (EWW3 CS)

Location: 36° 3 19.5 N, 84° 25 12.6 W, elevation 617 m
The measurements for this control site were located on the Pib, on an ultisol unit (Lily-Gilpin complex). The land at this site was used for deer hunting, as evidenced by discussions with the land owner and by the presence of deer fecal matter and carcasses. Only unexcavated measurements were conducted at this site.

Chapter 5

Results

5.1 Objective 1: Quantify CH_4 and CO_2 Fluxes

5.1.1 Fall Measurements: Meteorological Conditions and Soil Characterization

Several measurements were made to quantify meteorological conditions. These data are generated single data point measurements taken from a soil thermometer and atmospheric pressure gauge. Table 5.1 displays the meteorological conditions measured at the sampling locations.

TABLE 5.1: Meteorological conditions for fall sampling locations.

Location	Soil Temperature (°C)	Atmospheric Pressure (atm.)
BHCS	18.6	0.96
WMCS	17.9	0.96
LC3S	19.5	0.96

The soil was also characterized through a variety of measurements. Table 5.2 illustrates the soil type, carbon content, stable carbon isotope composition δ^{13}C, soil moisture content, and soil density.

TABLE 5.2: Soil characterization for fall sampling locations. Note that BCHS is not listed due logistical constraints on making measurements.

Location	Soil Type Complex	Carbon Content (%)	δ^{13}C (‰)	Soil Moisture Content (% H_2O)	Soil Density (g cm^{-3})
WMCS	Ultisol	2.86	-28.5	49	1.10
LC3S	Ultisol	1.90	-27.2	30	1.47

5.1.2 Fall Measurements: Concentration-Time Profiles

The primary research objective was to measure the rate of CH_4 and CO_2 exchanged at the soil-atmosphere interface. In making these measurements, the ancillary objective RO.02 was to assess if there is a diurnal effect on methanotrophs by making measurements at the BHCS site both during the day and at night in order to assess the impact of the diurnal signal on the chamber measurements.

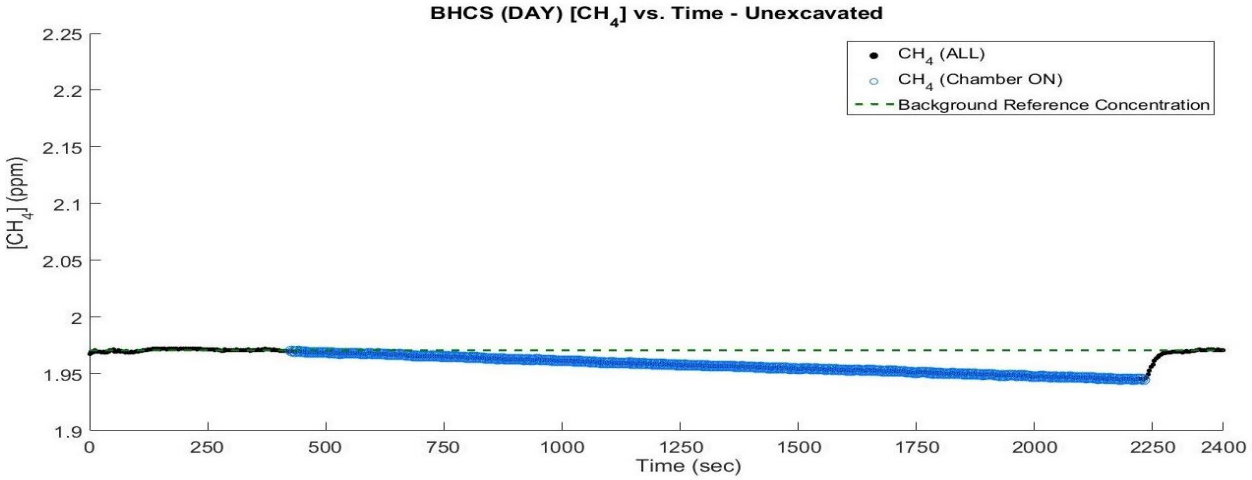

(A)

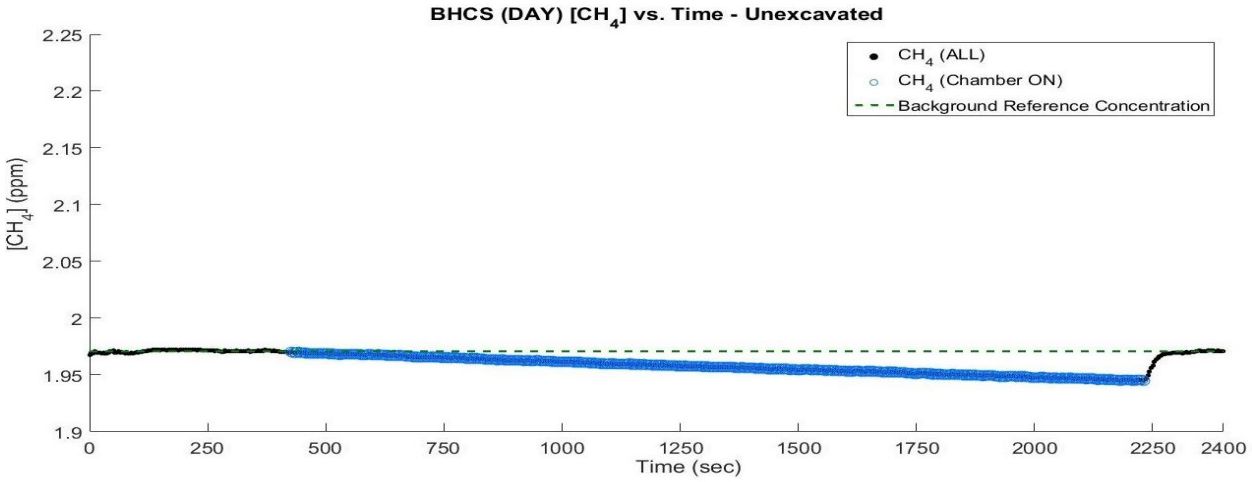

(B)

FIGURE 5.1: Autochamber-Picarro [CH_4] versus time measurements taken at the control site, BHCS, during October 2015. (A) shows the DAY measurements and (B) shows the NIGHT measurements. The x- and y-axis have been scaled equally for both graphs and for all proceeding concentration-time profiles. The Background Reference Concentration represents the mean value of the pre- and post-background measurements (black dots).

From visual inspection of the these two graphs (Figure 5.1), it is clear that the difference between

making measurements during the day and at night are inconsequential. A paired difference t-test confirms this by supporting the null hypothesis of no significant difference between day and night treatments at the BHCS site ($p < 0.001$).

The concentration profile for WMCS (Figure 5.2) was fairly flat and was mostly indifferent from the background reference concentration throughout the measurement period. This difference is expressed quantitatively through the mean and standard deviation for the [CH_4] values for the closed chamber period (2.011 ± 0.001 ppm) and the pre- and post-measurement (2.012 ± 0.005 ppm) measurements.

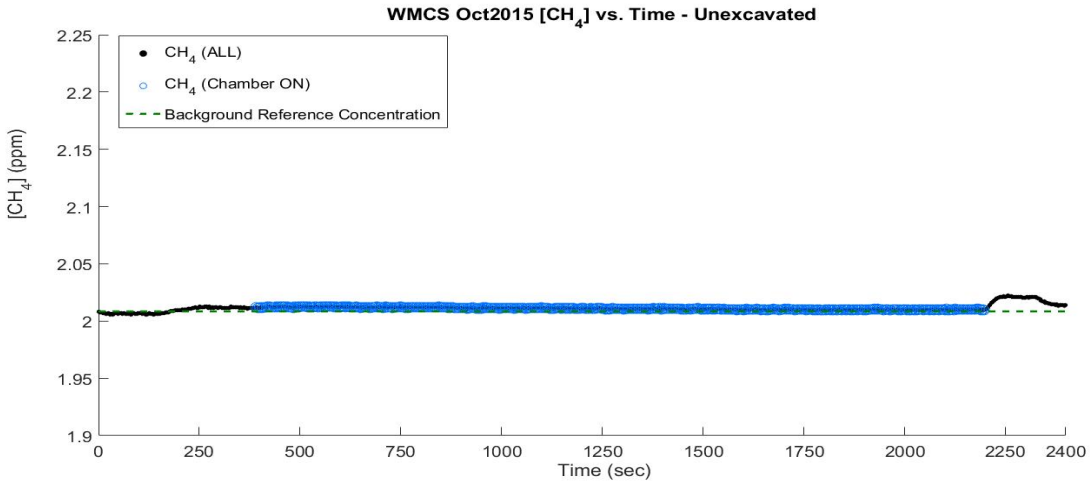

FIGURE 5.2: [CH_4] versus Time at the control site, WMCS.

The fall measuring session also illustrated elevated emissions of CH_4 at the test site (LC3S) versus the two control sites (WMCS and BHCS). This was evident across two types of measurements. First, the pre- and post-measurement of CH_4 at the three sites showed a higher atmospheric concentration at LC3S than at WMCS or BHCS (Figure 5.3). The median background [CH_4] for LC3S is significantly different at the 95% confidence level and greater in magnitude than the background measurements for WMCS and BHCS (both day and night).

The second piece of evidence that demonstrated an elevated [CH_4] at the test site in comparison to the control sites comes in the form of the concentration profiles. The control sites exhibited a decrease in [CH_4] over time (negative fluxes, Figures 5.1 and 5.3), whereas the test site presented an increase in [CH_4] over time (positive flux, Figure 5.4).

More specifically, the test site exhibits an increase in [CH_4] during the first 120 seconds of the measuring period but for the remaining 2275 seconds the profile exhibits a decrease in [CH_4] over time similar to the control sites (Figure 5.4).

The trends in CO_2 measurements across both the test and control sites were indistinct from one another. The primary difference between the different locations is the range in [CO_2] values. The

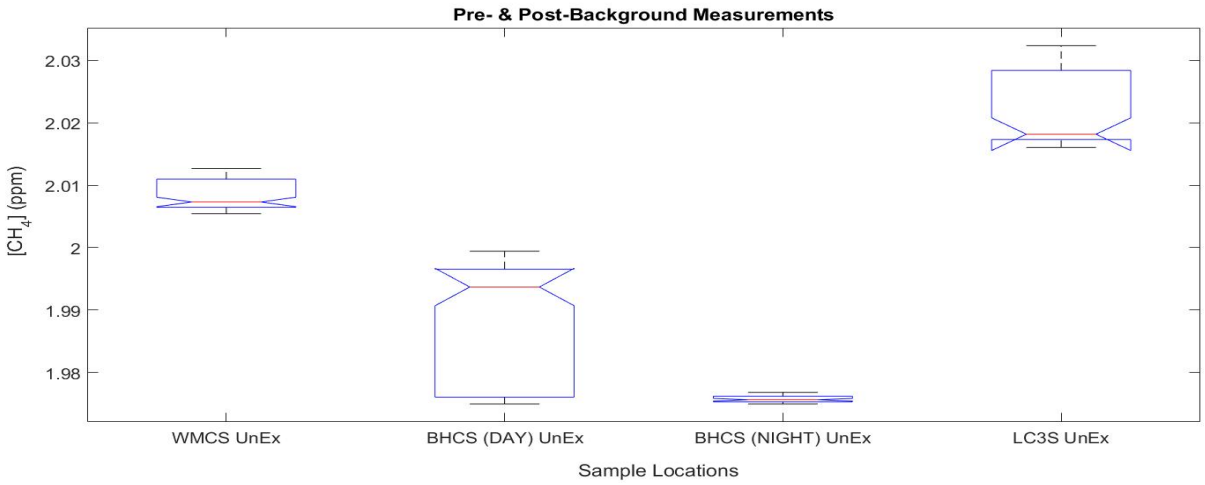

FIGURE 5.3: Boxplot of pre- and post-background for measurements made during October 2015. The red line within the boxplot represents the median value. The notches provide a point of comparison between the medians. If notches do not overlap, the result is that the medians are significantly different at the 95% confidence level.

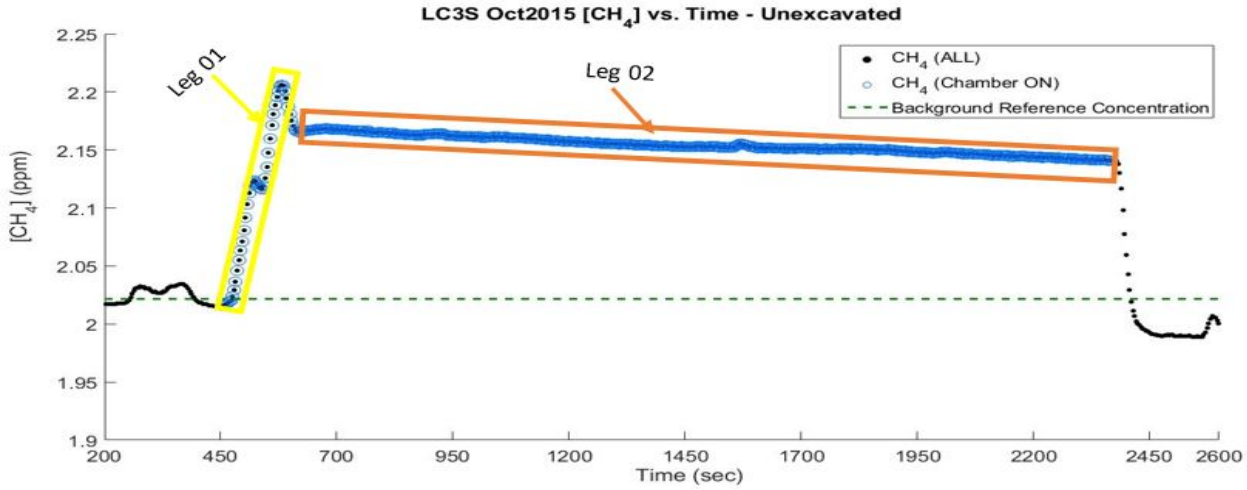

FIGURE 5.4: The fall measurement for CH_4 profile for the LC3S test site. Leg 01 exemplifies a sharp increase in CH_4, and Leg 02 illustrates a steady decrease in $[CH_4]$ with time. Time was shifted by 200 seconds for this site.

control sites tended to exhibit greater ranges (> 900 ppm) in measured $[CO_2]$ than the test site (approx. 300 ppm) (Figures 5.5-5.7).

5.1.3 Fall measurements: Flux Results Summary

From the concentration measurements, the initial flux (F_0) of each gas was calculated at each sampling location. This initial flux provides information on the maximum rate at which each gas

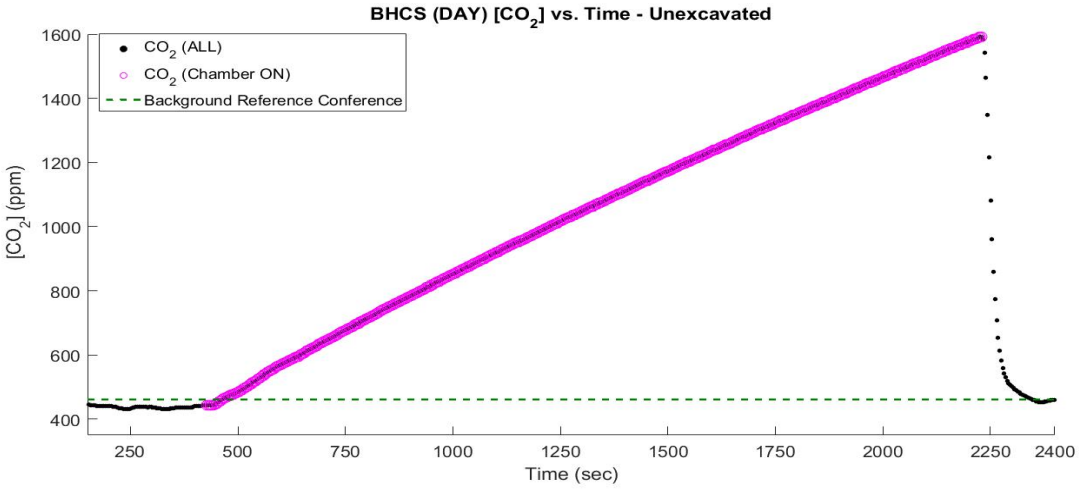

(A)

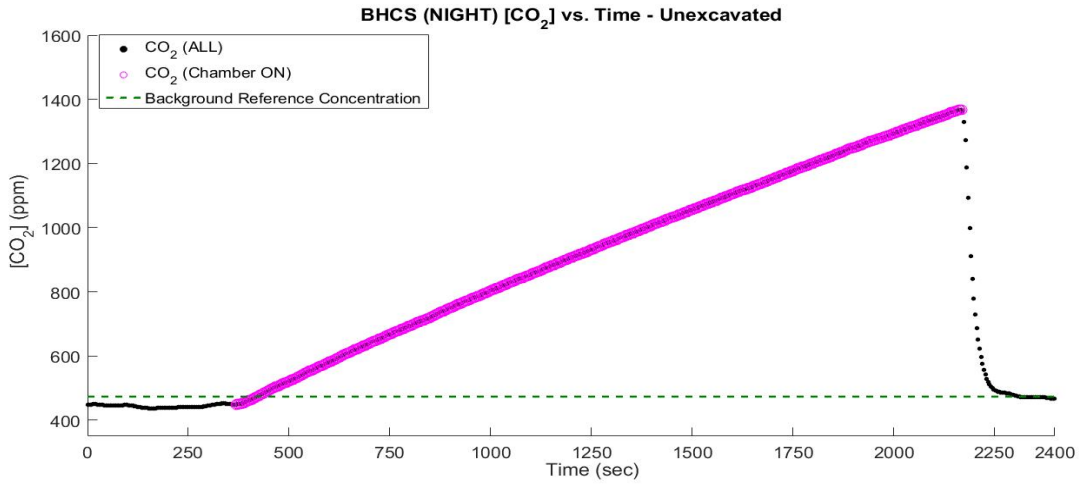

(B)

FIGURE 5.5: The fall measurement CO_2 profile at the BHCS location, where (A) represents the DAY measurements and (B) shows the NIGHT measurements. Note that the y-axis has been scaled to the same magnitude for both profiles in order to express the differences in the ranges of $[CO_2]$. The y-axis for the remaining $[CO_2]$-time profiles in this section also scaled identically.

escapes from the subsurface into the atmosphere.

5.1.4 Winter Measurements: Meteorological Conditions and Soil Characterization

Measurements of the meteorological conditions and the soil characterization metrics for the winter session are presented in Tables 5.4-5.5.

The values within parentheses represent temperatures taken with the soil thermometer. The other value indicates the mean temperature from the TDR probes.

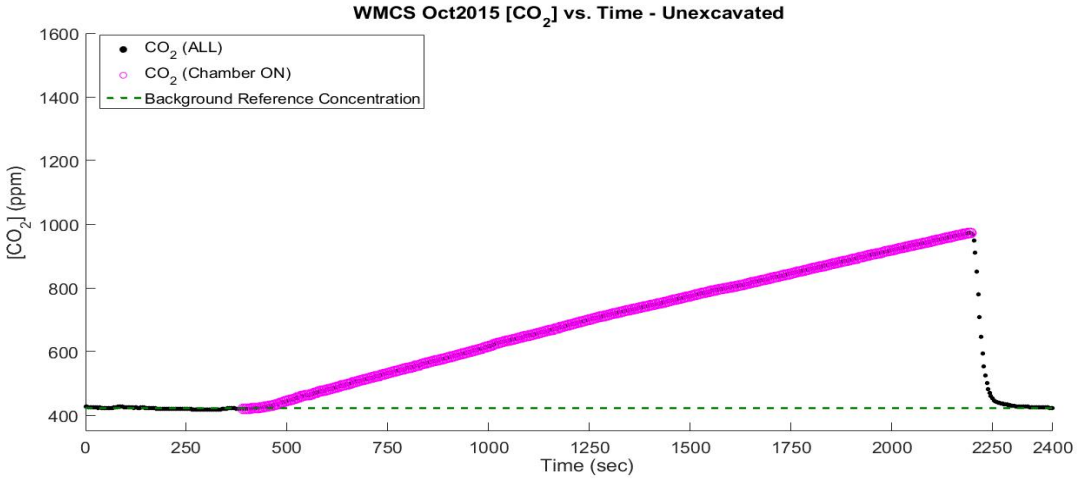

FIGURE 5.6: The fall measurements for the [CO_2]-time profile at the WMCS location.

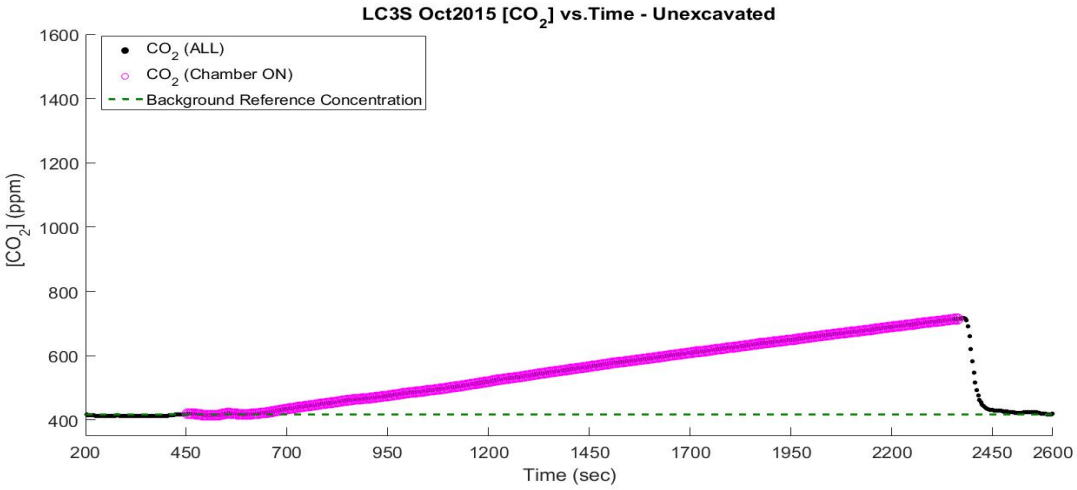

FIGURE 5.7: Fall measurements for the LC3S location.

TABLE 5.3: Flux measurements for both the control and test sites in October 2015. The same initial flux was used for both legs at LC3S. The uncertainties represent a 95% confidence interval.

Location	CH_4 Initial Flux ($F_0, \mu g\, m^{-3}\, s^{-1}$)	CO_2 Initial Flux ($F_0, \mu g\, m^{-3}\, s^{-1}$)
WMCS	-1.8E-04 $\pm$ 1.3E-04	4.2E+01 $\pm$ 3.8E-01
BHCS (DAY)	-1.6E-03 $\pm$ 1.6E-04	8.7E+01 $\pm$ 3.1E-01
BHCS (NIGHT)	-2.0E-03 $\pm$ 1.4E-04	6.7E+01 $\pm$ 3.8E-01
LC3S (Leg 01)	1.9E-01 $\pm$ 1.3E-01	2.1E+01 $\pm$ 4.9E-02
LC3S (Leg 02)	-1.6E-03 $\pm$ 5.0E-04	Same as Leg 01

It is important to note that the soil thermometer temperature measurements represent conditions at the beginning of the pre-background measurements. Using a soil thermometer, the soil temperatures for LC3S, EWW1, and EWW1 CS were 7.9, 13.5, and 15.3°C at the beginning of each

TABLE 5.4: Meteorological conditions for all winter sampling locations. EWW3 is lacking an atmospheric measurement due to equipment failure, and only the soil thermometer measurement was available for EWW3 CS.

Location	Soil Temperature (°C)	Atmosphere (atm.)
LC3S Feb2016	13.4 (7.9)	0.96
EWW1	20.5 (13.5)	0.97
EWW1 CS	16.1 (15.3)	0.97
EWW3	16.1	Not measured
EWW3 CS	(8.4)	0.93

of the measuring sessions, respectively (Table 5.4). However, the soil thermometers, at best, can only provide a low frequency account of any changes in temperature during the measurement. To better account for any change in meteorological conditions, two TDR probes and a data logger were used to calculate the soil temperature (and soil moisture) at a greater frequency, roughly one measurement every minute. These data are averaged and presented in Table 5.4 and are presented in a time series format as well (Figure 5.8).

Bulk soil measurements are presented in Table 5.5; these data were again collected through methods previously described in the "Research Methods section. All data presented are mean values of at least two samples.

TABLE 5.5: Bulk soil characterization for all winter sampling locations.

Location	Soil Type	Carbon Content (% C)	δ^{13}C (‰)	Soil Moisture (% H_2O)	Soil Density (g cm^{-3})
LC3S Feb2016	Ultisol	1.97	-28.0	21	1.05
EWW1	Entisol	5.02	-23.8	12	0.77
EWW1 CS	Ultisol	5.38	-25.3	19	1.03
EWW3	Ultisol	2.22	-27.6	11	0.73
EWW3 CS	Ultisol	4.64	-27.7	25	0.67

The pre- and post-background of the wintertime measurements demonstrated median values that were not significantly different at the EWW1 test and control sites (Figure 5.9). On the other hand, the pre- and post-background measurements showed that EWW3 CS had a significantly greater median background [CH_4] than EWW3. For LC3S, the winter measurements yielded significantly lower [CH_4] than in the fall.

5.1.5 Winter Measurements: Concentration Profiles

The winter measurement session produced more concentration profiles than the fall session because measurements were made at more sites, and because both unexcavated and excavated measurements were conducted at the LC3S, EWW1, and EWW1 CS sites. Time values on the x-axes

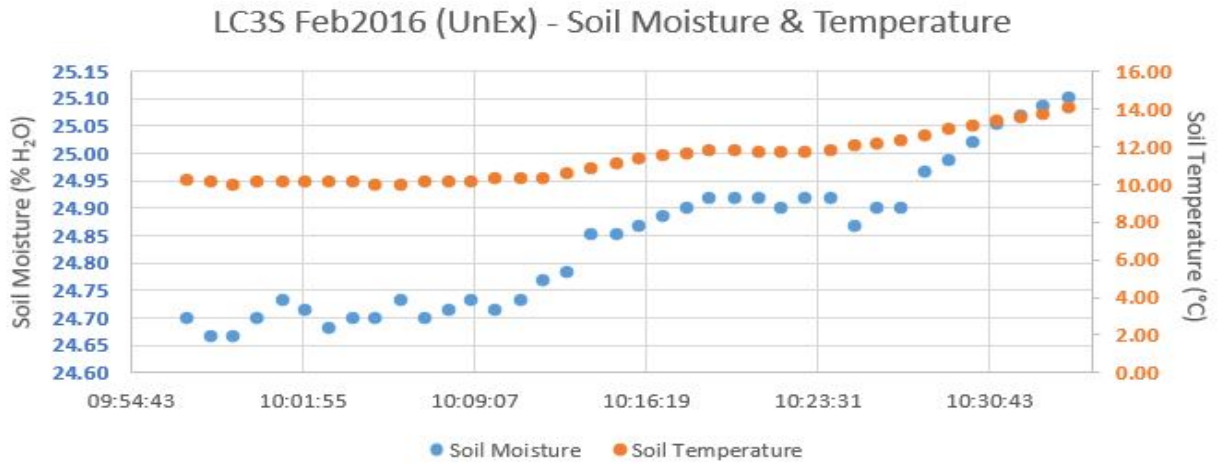

(A)

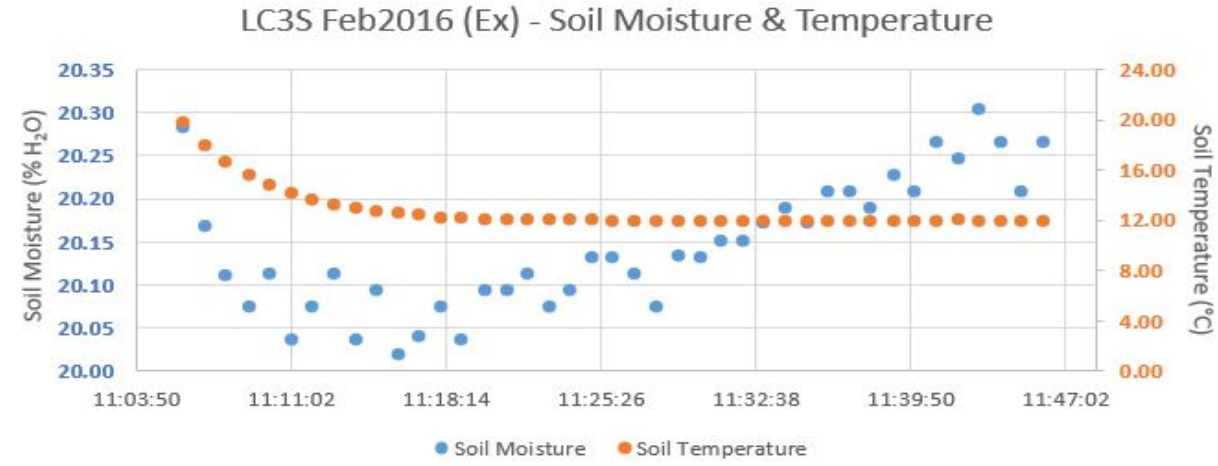

(B)

FIGURE 5.8: Soil moisture and soil temperature for LC3S. The unexcavated measurement is presented in (A) and the excavated measurement as (B). The TDR data for the remaining measured sites are located in Appendix A.

show different numerical values for the excavated measurements, but they all span roughly 2400 seconds.

Visual inspection reveals a large difference in the [CH_4] vs. time profiles between the two treatments at the LC3S site (Figure 5.10). Over time, the excavated measurements show an order of magnitude greater range of [CH_4], 0.16 ppm, over the same period as the unexcavated measurements, 0.01 ppm. Direct test-control comparisons could not be made for LC3S during the winter session due to the fact weather and logistical reasons prevented measurements at a corresponding control site.

At the control site, EWW1 CS, the [CH_4] versus time profiles for the unexcavated and excavated

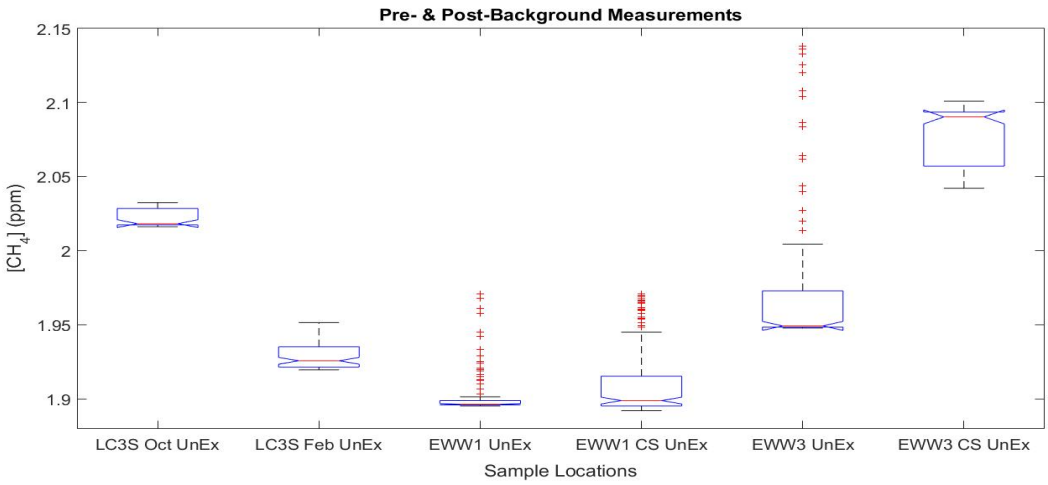

FIGURE 5.9: Boxplot of pre- and post-background measurements for the unexcavated winter sampling locations. A boxplot of the excavated sites is located in Appendix B.

experiments are also visually distinct during the first 300 seconds (Figure 5.11). In the unexcavated treatment, measured [CH_4] are similar to the mean background concentration throughout the measurement period. In contrast, for the excavated experiment [CH_4] exhibits a decrease and then returns to background concentrations.

At EWW1, the concentration profile for the unexcavated treatment showed a large increase in [CH_4] and return to background levels during the first 300 seconds (Figure 5.12). With the exception of the large spike and decrease, the measurements between the two treatments were fairly similar.

To compare the [CH_4] values between the test and control sites, EWW1 and EWW1 CS, a paired difference t-test was applied to both treatments. The mean difference between the unexcavated measurements at EWW1 and EWW1 CS was 0.098 ± 0.148 ppm and 0.067 ± 0.028 ppm (1σ) for the excavated measurements. Both of these mean differences were statistically significant in comparison to the null mean difference of zero ($p << 0.001$ ppm).

At EWW3, there were no excavated measurements, thus, leaving only test-control comparisons to present. At EWW3 [CH_4] showed a continuous increase at the test site and continuous decrease at the control site. At the control site, EWW3 CS, [CH_4] decreased without interruption but the concentration range (0.01 ppm) was greater than for the test site. At the test site, [CH_4] increased steadily without interruption until the chamber reopened, however, the range was small (0.1 ppm) (Figure 5.14).

At LC3S, the [CO_2] versus time profile define a linear trend with a positive slope. This behavior is largely similar to the observations made during the fall measuring period. Similar to the [CH_4]

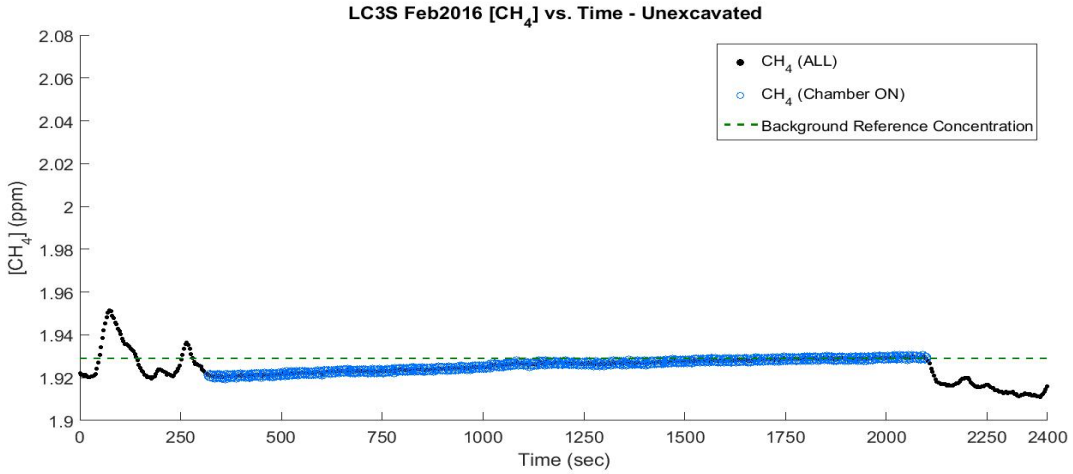

(A)

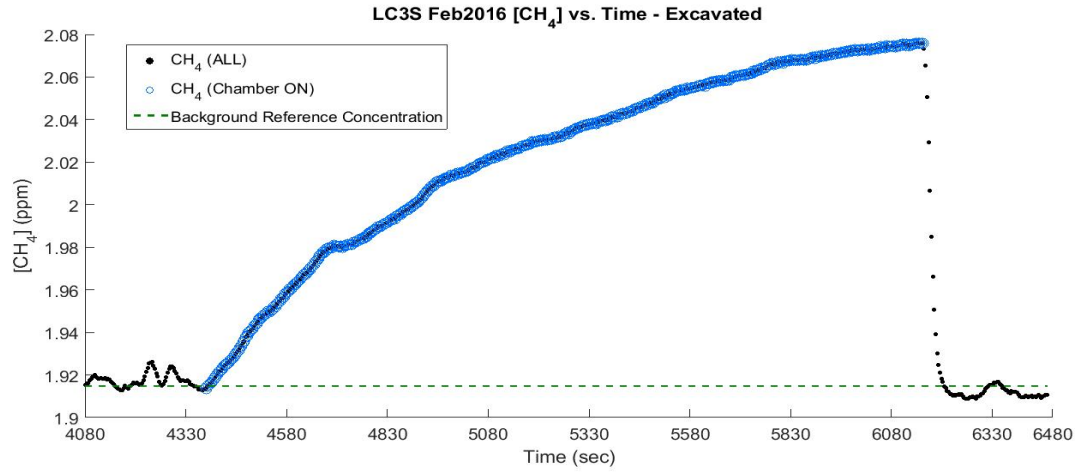

(B)

FIGURE 5.10: $[CH_4]$ vs. Time profile for the unexcavated (A) and the excavated (B) measurement at LC3S. Both the x- and y-axis are scaled identically to reflect the differences between the unexcavated and excavated treatments. This is true for all other $[CH_4]$ vs. time plots.

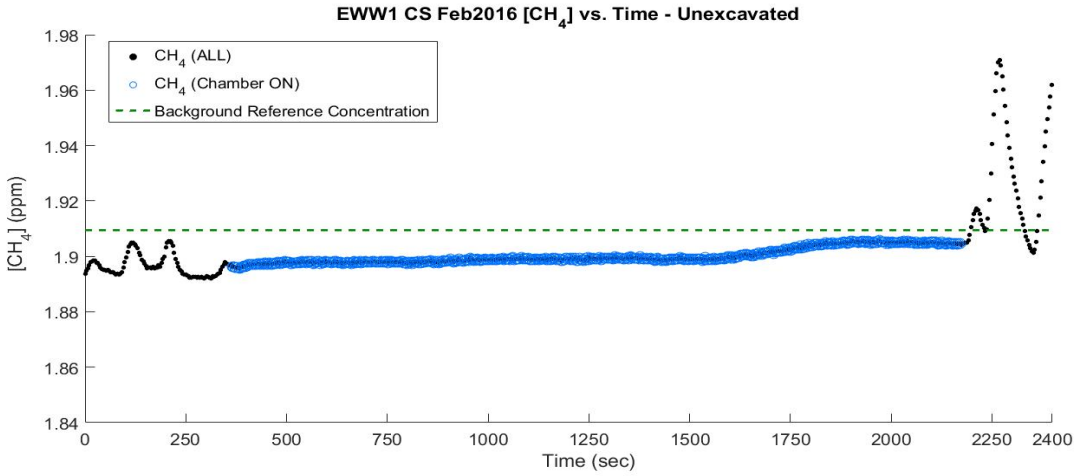

(A)

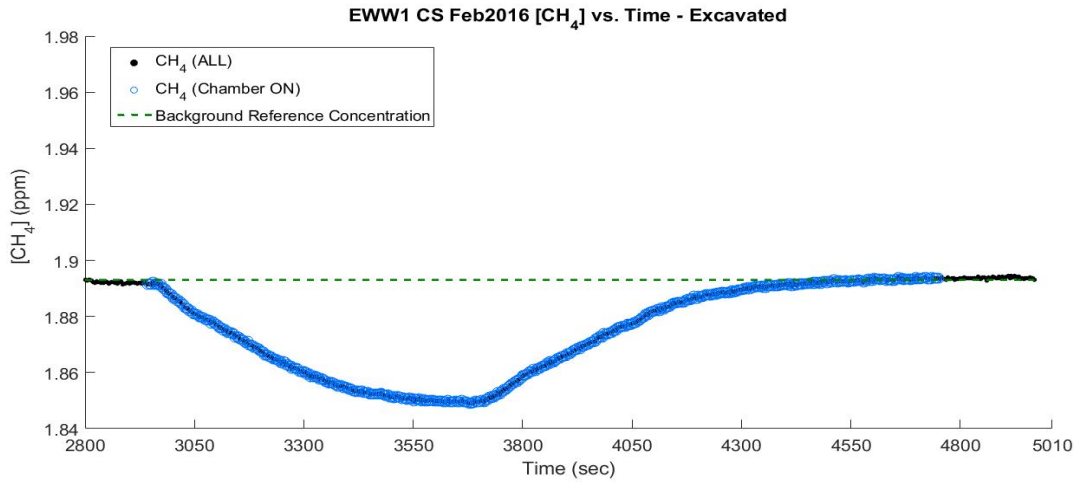

(B)

FIGURE 5.11: [CH_4] vs. time profile for EWW1 CS for both the unexcavated (A) and the excavated (B) treatments.

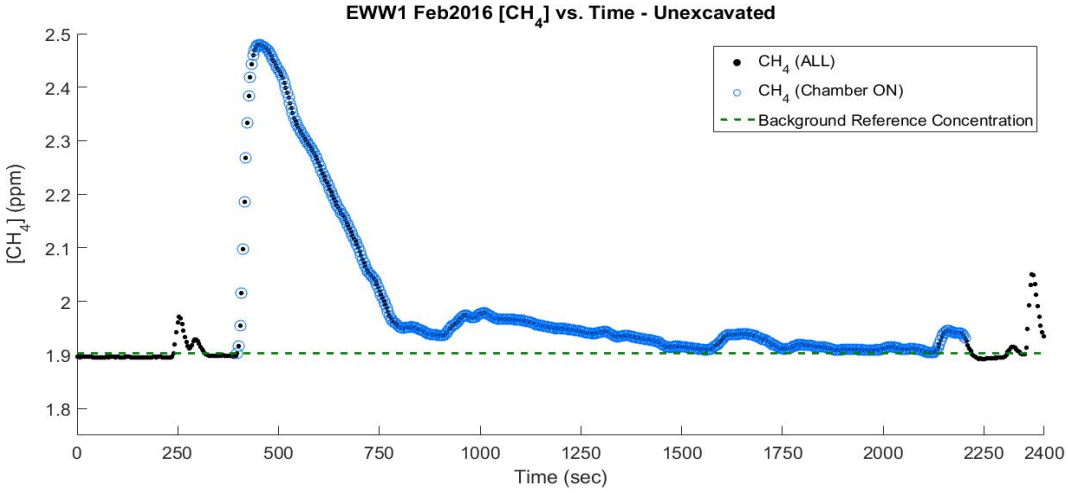

(A)

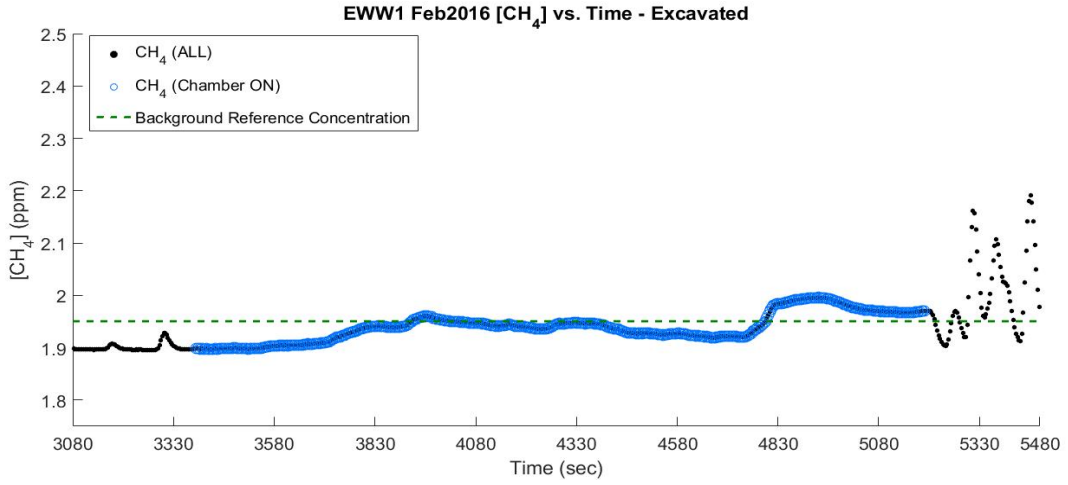

(B)

FIGURE 5.12: $[CH_4]$ vs. time profile for EWW1 for both the unexcavated (A) and the excavated (B) treatments.

profiles, the CO_2 profiles show a far greater range in the $[CO_2]$ for the excavated treatment relative to the unexcavated treatment.

The CO_2 profiles for EWW1 CS, were not too dissimilar in the $[CO_2]$ range but the shape of the profiles were different. The CO_2 in the unexcavated treatment was emitted at a linear rate without interruption (Figure 5.16A). However, the profile for the excavated treatment increased to maximum $[CO_2]$ of 868 ppm in the first 700 seconds and remained steady at that concentration for the remainder of the closed measuring period (Figure 5.16B).

At EWW1, the CO_2 profiles for both treatments were the most unique among all measured CO_2 profiles. The $[CO_2]$ ranges for the unexcavated (314 ppm) and excavated (318 ppm) treatments were similar. However, visual inspection of the two graphs (Figure 5.17) shows a rough and jerky

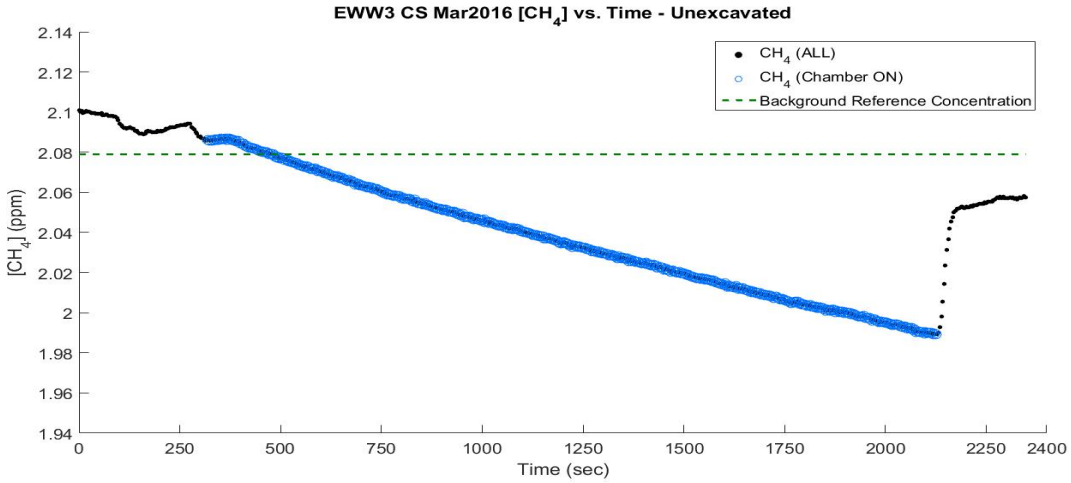

FIGURE 5.13: [CH_4] vs. Time for the EWW3 CS site. Only unexcavated measurements were made at this site.

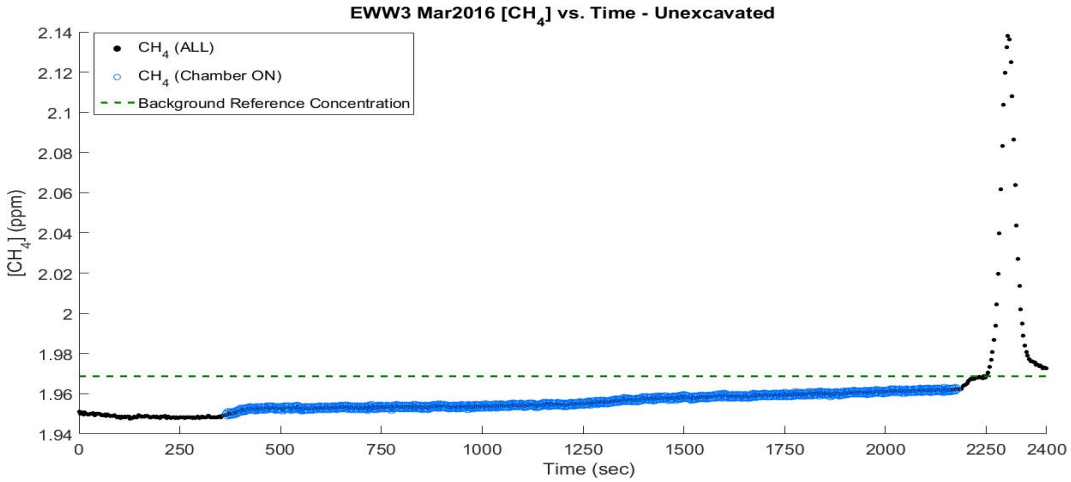

FIGURE 5.14: [CH_4] vs. Time for the EWW3 CS site. Only unexcavated measurements were made at this site.

profile over the entire course of the measuring period, which is highly irregular with respect to all measured profiles regardless of gas or treatment.

5.1.6 Methane Flux Results Summary: Fall & Winter

Using the CH_4 profiles, the initial flux was calculated as per the description in the "Research Methods section (Equation 4.1). The results of these initial fluxes are presented in Tables 5.6-5.7.

Initial flux estimates for test and control sites are presented in Table 5.8. A paired difference two tailed t-test analysis demonstrates no significant difference between test and control sites ($p = 0.272$). However, the power of the performed t-test was 0.16, which is far lower than the desired

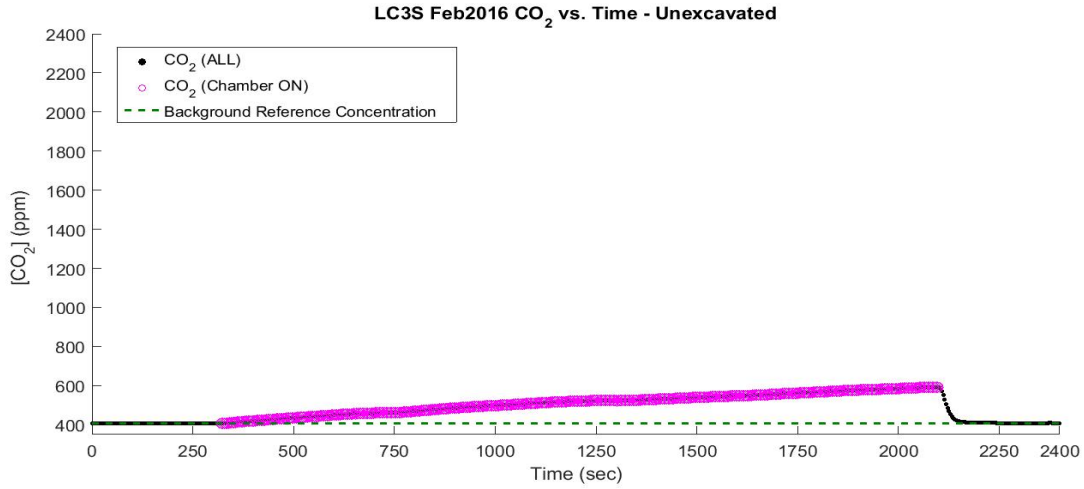

(A)

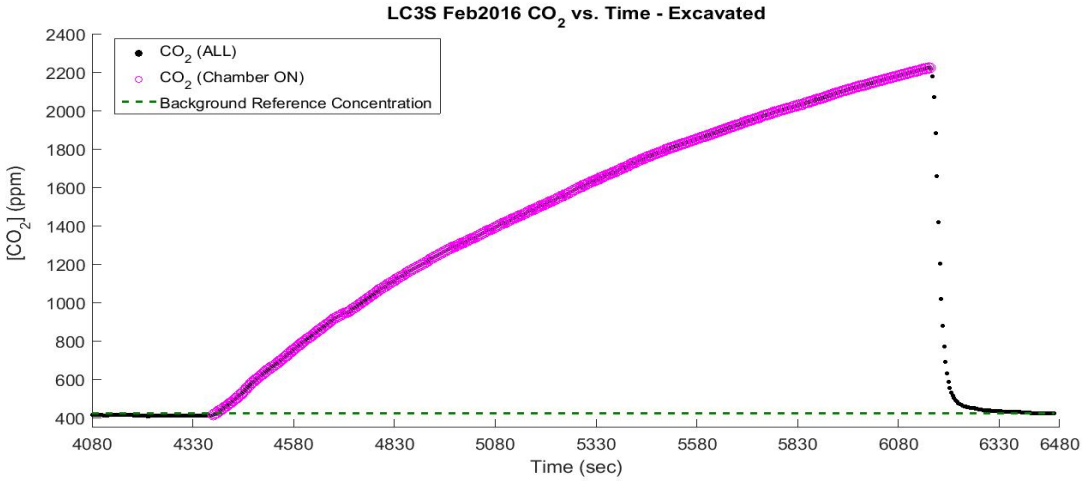

(B)

FIGURE 5.15: $[CO_2]$ vs. Time profiles at the LC3S location. X- and y-axis have been scaled identically to provide an easier comparison between the unexcavated profile (A) and the excavated profile (B).

power of 0.80. Using this data, the number of samples needed to provide a t-test with the desired power is 79 test-control pairs.

5.2 Objective 2: Quantify the Isotopic Composition of CH_4

5.2.1 Fall Measurements: Keeling Plots

The second objective of this study was to collect isotopic data for the CH_4 and CO_2 escaping from the soil. The isotopic data is used to identify the source of the escaped gas by plotting the inverse

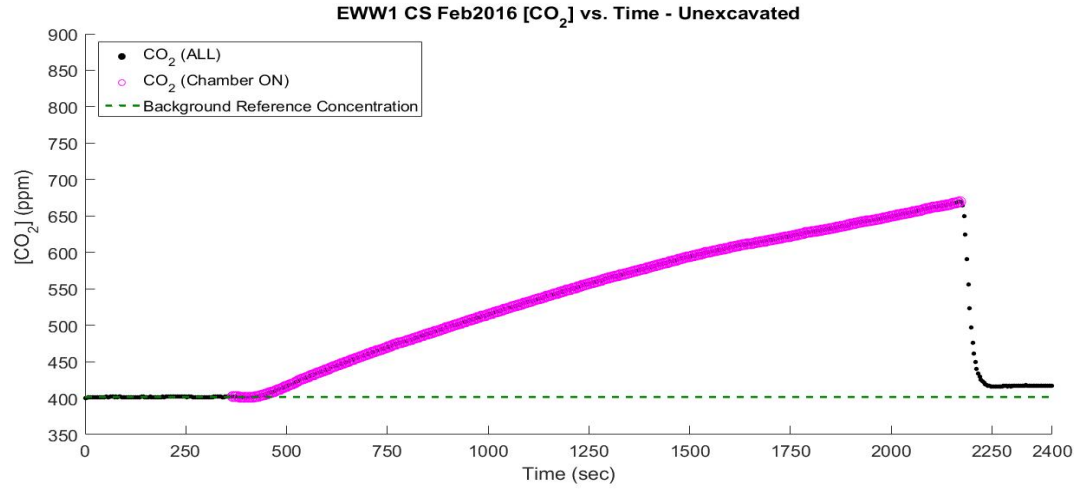

(A)

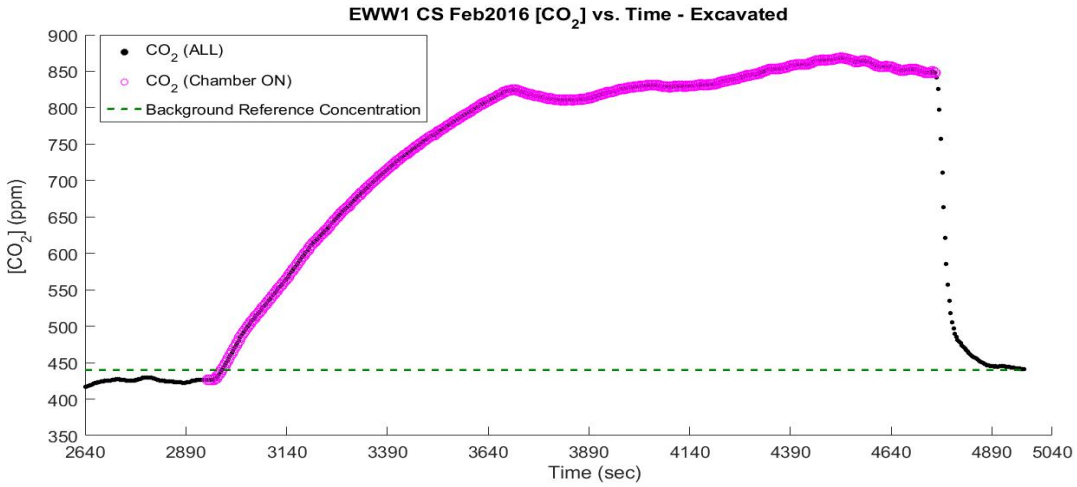

(B)

FIGURE 5.16: $[CO_2]$ vs. time profiles at the EWW1 CS location, where the unexcavated profile is (A) and the excavated profile (B).

concentration of the gas versus the stable carbon isotope composition. As described in detail in the "Research Materials and Methods section, this relationship is known as a Keeling plot. Fitting a least squares linear regression to the data yields a y-intercept value for $\delta^{13}C$ that is used to identify the source using known ranges of various sources (Table 5.9).

The $\delta^{13}C$ of the CH_4 source (y-intercepts) for the control plots demonstrated mixed results. For WMCS, BHCS (DAY), and BHCS (NIGHT), the y-intercepts were $-346 \pm 431‰$, $-28 \pm 54‰$, and $-59 \pm 53‰$ (uncertainty represents a 95% confidence interval), respectively. The large uncertainties in the values of the y-intercepts and the impossibly low value for WMCS make comparisons with known source isotopic composition ranges (Table 5.9) inconclusive.

At the test site LC3S the $\delta^{13}C$ of the CH_4 source was $-45 \pm 18‰$ (Figure 5.19). Though this value is

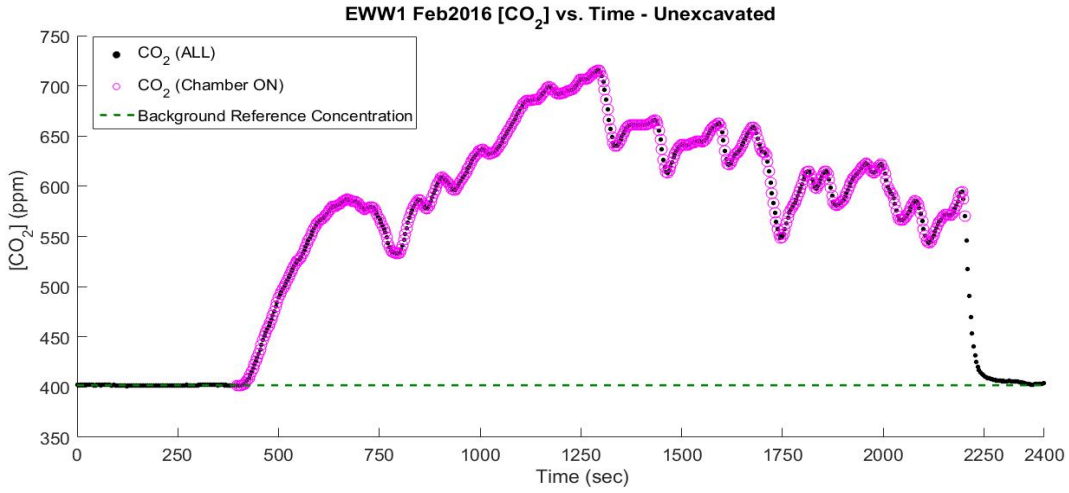

(A)

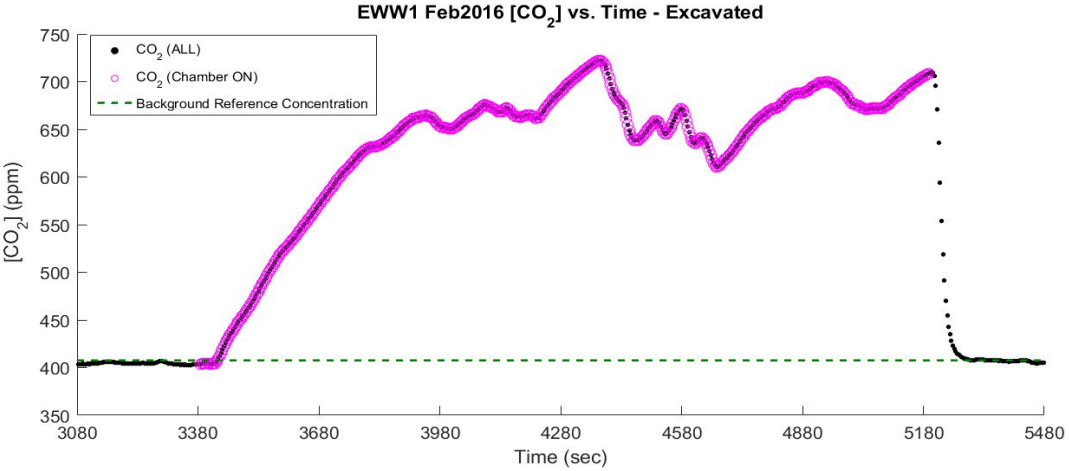

(B)

FIGURE 5.17: $[CO_2]$ vs. time profiles at the EWW1 location, where the unexcavated treatment is shown (A) and the excavated treatment shown in (B).

within the thermogenic zone, the confidence interval is too large to be confined solely within the thermogenic zone (Table 5.9).

5.2.2 Winter Measurements: Keeling Plots

The measurements made during the winter session produced Keeling plots for both unexcavated and excavated treatments for LC3S, EWW1, and EWW1 CS; for the measurements conducted at EWW3 and EWW3 CS, only the unexcavated treatment was measured.

For test site LC3S, the results for the Keeling plot measurements were in stark contrast between the two treatments (Figure 5.20). The unexcavated measurements produced a value of $+95 \pm 143‰$

TABLE 5.6: *Initial flux results of CH_4 for control and test sites during both sessions.

Location	Season	Initial Flux ($F_0, \mu g\, m^{-3}\, s^{-1}$) [UnEx]	Initial Flux ($F_0, \mu g\, m^{-3}\, s^{-1}$) [Ex]
WMCS	Oct 2015	-1.8E-04 $\pm$ 1.3E-04	Not measured
BHCS (DAY)	Oct 2015	-1.6E-03 $\pm$ 1.6E-04	Not measured
BHCS (NIGHT)	Oct 2015	-2.0E-03 $\pm$ 1.4E-04	Not measured
LC3S Oct2015	Oct 2015	+2E-01 $\pm$ 1E-01	Not measured
LC3S Feb2016	Feb 2016	+1.0E-03 $\pm$ 2.7E-04	+2.7E-02 $\pm$ 5.3E-04
EWW1 CS	Feb 2016	+3.1E-04 $\pm$ 1.4E-04	-1.1E-02 $\pm$ 1.8E-04
EWW1	Feb 2016	Measurements were not meaningful	Measurements were not meaningful
EWW3 CS	Mar 2016	-8.6E-04 $\pm$ 1.7E-04	Not measured
EWW3	Mar 2016	+2.2E-04 $\pm$ 1.4E-04	Not measured

*For LC3S Oct 2015, only Leg01 was reported in the table. Leg 02 was measured to be -1.6E03.

TABLE 5.7: *Test-control pairs for measurements of CH_4 initial flux for both seasons.

Location	Control ($\mu g\, m^{-3}\, s^{-1}$)	Test ($\mu g\, m^{-3}\, s^{-1}$)
LC3S Oct2015 (Unexcavated)	-1.3E-03 $\pm$ 9.7E-04	+1.9E-01 $\pm$ 1.3E-01
LC3S Feb2016 (Unexcavated)	+3.1E-04 $\pm$ 1.4E-04	+1.0E-03 $\pm$ 2.7E-04
LC3S Feb2016 (Excavated)	-1.1E-03 $\pm$ 1.8E-04	+2.7E-02 $\pm$ 5.3E-04
EWW3 (Unexcavated)	-8.6E-03 $\pm$ 1.7E-04	+2.2E-04 $\pm$ 1.4E-04

*The control site paired with LC3S Oct2015 is an average of WMCS, BHCS (DAY), and BHCS (NIGHT). A control site for LC3S Feb2016 was not measured due to logistical reasons; therefore, the test site was paired with EWW1 CS.

TABLE 5.8: Initial flux results of CO_2 for control and test sites during both sessions.

Location	Season	Initial Flux ($F_0, \mu g\, m^{-3}\, s^{-1}$) [UnEx]	Initial Flux ($F_0, \mu g\, m^{-3}\, s^{-1}$) [Ex]
WMCS	Oct 2015	+4.2E+01 $\pm$ 3.8E-01	Not measured
BHCS (DAY)	Oct 2015	+8.7E+01 $\pm$ 3.1E-01	Not measured
BHCS (NIGHT)	Oct 2015	+6.9E+01 $\pm$ 3.8E-01	Not measured
LC3S Oct2015	Oct 2015	+2.1E+01 $\pm$ 4.9E-02	Not measured
LC3S Feb2016	Feb 2016	+1.8E+01 $\pm$ 8.8E-02	+2.2E+02 $\pm$ 2.2E00
EWW1 CS	Feb 2016	+2.7E+01 $\pm$ 2.2E-01	+8.5E+01 $\pm$ 6.0E-01
EWW1	Feb 2016	Measurements were not meaningful	Measurements were not meaningful
EWW3 CS	Mar 2016	+8.2E+01 $\pm$ 6.6E-01	Not measured
EWW3	Mar 2016	+4.5E+01 $\pm$ 5.2E-01	Not measured

for the δ^{13}C-CH_4 intercept, whereas, the δ^{13}C-CH_4 intercept for the excavated measurement was $-38 \pm 10‰$ (Table 5.10). The result of the excavated measurement is important as the isotopic

TABLE 5.9: Stable carbon isotopic composition ranges for classification of CH_4 sources.

Classification of Source	Stable Carbon Isotope Range (δ^{13}C, ‰)
Biogenic	Between -110 and -60
Mixed	Between -60 and -50
Thermogenic	Between -50 and -25

composition (including its confidence levels) falls within the thermogenic zone (Figure 5.26). Furthermore, Figure 20 depicts δ^{13}C data for CH_4 and CO_2 measured in unexcavated and excavated experiments at LC3S.

At EWW1 CS, the δ^{13}C-CH_4 intercept for the unexcavated treatment was $+76 \pm 159‰$ and the excavated treatment was $-89 \pm 26‰$. When the confidence intervals are taken into account, the δ^{13}C-CH_4 intercept for the excavated treatment lies within the biogenic zone (Table 5.10, Figure 5.26).

For test site EWW1, the Keeling plots highlight similar δ^{13}C-CH_4 intercepts, $-39 \pm 3‰$ and $-36 \pm 16‰$, for the unexcavated and the excavated treatments, respectively (Figure 5.22). Measurements at this site across both treatments are within the thermogenic zone (Table 5.10, Figure 5.26). In comparison to the excavated treatment at the control site, the δ^{13}C-CH_4 composition of the source at the test site is more enriched in ^{13}C signaling the presence of CH_4 from a thermogenic source.

The δ^{13}C-CH_4 intercepts for the control site provided a value that corresponded with a biogenic signature, and the test sites at EWW3 had very large uncertainties, making source classification inconclusive (Figure 5.24). Only unexcavated measurements were conducted at these sites, where the control, EWW3 CS, presented a δ^{13}C-CH_4 composition of $-62 \pm 13‰$ and for the test site, EWW3, $+15 \pm 128‰$ (Figure 5.25).

TABLE 5.10: Summary of δ^{13}-CH_4 compositions for sources measured at all control and test sites. Values within the parenthetical indicate the range of the 95% confidence interval.

Location	Unexcavated (‰)	Excavated (‰)	Classification of Source	
WMCS	-346 (-777, -85)	Not measured	Mixed (Unexcavated)	N/A
BHCS (DAY)	-28 (-82, +26)	Not measured	Mixed (Unexcavated)	N/A
BHCS (NIGHT)	-59 (-113, -5)	Not measured	Mixed (Unexcavated)	N/A
LC3S Oct2015	-46 (-63, -28)	Not Measured	Mixed (Unexcavated)	N/A
LC3S Feb2016	+95 (-49, +239)	-38 (-48, -29)	Mixed (Unexcavated)	Thermogenic (Excavated)
EWW1 CS	+76 (-83, +235)	-89 (-115, -64)	Mixed (Unexcavated)	Biogenic (Excavated)
EWW1	-39 (-42, -36)	-36 (-52, -20)	Thermogenic (Unexcavated)	Thermogenic (Excavated)
EWW3 CS	-62 (-77, -49)	Not measured	Biogenic (Unexcavated)	N/A
EWW3	+15 (-114, +143)	Not measured	Mixed (Unexcavated)	N/A

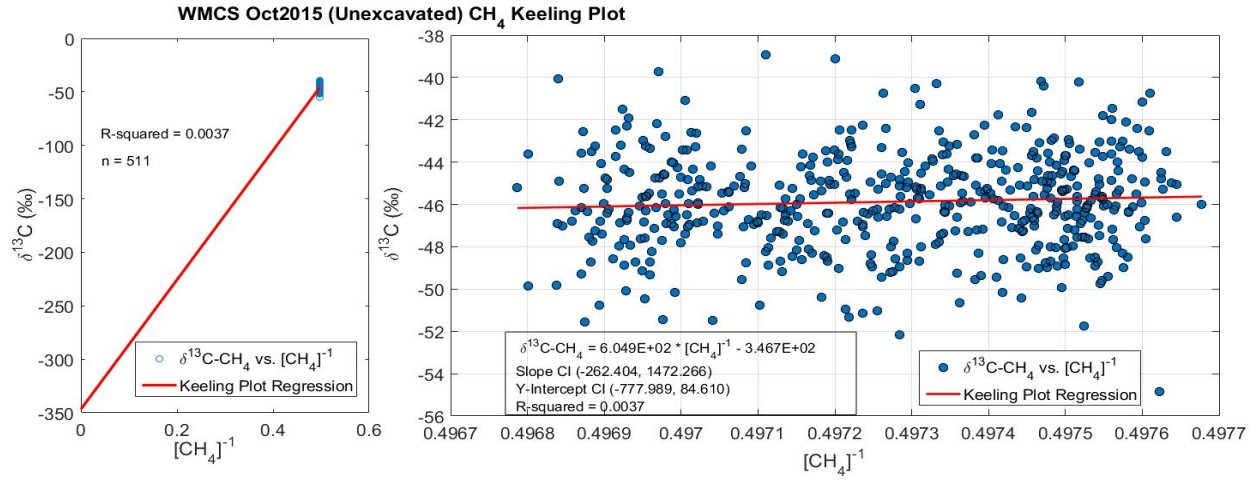

(A)

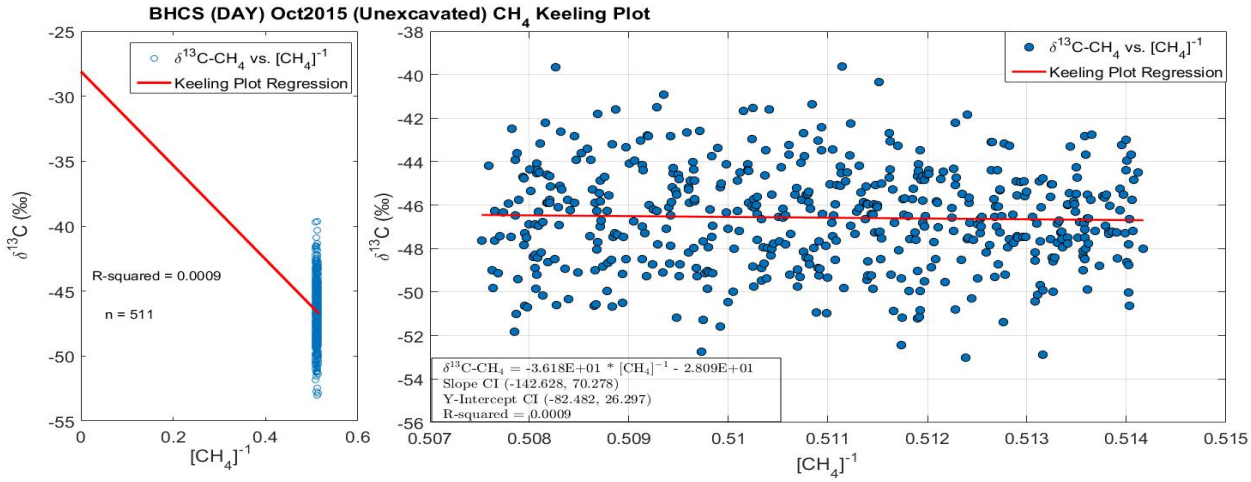

(B)

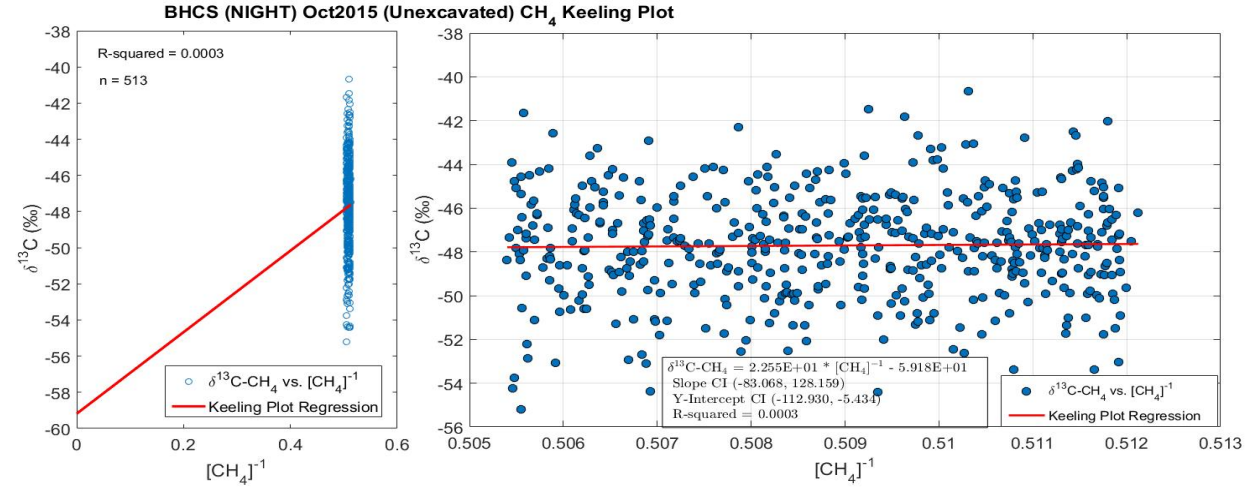

(C)

FIGURE 5.18: Keeling plots for the control sites during the fall measurement session, presented, from top to bottom, WMCS, BHCS (DAY), and BHCS (NIGHT). The left panel shows a full view of the data in which the regression is allowed to extend to the point where the regression crosses the y-axis (y-intercept) at $x = 0$. The right panel is a close-up view of the data.

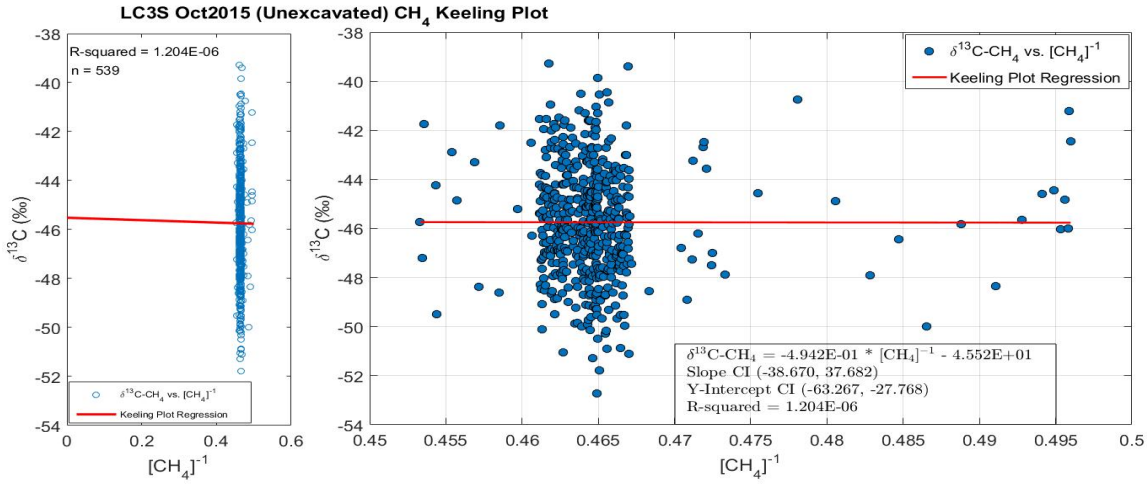

FIGURE 5.19: Keeling plot for the test site during the fall measurement session, LC3S.

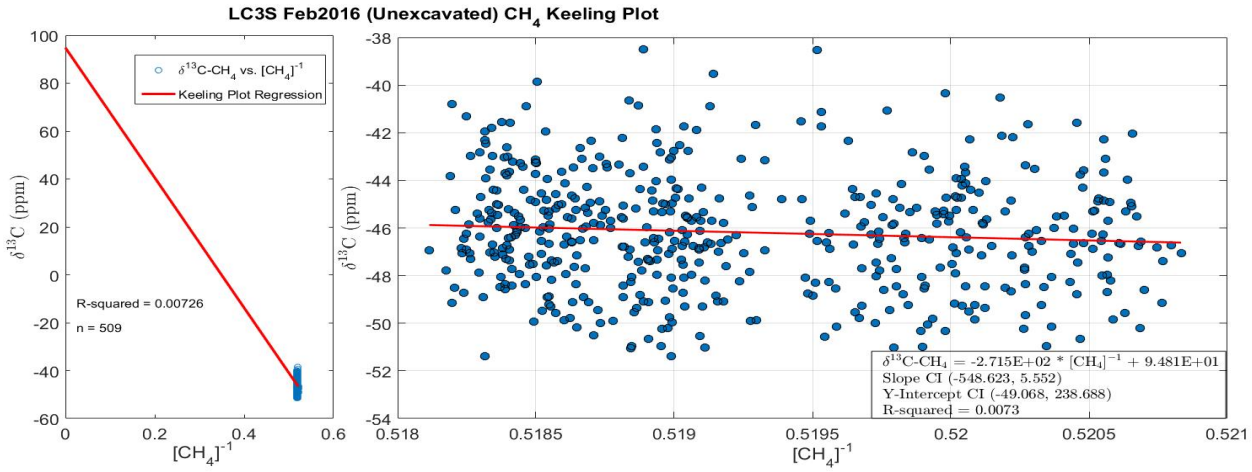

(A)

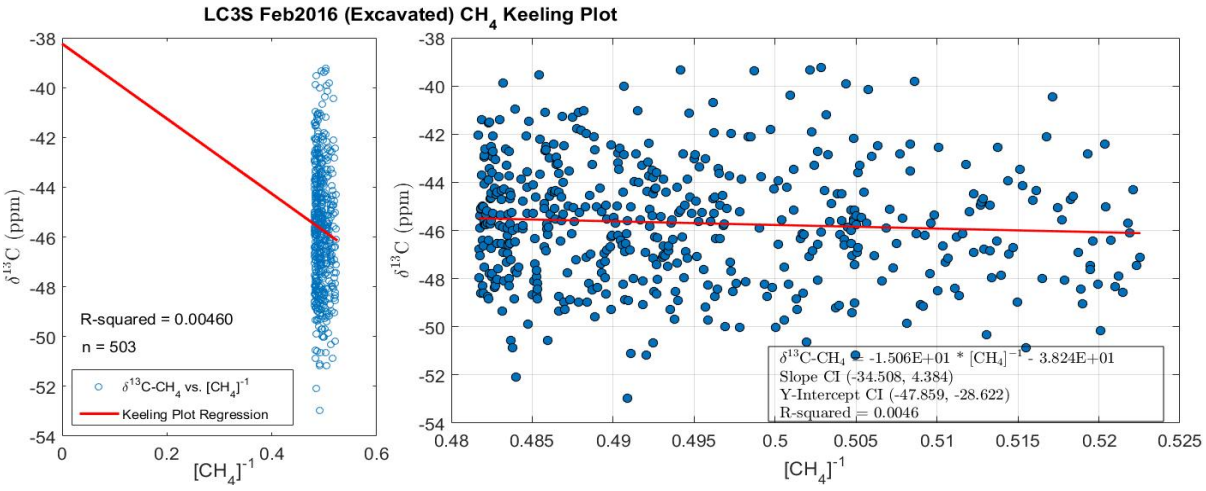

(B)

FIGURE 5.20: Keeling plots for winter measurements at LC3S, where the unexcavated treatment is (A) and the excavated treatment (B).

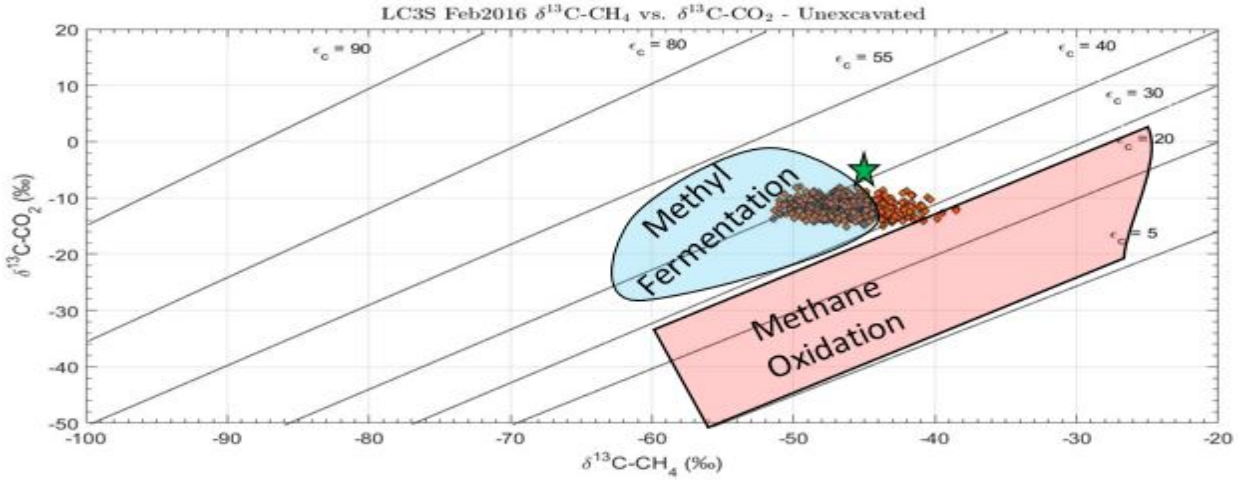

(A)

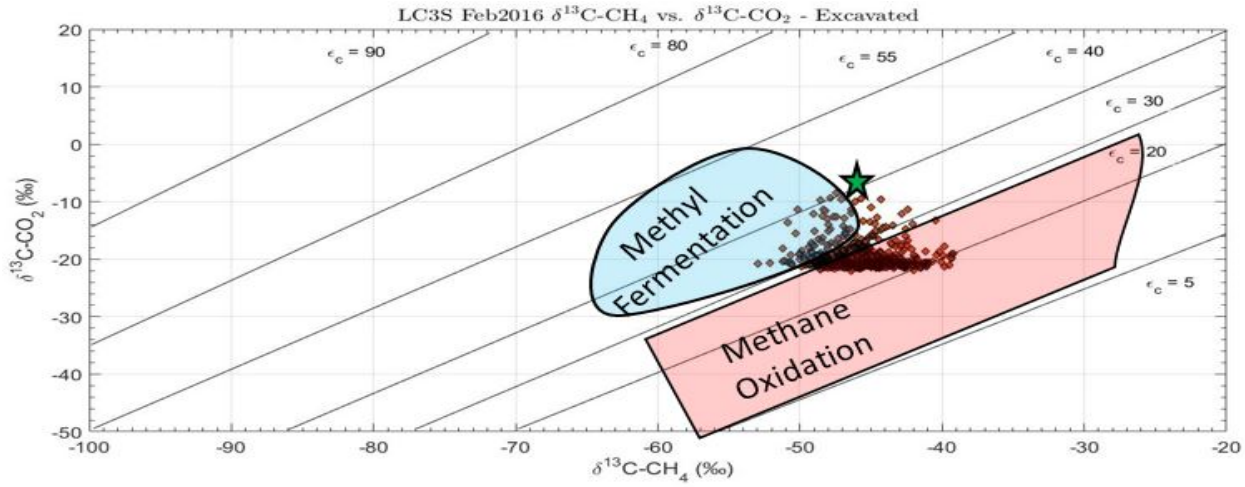

(B)

FIGURE 5.21: δ^{13}C isotopic results at test site LC3S for both CH_4 and CO_2, where the unexcavated measurements are presented in (A) and the excavated treatments is presented in (B). The green star represents the approximate composition of the atmosphere.

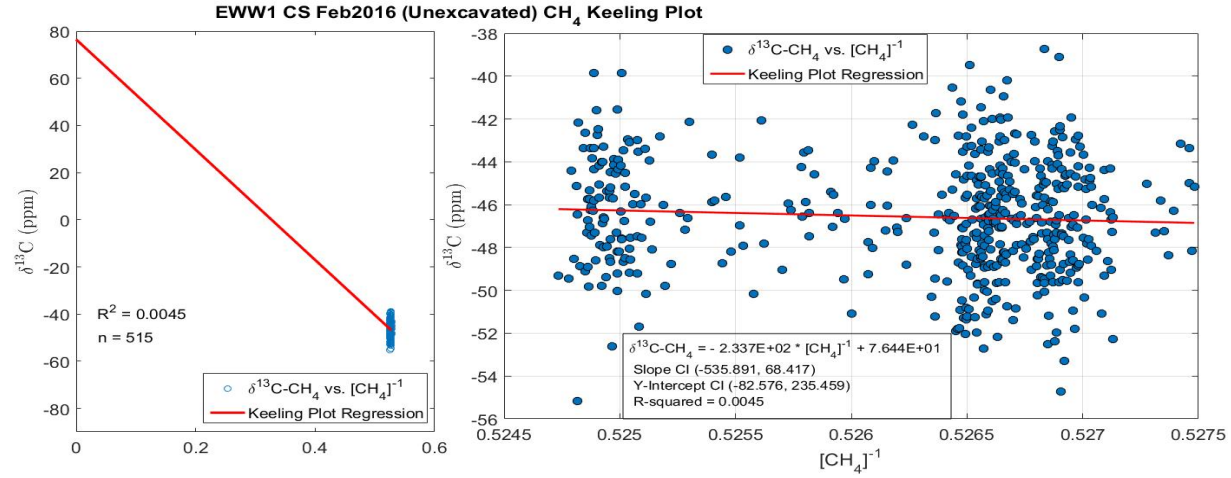

(A)

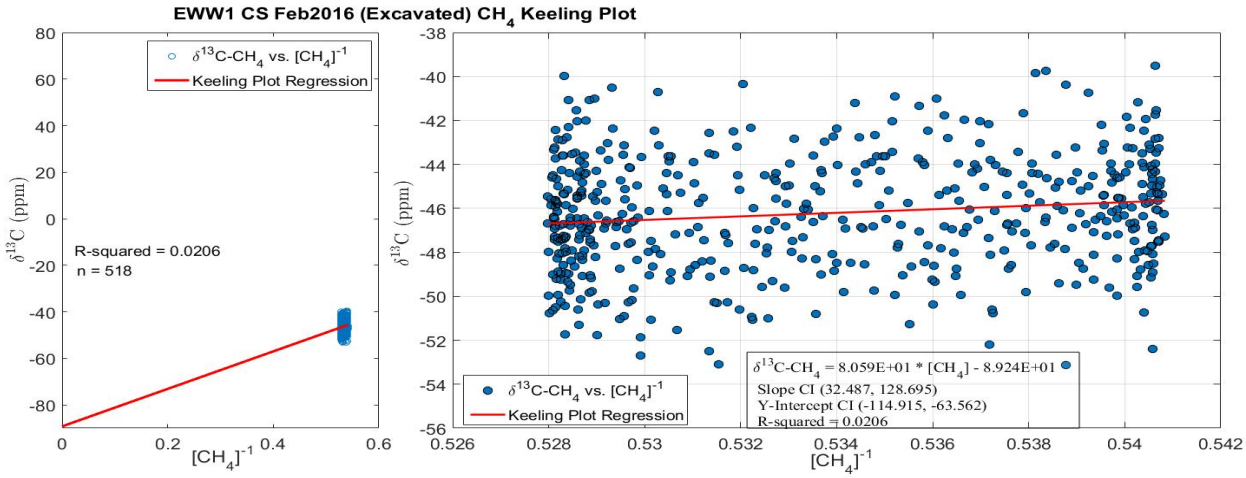

(B)

FIGURE 5.22: Keeling plots for the control site, EWW1 CS, showing the unexcavated treatment on top and the excavated treatment on bottom.

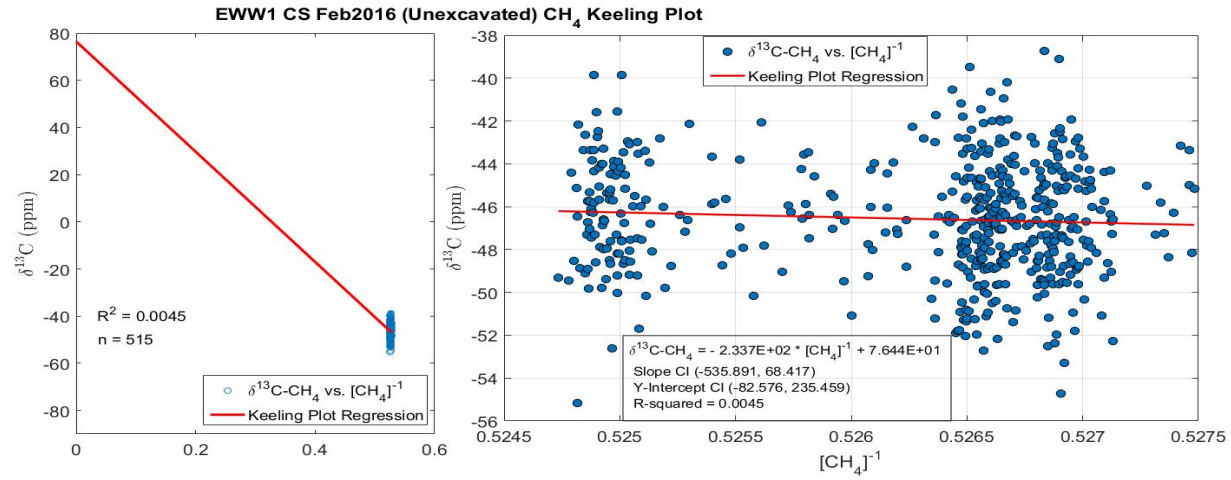

(A)

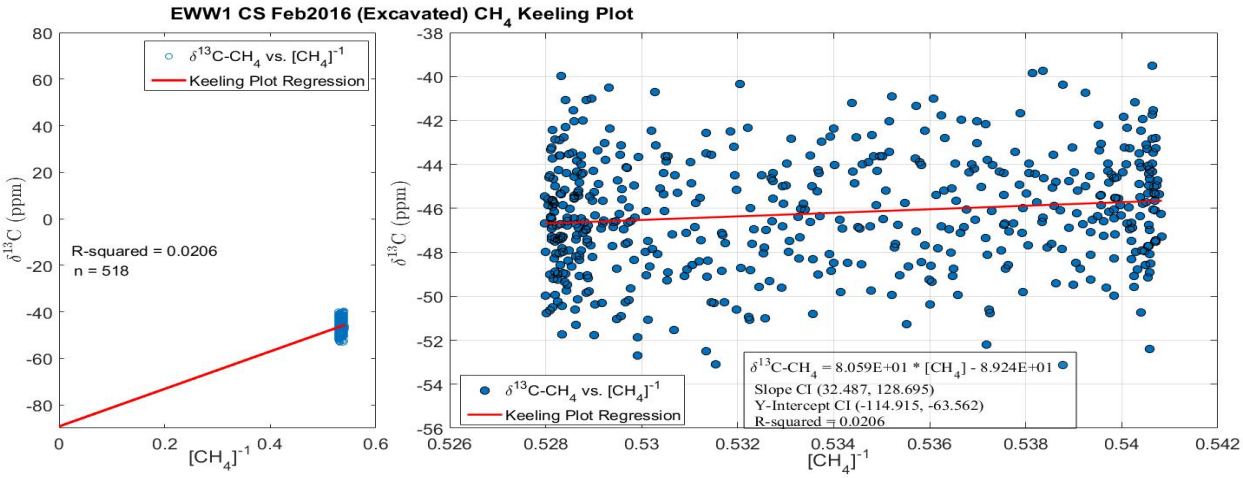

(B)

FIGURE 5.23: Keeling plots for the control site, EWW1 CS, showing the unexcavated treatment on top and the excavated treatment on bottom.

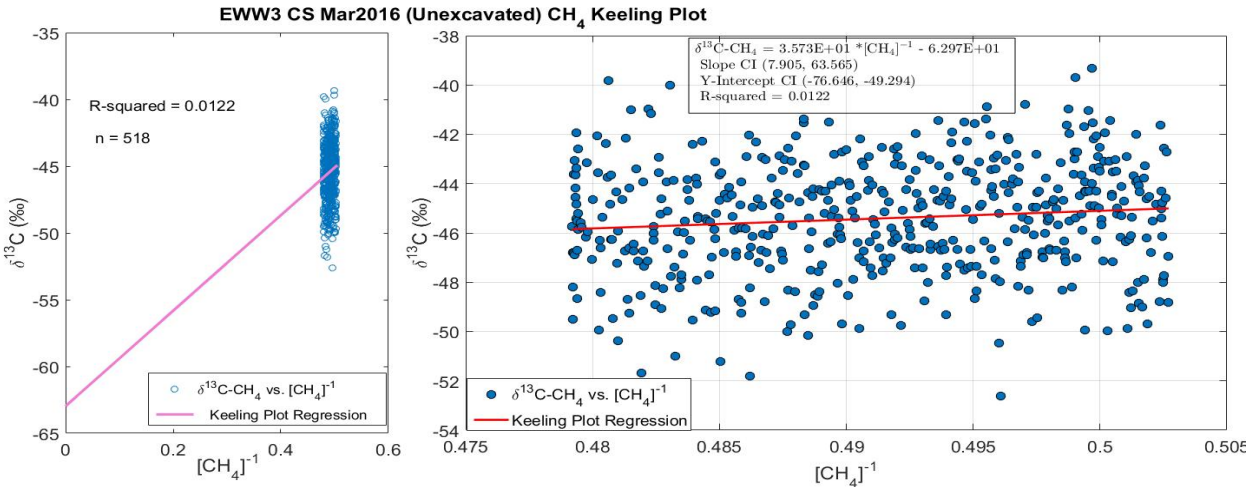

FIGURE 5.24: Keeling plot for control site, EWW3 CS. Measurements reflect an unexcavated treatment.

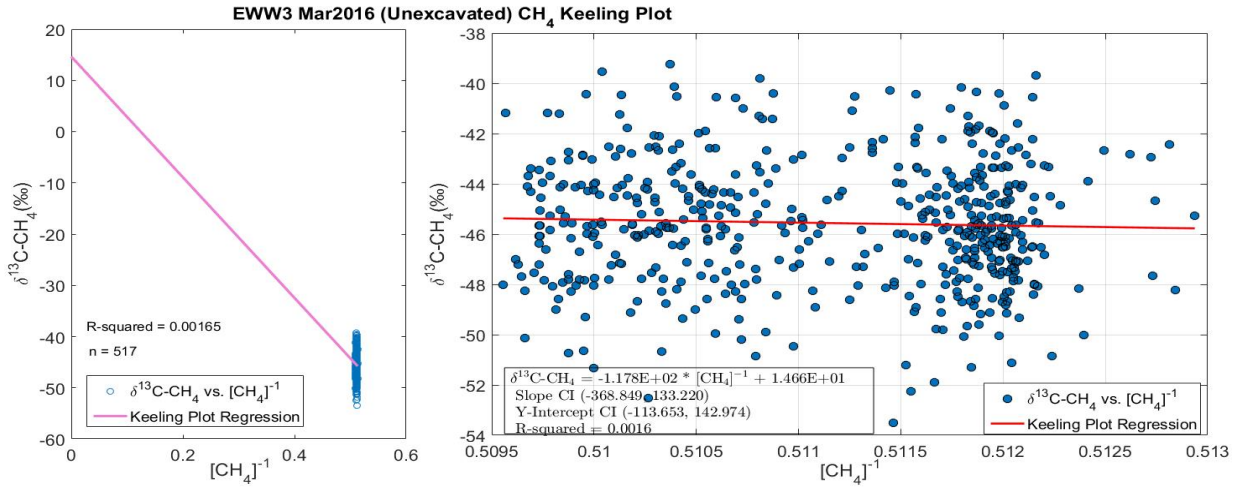

FIGURE 5.25: Keeling plot for test site, EWW3. Measurements reflect an unexcavated treatment.

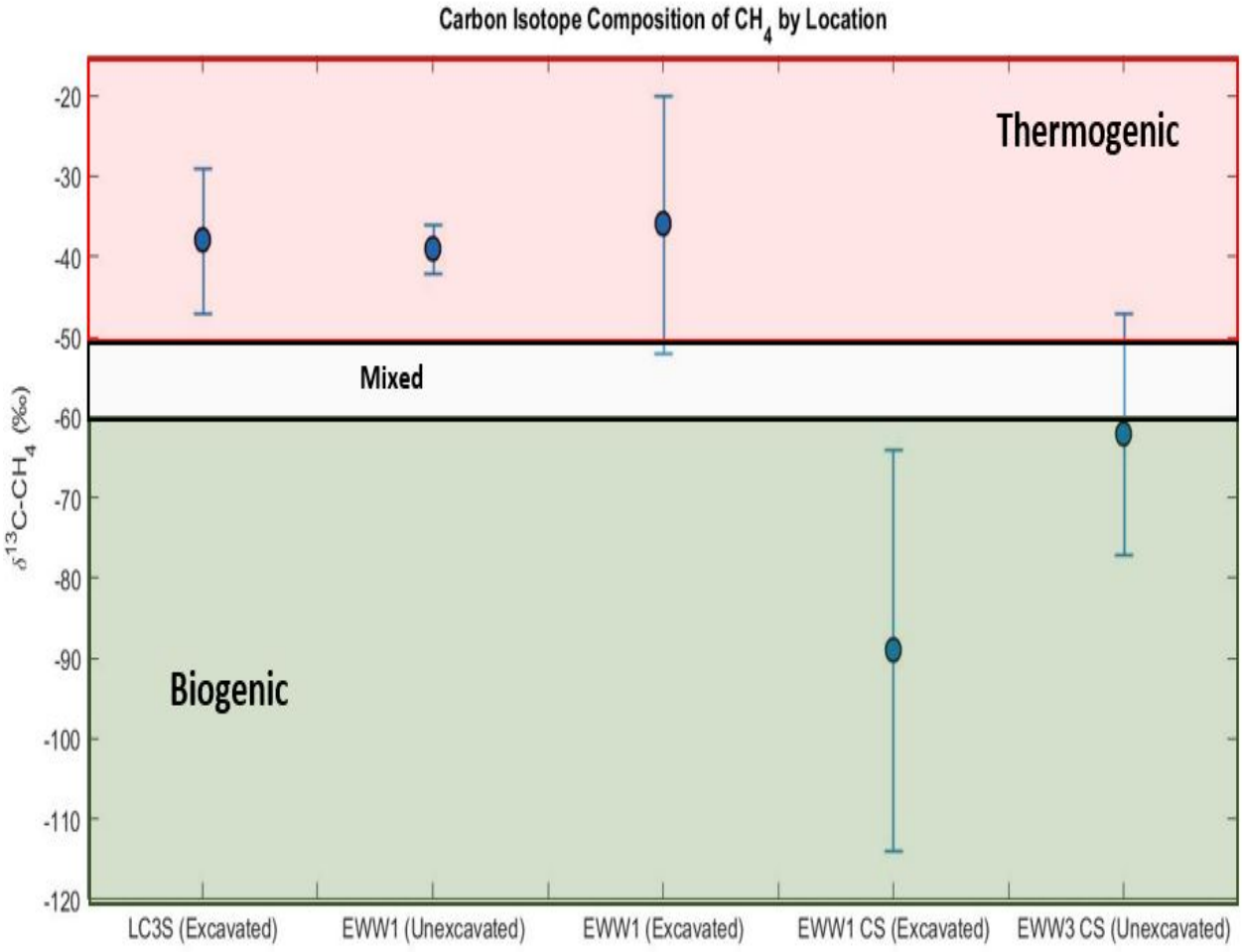

FIGURE 5.26: Stable carbon isotope compositions by location. Only the conclusive signatures are presented.

Chapter 6

Discussion

6.1 Fall Measurements: Concentrations & Fluxes

Due to the presence of microbes in the soil, it was important to better understand whether a diurnal cycle had an effect on the microbial activity. At the BHCS location, the DAY and NIGHT treatments exhibited similar CH_4 fluxes (Table 5.2). Furthermore, a paired difference t-test demonstrated that the two treatments were not significantly different. These results lead to the conclusion that diurnal changes in the activity of methanotrophs are insignificant, which reduces concern for making the majority of measurements during daytime hours.

The concentration-time profiles for all of the CH_4 measurements were telling of methanotrophic behavior. Each of the profiles, excluding Leg 01 LC3S, exhibited a negative slope, thus indicating consumption of atmospheric CH_4 over time. Generally, methanotrophic activity is common in warm and well drained soils. As a result, CH_4 fluxes in temperate forests are generally negative (Topp and Pattey, 1997). Both the control and test sites recorded warm temperatures and were moderately drained. These factors, particularly the temperature, contributed to the methanotrophic activity.

Flux estimates reinforce the presence of methanotrophy and provide details about site to site variation (Table 5.9). The control sites WMCS and BHCS (both DAY and NIGHT) had negative fluxes, but the flux was an order of magnitude lower for WMCS (Table 06). This may have been due to the light rainfall during measurement of WMCS and the soil temperature was slightly lower than at BHCS (Table 02).

However, the most important finding is the differences in flux results between the control and test sites. The positive flux measurement (Leg 01) at LC3S was two order of magnitudes greater than at BHCS and three orders of magnitude greater than at WMCS. But this positive flux only lasted 130 seconds, and was followed by a negative flux indicative of methanotrophic behavior (Leg 02). In comparison, $[CH_4]$ observed at the control sites decreased steadily from the time at which the chamber closed until the chamber was reopened. One reason for the large CH_4 flux for Leg 01 could be a macropore. A macropore enhances the flux by acting as both a reservoir

and as a conduit for gas to escape from the subsurface to the atmosphere. The explanation of the delayed methanotrophic activity in Leg 02 after the initial positive flux is explained through the idea of equilibration. Methanotrophy was activated after the CH_4 saturated the headspace of the chamber and thus provided the methanotrophs an opportunity to consume CH_4 escaping from the soil.

The first conclusion that can be drawn from the fall session CH_4 flux measurements is that there is definitely an excess of methane at the test site relative to the control sites. This excess is evidenced by both the greater background [CH_4] (Figure 5.3) and the greater initial CH_4 initial flux (Table 5.6) measured at the test site relative to the control sites. The positive flux at LC3S indicates that methanotrophy can falter or be delayed, thus permitting gas to escape from the soil into the atmosphere. This delayed reaction by the methanotrophs was clearly exhibited at the LC3S location through Leg 01.

Measured [CO_2] demonstrated a greater range at the control sites than the test site. Furthermore, the CO_2 fluxes for control sites were two to four times higher than the test site (Table 5.3). These observations support the idea that there is an excess amount of CH_4 in the soil at the test site that is not consumed and transformed into CO_2. Instead, the CH_4 escapes and thus the amount of CO_2 is relatively lower at the test site compared to the control sites. On the other hand, higher soil [CO_2] at the control sites may result from higher organic carbon content (mean %C = 2.86) than at the test site (1.90 %C). A greater amount of organic material in the soil would result in more microbial and root respiration, thus increasing the amount of CO_2 measured in the soil.

6.2 Winter Measuurements: Concentration Profiles & Fluxes

The concentration-time profiles for LC3S unexcavated and excavated experiments were very different (Figure 5.10). The excavated treatment showed a range (0.16 ppm) in [CH_4] that was an order of magnitude greater than the unexcavated treatment (0.01 ppm). Due to the fact that the majority of methanotrophic reactions require O_2, the distance from the soil-atmosphere interface at which the measurement takes place is important. In the excavated treatment taking place 30 cm beneath the original ground surface, where there was likely less O_2 and thus less methanotrophic activity, resulting in higher measured [CH_4].

Dissimilar results were also found between the unexcavated and excavated treatments at EWW1 and EWW1 CS. However, the concentration-time profiles are irregular (Figures 5.11-12), making interpretations more uncertain. The difficulty in interpreting the [CH_4]-time profiles at EWW1 may be due to the rocky soil matrix where the measurements took place. When soil is homogeneous, permeable and fine-grained, chamber concentration-time profiles show a high initial slope (flux) that gradually decreases to zero as the saturation concentration is reached (e.g. Figure 5.14 for CO_2). The soil at EWW1 was heterogeneous, consisting of clasts 2-6 cm in length contained

within a finer-grained matrix. This textural heterogeneity would increase spatial variability in permeability, biological activity, and fluxes. The resulting [CH_4]-time profiles were too irregular to glean useful information on the effects of methanogenesis and/or methanotrophy.

For the control versus test site comparison of the [CH_4] for the excavated treatments at EWW1, the primary expectation that could be made is a greater [CH_4] and flux would be measured at the test site due to subsurface leakage from the well. The data agreed with the first expectation in that the mean concentration of [CH_4] at the test site is 1.94 ± 0.03 ppm, whereas the mean at the control site is 1.87 ± 0.02 ppm. The data for EWW1 also suggests an agreement with the second expectation in that the test site showed a small positive initial slope, but the control site showed a negative slope, causing [CH_4] to decrease before recovering to the background value.

The unusual concentration-time profile observed at the EWW1 test site made the flux estimate meaningless. At the control site, EWW1 CS, the flux results showed a small positive flux (3.1E-04 $\pm$ 1.4E-04 μg m^{-2} s^{-1}) for the unexcavated treatment and a flux (-1.1E-02 $\pm$ 1.8E-04 μg m^{-2} s^{-1}), two orders of magnitude greater, but negative for the excavated treatment. These results at first glance indicate that the positive flux in the unexcavated treatment was caused by methanogenesis, and the negative flux in the excavated treatment by methanotrophy. But on closer inspection, the small positive flux (3.1E-04 $\pm$ 1.4E-04 μg m^{-2} s^{-1}) for the unexcavated measurement does not provide a great deal of confidence in concluding methanogenesis. The small flux and the addition of the large spikes (likely due to the enteric fermentation from the cows surrounding the field site) of background CH_4 detracts from methanogenesis. Furthermore, the negative flux for the excavated treatment only persists for 500 of the 2100 (24%) seconds of the closed-chamber portion of the measurement before returning to background. This non-continuous behavior detracts from producing a confident conclusion of methanotrophy. In the end, addressing the CH_4 measurements in the context of microbial activity is inconclusive based on the presented data.

Due to the fact that LC3S lacked a geologic-specific control and EWW1 lacked useable flux values, EWW1 CS was used as the control site for LC3S. In evaluating the fluxes, it is first important to note that the excavated flux for LC3S was an order of magnitude greater than the unexcavated treatment (Table 5.6). Removal of methanogens in the top 30 cm of soil explains this result. Flux values are one order of magnitude greater for the test site LC3S than for the control site EWW1 CS for each respective treatment (Table 5.6). This result demonstrates that the rate of emissions at the test site is greater than at the control site, in which the difference can be presented as conceivably connected with HVHF activity.

There were no excavated measurements made at the EWW3 site, but the differences observed between unexcavated treatments at the test and control sites are worth discussion (Figure 5.13). The test site showed an increase in [CH_4] of 0.01 ppm over time, whereas the control site showed a larger (0.1 ppm) decrease in [CH_4] over time . This decrease in [CH4] exemplifies the presence

of methanotrophic activity at the control site. It is also important to consider that the mean background [CH_4] was greater at the control site (2.04 $\pm$ 0.03 ppm) than at the test site (1.96 0.003 ppm). The greater background concentration of CH_4 at the control site may have resulted from the observed decomposing deer carcasses and deer fecal matter. From the concentration profiles, the CH_4 flux magnitude was 10 times lower at the test site than the control site (Table 5.2). The large negative flux at the control site likely was due to greater methanotrophic activity. In the end, it can be stated for EWW3 that the test site showed a positive flux of methane from the subsurface into the atmosphere, but the flux magnitude was an order of magnitude less than the flux of methane from the atmosphere into the subsurface at the control site.

6.3 Fall Measurements: Stable Carbon Isotope Analysis

Keeling plots served as the primary tool for analyzing the δ^{13}C data. In using a Keeling plot, two assumptions are made: 1) the observed gas is a mixture of background (i.e. atmospheric) and soil gases, and 2) the isotopic compositions of the two endmembers are static. Due to the fact that a Keeling plot compares the isotopic composition of the measured species versus the inverse concentration with a least squares regression, one can expect the first assumption to hold true because the isotopic compositions of the two endmembers would not change during the course of the measurement. The second assumption was not likely violated due to the fact that spatial coverage at site was very limited and the δ^{13}C signatures are static over time, thus reducing the likelihood that the isotopic compositions of the endmembers were static from a site to site basis.

The isotopic composition of the source for the control plots, as determined by the Keeling plots, were varied. For the control site, WMCS, the δ^{13}C-CH_4 signature was very negative but the uncertainty was also very large as well (Table 5.12). Similarly, the δ^{13}C-CH_4 signature for the BHCS (NIGHT) control site also produced an unusual result with a great amount of uncertainty (Table 5.12). Likewise, the BHCS (DAY) measurement produced an unusual result but this value loses its significance because the uncertainty is too great to classify the measurement into a particular zone (Table 5.12). The high degree of uncertainty for all of these sites makes it impossible to classify the sources into a specific zones category (i.e. biogenic, thermogenic, and mixed). This is also true when making the comparison between the control sites and the test site (LC3S Oct2015); though the δ^{13}C-CH_4 measurement for LC3S is within the thermogenic zone the uncertainty is too great to conclusively claim that the source of the CH_4 is thermogenic (Table 5.12).

6.4 Winter Measurements: Stable Carbon Isotope Analysis

The test site, LC3S demonstrated uncertain results through the unexcavated treatment due to the high degree of uncertainty that expanded across two different zones. However, for the excavated

treatment the Keeling plot clearly demonstrated that the source of the CH_4 at LC3S is thermogenic (Table 5.12). Though the unexcavated treatment was uncertain, the conclusiveness of the δ^{13}C-CH_4 signature using the excavated treatment shows that there is thermogenic gas present at the site and that using the excavated method improves the detection of the source of the subsurface gases.

EWW1 shows δ^{13}C-CH_4 values with a low uncertainties plotting within the thermogenic zone for both treatments (Figure 5.22 and Table 5.12). The fact both treatments produced a conclusive result may speak to a lack of microbial activity at this site. The absence or scarcity of microbes would reduce the likelihood of a detectable difference between the δ^{13}C-CH_4 signatures between the two treatments.

Keeling plot intercepts for EWW1 CS show a wide difference between the unexcavated (+76 $\pm$ 156‰) and excavated treatments (-89 $\pm$ 25‰) (Figure 5.21 and Table 5.12). Although the excavated treatment δ^{13}C-CH_4 has a large uncertainty, the error bars lie within the biogenic zone (Table 5.6).

The EWW3 site yielded uncertain results due to the wide margin of error regarding the δ^{13}C-CH_4 value. The lack of a certain δ^{13}C-CH_4 signature at EWW3 may suggest the necessity of excavating a pit to reduce the microbial activity.

At the control site, EWW3, a conclusive biogenic source was found. Though it is important to note that the upper limit of the confidence interval is on the positive boundary of the biogenic zone. An excavated treatment may be useful in reducing the uncertainty.

In addition to the Keeling plots, δ^{13}C-CH_4 results in combination with δ^{13}C-CO_2 can provide more information regarding the classification of the source of the emitted gas. In assessing the relationship between δ^{13}C-CO_2 versus δ^{13}C-CH_4, it is possible to determine the pathway of methane formation. In a freshwater system, there are two primary pathways towards the generation of CH_4 from CO_2 (Figure 5.26).

The winter session measurements taken at LC3S are a good illustrator of this concept. The majority of the δ^{13}C-CO_2 versus δ^{13}C-CH_4 data plotted within the methyl fermentation field for the unexcavated treatment, whereas the bulk proportion of the data plotted in the methane oxidation field for the excavated treatment (Figure 5.19). Methyl fermentation reflects the production of CH_4 through the consumption of organic matter, primarily acetate (in freshwater systems), by microbes in the soil. The byproduct of this form of methanogenesis is carbon dioxide. Using the δ^{13}C compositions of CH_4 and CO_2, one can confirm that this form of methanogenesis is taking place, simultaneously confirming the production of biogenic gas. On the other hand, the methane oxidation pathway indicates that the CO_2 being produced is a product of CH_4 that was consumed by methanotrophs. Thus the source of CH_4 for these methanotrophs may be atmospheric, biogenic, or thermogenic. The isotopic data at LC3S eliminates the former two possibilities with the Keeling plot results (Tables 5.9 and 5.11), thereby leaving the only remaining possibility of a thermogenic

source. In other words, the CH4 that was oxidized most likely was sourced from thermogenic methane leakage at the test site.

In general, δ^{13}C-CO_2 signatures for all of the sites were near the value of $\delta^{13}C_{soil}$ regardless of treatment. For unexcavated treatments this is consistent with CO_2 being produced by respiration/decomposition of plant organic matter, since most soil gas carbon isotope compositions plot in the methyl fermentation field (Figure 5.19). Another factor to consider is the effect that plant respiration, specifically by roots and shoots, could have on the fractionation between bulk soil and CO_2. The small amount of δ^{13}C fractionation is expected due to the fact that the fractionation constant (α) for aerobic oxidation (i.e. methanotrophy) αCH_4-CO_2 is roughly equal to 1.039 (Templeton et al., 2006). Also, it was clear that the Keeling plots for the δ^{13}C-CO_2 signatures were associated with far less uncertainty than the δ^{13}C-CH_4. This was largely due to the greater range and magnitude of [CO_2] values as compared to [CH_4].

6.5 Summarizing Remarks

The theme of uncertain results through the majority of the unexcavated measurements with the certain results through the excavated treatments is important to understand because it demonstrates the need to make soil gas measurements at depth instead of at the natural surface. Of course, the next step to better understand how the surface CH_4 signal is affected by subsurface processes is by measuring [CH_4] and δ^{13}C-CH_4 at a series of depths below the soil-atmosphere interface. By collecting this data, an advection-diffusion model can be properly calibrated for CH_4.

Combining the flux results of LC3S with the corresponding isotopic data yields strong evidence of the presence of not only excess CH_4 in the subsurface but that the dominant source of the CH_4 is thermogenic. Furthermore, it is clear from the differences between the unexcavated and excavated treatments observed at multiple sites that future measurements should incorporate measurements using at least the excavated treatment, if not both. Finally, implementing calculations such as minimum detectable flux and geospatial analysis will increased the comprehensiveness of these results so that richer conclusions can be made to further the understanding of the relationship of HVHF activity and methane emissions.

BIBLIOGRAPHY

Arthur, J. Daniel, Brian Bohm, and Mark Layne (2008). *Hydraulic Fracturing Considerations for Natural Gas Wells of the Marcellus Shale*. Tech. rep.

Atkinson, G M et al. (2016). "Hydraulic Fracturing and Seismicity in the Western Canada Sedimentary Basin". In: *Seismological Research Letters* 87.3, pp. 631–647. ISSN: 0895-0695. DOI: 10.1785/0220150263.

Backman, Leif (2009). *Methane: Sources and Emissions*. Tech. rep. Ilmatieteen Laitos Meterologiska Institutet Fininish Meterolohical Institute. URL: http://www.epa.gov/outreach/sources.html.

Beaver, William (2014). "Environmental Concerns in the Marcellus Shale". In: *Business and Society Review* 119.1, pp. 125–146. ISSN: 00453609. DOI: 10.1111/basr.12027. URL: http://doi.wiley.com/10.1111/basr.12027.

Boyer, E.W. et al. (2011). *The Impact of Marcellus Gas Drilling on Rural Drinking Water Supplies*. Tech. rep. Penn State University, p. 26. URL: www.rural.palegislature.us/documents/reports/Marcellus{_}and{_}drinking{_}water{_}2011{_}rev.pdf.

Chapman, R. E. (1983). *Petroleum Geology*. New York: Elsevier, pp. 1–407.

Christiansen, Jesper Riis, Josh Outhwaite, and Sean M Smukler (2015). "Comparison of CO2, CH4 and N2O soil-atmosphere exchange measured in static chambers with cavity ring-down spectroscopy and gas chromatography". In: *Agricultural and Forest Meteorology* 211, pp. 48–57. ISSN: 0168-1923.

Crosson, E.R. (2008). "A cavity ring-down analyzer for measuring atmospheric levels of methane, carbon dioxide, and water vapor". In: *Applied Physics B* 92.3, pp. 403–408. ISSN: 0946-2171. DOI: 10.1007/s00340-008-3135-y. URL: http://link.springer.com/10.1007/s00340-008-3135-y.

Dale, A. W. et al. (2008). "Anaerobic oxidation of methane (AOM) in marine sediments from the Skagerrak (Denmark): II. Reaction-transport modeling". In: *Geochimica et Cosmochimica Acta* 72.12, pp. 2880–2894. ISSN: 00167037. DOI: 10.1016/j.gca.2007.11.039.

Darrah, T. H. et al. (2014). "Noble gases identify the mechanisms of fugitive gas contamination in drinking-water wells overlying the Marcellus and Barnett Shales". In: *Proceedings of the National Academy of Sciences*, pp. 1–6. ISSN: 0027-8424. DOI: 10.1073/pnas.1322107111. URL: http://www.pnas.org/cgi/doi/10.1073/pnas.1322107111.

Denmead, O. T. (2008). "Approaches to measuring fluxes of methane and nitrous oxide between landscapes and the atmosphere". In: *Plant and Soil* 309.1-2, pp. 5–24. ISSN: 0032-079X. DOI: 10.

1007/s11104-008-9599-z. URL: http://link.springer.com/10.1007/s11104-008-9599-z.

Ehhalt, D. H. and U. Schmidt (1978). "Sources and sinks of atmospheric methane". In: *Pure and Applied Geophysics PAGEOPH* 116.2-3, pp. 452–464. ISSN: 00334553. DOI: 10.1007/BF01636899.

EIA (2015). *Annual Energy Outlook*. Tech. rep. Wasington D.C.

– (2016a). *International Energy Outlook*. Wasington D.C. URL: https://www.eia.gov/forecasts/aeo/data/browser/{\#}/?id=6-IEO2016{\&}region=0-0{\&}cases=Reference{\&}start=2010{\&}end=2040{\&}f=A{\&}linechart={~}Reference-d021916a.3-6-IEO2016{~}Reference-d021916a.28-6-IEO2016{\&}ctype=linechart{\&}sourcekey=0.

– (2016b). *Natural Gas Gross Withdrawls and Production*. Washington, DC.

Ellsworth, William L. (2013). "Disposal of Hydrofracking Waste Fluid by Injection into Subsurface Aquifers Triggers Earthquake Swarm in Central Arkansas with Potential for Damaging Earthquake". In: *Seismological Research Letters* 83, pp. 250–260. ISSN: 0895-0695. DOI: 10.1785/gssrl.83.2.250.

EPA (2015). *Overview of Greenhouse Gases: Methane Emissions*. URL: http://www.epa.gov/climatechange/ghgemissions/gases/ch4.html (visited on 04/22/2015).

– (2016). *Inventory of U.S. Greenhouse Gas Emissions and Sinks: 1990 2014*. Tech. rep. Washington, DC, pp. 1990–1998. DOI: EPA430-R-13-001.

Etiope, Giuseppe and Ronald W. Klusman (2010). "Microseepage in drylands: Flux and implications in the global atmospheric source/sink budget of methane". In: *Global and Planetary Change* 72.4, pp. 265–274. ISSN: 09218181. DOI: 10.1016/j.gloplacha.2010.01.002.

Evenick, Nick and Bob Hatcher (2006). "Potential Subsurface Structures and Hydrocarbon Reservoirs in the Souther Appalachain Basin Beneath the Cumberland Plateau and Eastern Highland Rim, Tennessee, Kentucky, and Southwestern Virginia". PhD thesis. University of Tennesse - Knoxville.

Flewelling, Samuel A. and Manu Sharma (2014). "Constraints on upward migration of hydraulic fracturing fluid and brine". In: *Groundwater* 52.1, pp. 9–19. ISSN: 0017467X. DOI: 10.1111/gwat.12095.

Fowler, Bob (2013). *Energy firms attend UT Forest fracking conference*. Knoxville. URL: http://www.knoxnews.com/news/local-news/energy-firms-attend-ut-forest-fracking.

Gang, Duane W. (2013). *UT seeks bids for drilling in forest*. URL: http://archive.tennessean.com/article/20130608/NEWS04/306080043/UT-seeks-bids-drilling-forest.

Hatcher, Bob (2013). *Geology and Petroleum Resources of Tennessee and the Use of Fracking as a Drilling Tool*.

Hirji, Zahra and Lisa Song (2015). *The Fracking Boom, State by State*. URL: http://insideclimatenews.org/news/20150120/map-fracking-boom-state-state?utm{_}source=Inside+Climate+News{\&}utm{_}campaign=0d53133b4a-InsideClimate{_}News12{_}

}10{_}2014{\&}utm{_}medium=email{\&}utm{_}term=0{_}29c928ffb5-0d53133b4a-326458445.

Hornberger, George et al. (2015). *HEI Special Scientific Committee on Unconventional Oil and Gas Development*. URL: http://www.healtheffects.org/UOGD/UOGD.htm (visited on 07/13/2016).

Iea (2014). "Solar Photovoltaic Energy". In: *Technology Roadmap*, p. 60. DOI: 10.1007/SpringerReference_7300. URL: http://www.iea.org/publications/freepublications/publication/TechnologyRoadmapSolarPhotovoltaicEnergy{_}2014edition.pdf.

Jackson, Robert B. et al. (2013). "Increased stray gas abundance in a subset of drinking water wells near Marcellus shale gas extraction". In: *Proceedings of the National Academy of Sciences of the United States of America* 110.28, pp. 11250–5. ISSN: 1091-6490. DOI: 10.1073/pnas.1221635110. URL: http://www.pubmedcentral.nih.gov/articlerender.fcgi?artid=3710833{\&}tool=pmcentrez{\&}rendertype=abstract$\backslash$nhttp://www.pnas.org/content/110/28/11250.

Jackson, Robert B et al. (2014a). "Natural gas pipeline leaks across Washington, DC." In: *Environmental science & technology* 48.3, pp. 2051–8. ISSN: 1520-5851. DOI: 10.1021/es404474x. URL: http://www.ncbi.nlm.nih.gov/pubmed/24432903.

Jackson, Robert B. et al. (2014b). "The Environmental Costs and Benefits of Fracking". In: *Annual Review of Environment and Resources* 39, pp. 327–362. DOI: 10.1146/annurev-environ-031113-144051.

Kirschke, Stefanie et al. (2013). "Three decades of global methane sources and sinks". In: *Nature Geoscience* 6.10, pp. 813–823. ISSN: 1752-0894. DOI: 10.1038/ngeo1955. URL: http://www.nature.com/doifinder/10.1038/ngeo1955.

Klusman, W, M Emmelyn Leopold, and Michael P Leroy (2000). "Seasonal variation in methane fluxes from sedimentary basins to the atmosphere: Results from chamber measurements and modeling of transport from deep sources". In: *Geophysical Research* 105.D20, pp. 24,661–24,670. DOI: 10.1029/2000JD900407. URL: http://dx.doi.org/10.1029/2000JD900407.

Kort, Erica A. et al. (2014). "Four corners: The largest US Methane anomaly viewed from space". In: *AGU Geophysical Research Letters*, pp. 6898–6903. DOI: 10.1002/2014GL061503.Received.

Krevor, Samuel et al. (2010). "Rapid detection and characterization of surface CO2 leakage through the real-time measurement of δ13 C signatures in CO2 flux from the ground". In: *International Journal of Greenhouse Gas Control* 4.5, pp. 811–815. ISSN: 17505836. DOI: 10.1016/j.ijggc.2010.05.002. URL: http://dx.doi.org/10.1016/j.ijggc.2010.05.002.

Kvenvolden, Keith A. and Bruce W. Rogers (2005). "Gaia's breath - Global methane exhalations". In: *Marine and Petroleum Geology* 22.4 SPEC. ISS. Pp. 579–590. ISSN: 02648172. DOI: 10.1016/j.marpetgeo.2004.08.004.

Lampe, Carolyn et al. (2012). "Fault control on hydrocarbon migration and accumulation in the Tertiary Dongying depression, Bohai Basin, China". In: *AAPG Bulletin* 96.6, pp. 983–1000. ISSN: 01491423. DOI: 10.1306/11031109023.

Long, Jane C S and Daniel Billaux (1987). "From Field Data to Fracture Network Modeling' An Example Incorporating Spatial Structure". In: *Water Resources Research* 23.0043.

Maher, Damien T., Isaac R. Santos, and Douglas R. Tait (2014). "Mapping Methane and Carbon Dioxide Concentrations and δ13C Values in the Atmosphere of Two Australian Coal Seam Gas Fields". In: *Water, Air, & Soil Pollution* 225.12, p. 2216. ISSN: 0049-6979. DOI: 10.1007/s11270-014-2216-2. URL: http://link.springer.com/10.1007/s11270-014-2216-2.

Martini, Anna M. et al. (2003). "Microbial production and modification of gases in sedimentary basins: A geochemical case study from a Devonian shale gas play, Michigan basin". In: *AAPG Bulletin* 87.8, pp. 1355–1375. ISSN: 01491423. DOI: 10.1306/031903200184.

Megonigal, J. P., M. E. Hines, and P. T. Visscher (2003). *Anaerobic Metabolism: Linkages to Trace Gases and Aerobic Processes*. 10th ed. Vol. 10. Elsevier Ltd., pp. 273–359. ISBN: 9780080983004. DOI: 10.1016/B978-0-08-095975-7.00808-1. URL: http://dx.doi.org/10.1016/B978-0-08-095975-7.00808-1.

Miller, Scot M et al. (2013). "Anthropogenic emissions of methane in the United States". In: *Proceedings of the National Academy of Sciences* 110.50, pp. 20018–20022. DOI: 10.1073/pnas.1314392110. URL: http://www.pnas.org/content/110/50/20018.abstract.

Pataki, D. E. et al. (2003). "The application and interpretation of Keeling plots in terrestrial carbon cycle research". In: *Global Biogeochemical Cycles* 17.1, n/a–n/a. ISSN: 08866236. DOI: 10.1029/2001GB001850. URL: http://doi.wiley.com/10.1029/2001GB001850.

Pihlatie, Mari K. et al. (2013). "Comparison of static chambers to measure CH4 emissions from soils". In: *Agricultural and Forest Meteorology* 171-172, pp. 124–136. ISSN: 01681923. DOI: 10.1016/j.agrformet.2012.11.008. URL: http://linkinghub.elsevier.com/retrieve/pii/S0168192312003450.

Pumpanen, Jukka et al. (2004). "Comparison of different chamber techniques for measuring soil CO 2 efflux". In: *Agricultural and Forest Meteorology* 123.3, pp. 159–176. ISSN: 0168-1923.

Rooney, M. A., G. E. Claypool, and H. M. Chung (1995). "Modeling thermogenic gas generation using carbon isotope ratios of natural gas hydrocarbons". In: *Chemical Geology* 126, pp. 219–232. ISSN: 0009-2541. DOI: 10.1016/0009-2541(95)00119-0. URL: {\textless}GotoISI{\textgreater}://WOS:A1995TQ07000002.

Schoell, Martin (1988). "Multiple origins of methane in the earth". In: *Chemical Geology* 71, pp. 1–10. URL: http://ac.els-cdn.com/0009254188901015/1-s2.0-0009254188901015-main.pdf?{_}tid=041c42e2-7cc1-11e4-80e3-00000aab0f26{\&}acdnat=1417813096{_}6a2fb4790c71d87e9d1b3419793a2154.

Sharp, Zachary (2007). "Carbon in the Low-Temperature Environment". In: *Stable Isotopes Geochemistry*. Ed. by Chris Rapp. Pearson. Chap. 7, pp. 150–178.

Stolper, D A et al. (2014). "Formation temperatures of thermogenic and biogenic methane". In: *Science* 344.

TDEC (2015). *Oil and Gas Well Permits*. URL: http://environment-online.state.tn.us:8080/pls/enf{_}reports/f?p=9034:34300:0::NO:::.

TDEC (2016). *Oil and Gas Well Database*. Nashville. URL: http://tdec.tn.gov:8080/pls/enf{_}reports/f?p=9034:34300:0::NO:::.

Teasdale, Christopher J et al. (2014). "Ground Gas Monitoring : Implications for Hydraulic Fracturing and". In: *Environmental Science & Technology* 48, pp. 13610–13616. DOI: dx.doi.org/10.1021/es502528c.

Templeton, Alexis S. et al. (2006). "Variable carbon isotope fractionation expressed by aerobic CH4-oxidizing bacteria". In: *Geochimica et Cosmochimica Acta* 70.7, pp. 1739–1752. ISSN: 00167037. DOI: 10.1016/j.gca.2005.12.002.

Topp, Edward and Elizabeth Pattey (1997). "Soils as sources and sinks for atmospheric methane". In: *Canadian Journal of Soil Science* 77.2, pp. 167–177. ISSN: 0008-4271. DOI: 10.4141/S96-107. URL: http://pubs.aic.ca/doi/abs/10.4141/S96-107.

USGS (2016). *Fort Payne Formation and Chattanooga Shale*. URL: http://mrdata.usgs.gov/geology/state/sgmc-unit.php?unit=TNMfp;8 (visited on 02/24/2016).

Wang, Qiang et al. (2014). "Natural gas from shale formation - The evolution, evidences and challenges of shale gas revolution in United States". In: *Renewable and Sustainable Energy Reviews* 30, pp. 1–28. ISSN: 13640321. DOI: 10.1016/j.rser.2013.08.065. URL: http://dx.doi.org/10.1016/j.rser.2013.08.065.

Whiticar, Michael J (1999). "Carbon and hydrogen isotope systematics of bacterial formation and oxidation of methane". In: *Chemical Geology* 161.13, pp. 291–314. ISSN: 0009-2541. DOI: http://dx.doi.org/10.1016/S0009-2541(99)00092-3. URL: http://www.sciencedirect.com/science/article/pii/S0009254199000923.

Wilson, Charles W. and Richard G. Stearns (1958). "Structure of the Cumberland Plateau, Tennssee". In: *BULLETIN OF THE GEOLOGICAL SOCIETY OF AMERICA* 69.October, pp. 1283–1296.

Zhang, Liwei et al. (2014). "Leakage Detection of Marcellus Shale Natural Gas at an Upper Devonian Gas Monitoring Well: A 3-D Numerical Modeling Approach". In:

Appendix A

Appendix: Soil Moisture & Soil Temperature Data

The following are graphs of soil moisture and soil temperature data. Data is unavailable for the fall and EWW3 CS.

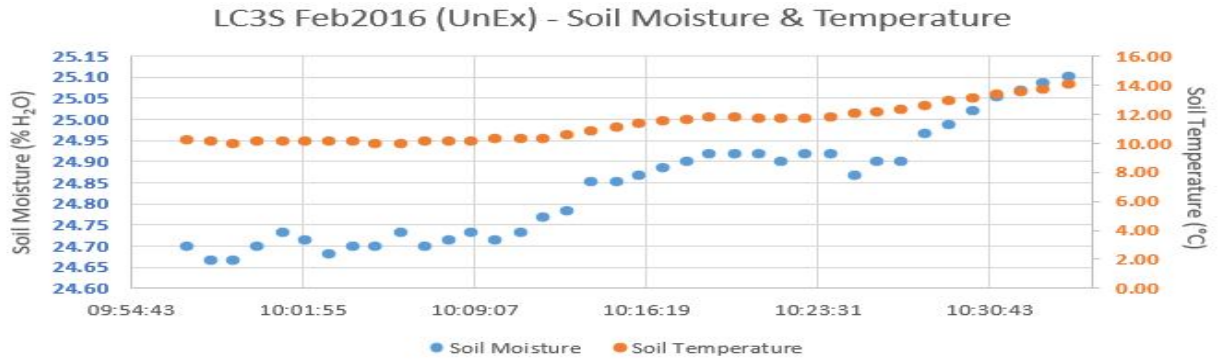

(A) LC3S Feb 2016 (Unexcavated)

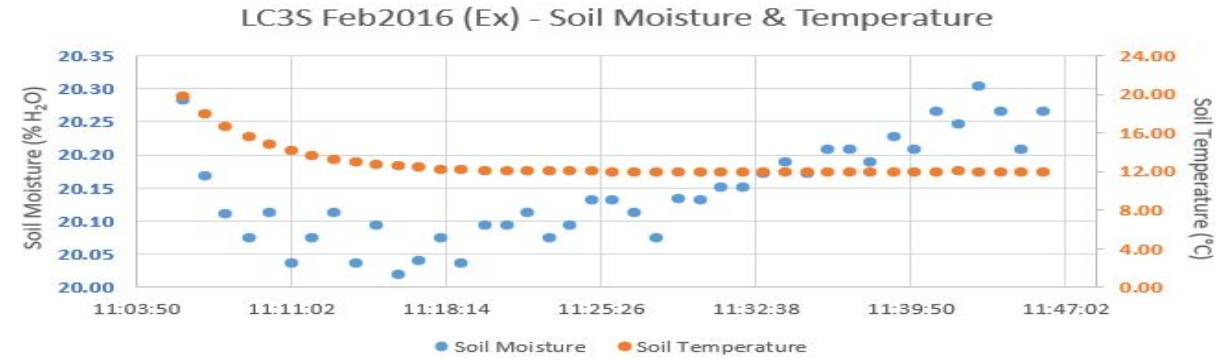

(B) LC3S Feb 2016 (Excavated)

FIGURE A.1: Soil moisture and temperature data for LC3S Feb 2016. All measurements were collected with a time-domain reflectometer instrument that logged these metrics on a minute-by-minute basis.

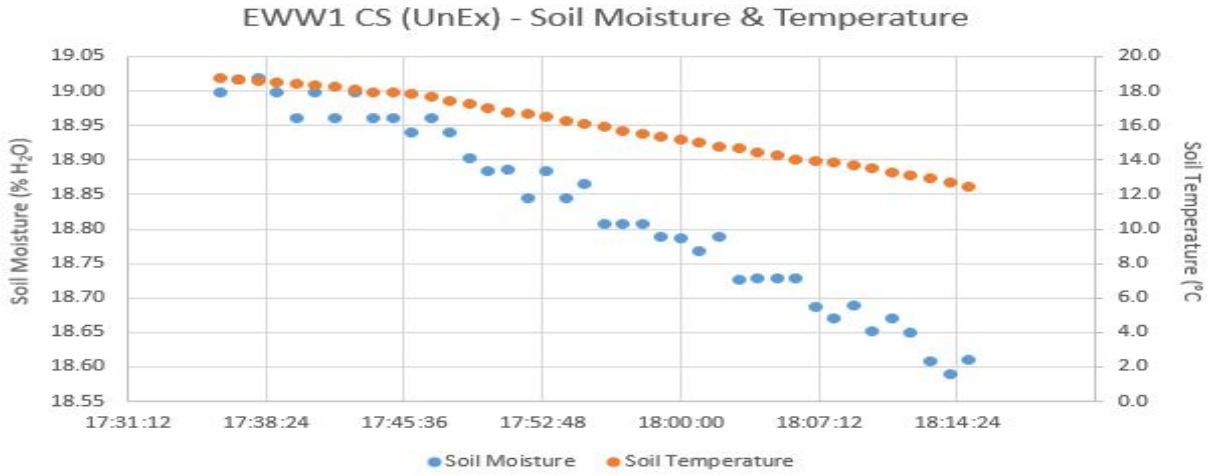

(A) EWW1 CS (Unexcavated)

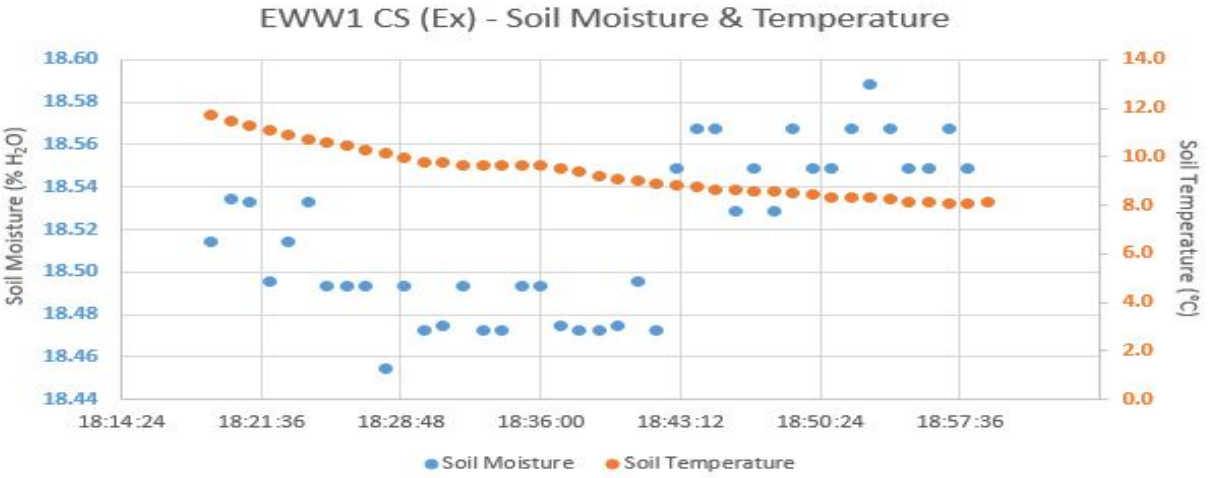

(B) EWW1 CS (Excavated)

FIGURE A.2: Soil moisture and temperature data for EWW1 CS.

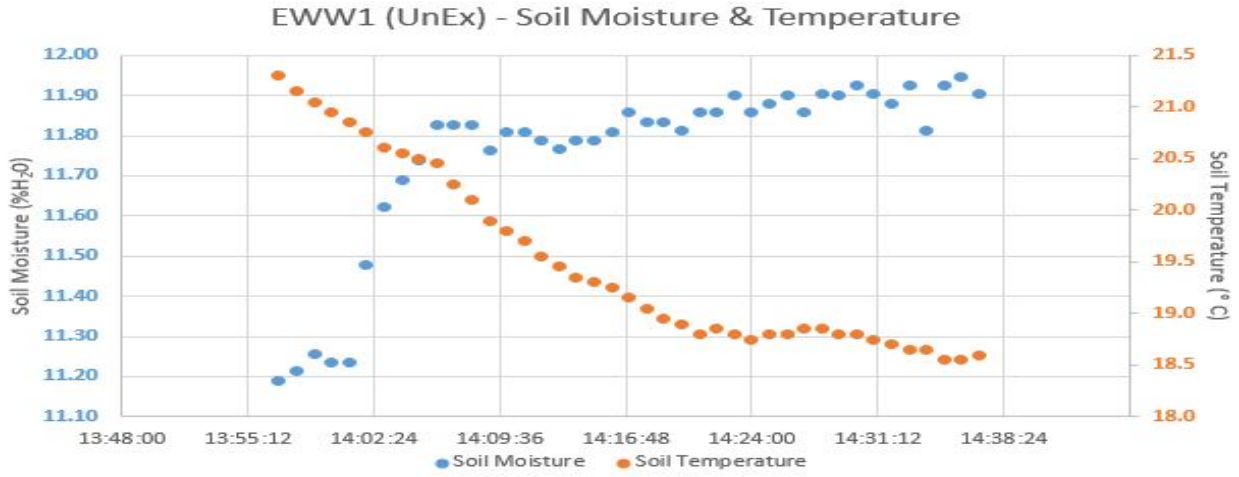

(A) EWW1 (Unexcavated)

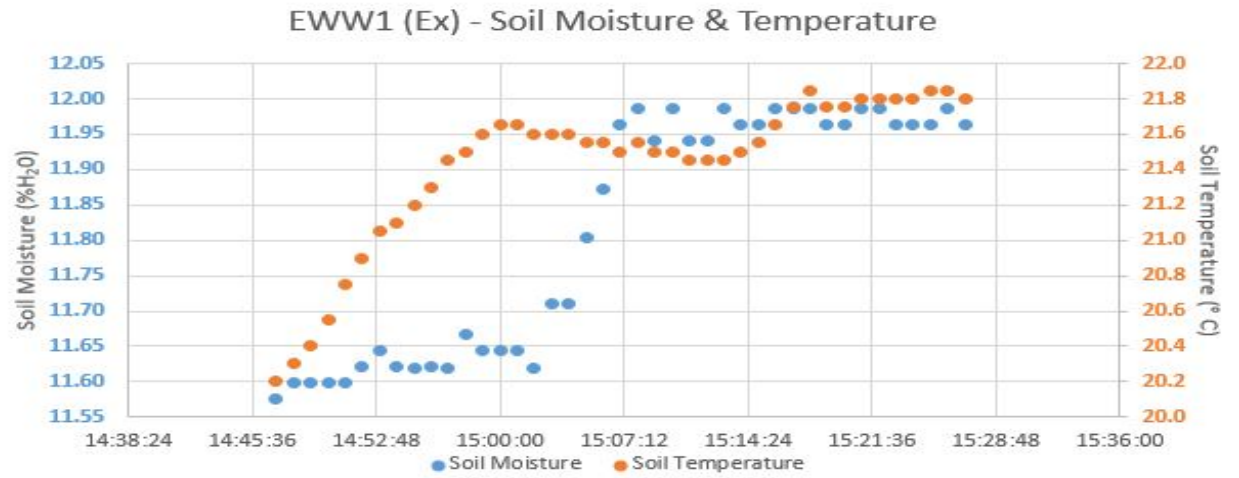

(B) EWW1 (Excavated)

FIGURE A.3: Soil moisture and temperature data for EWW1.

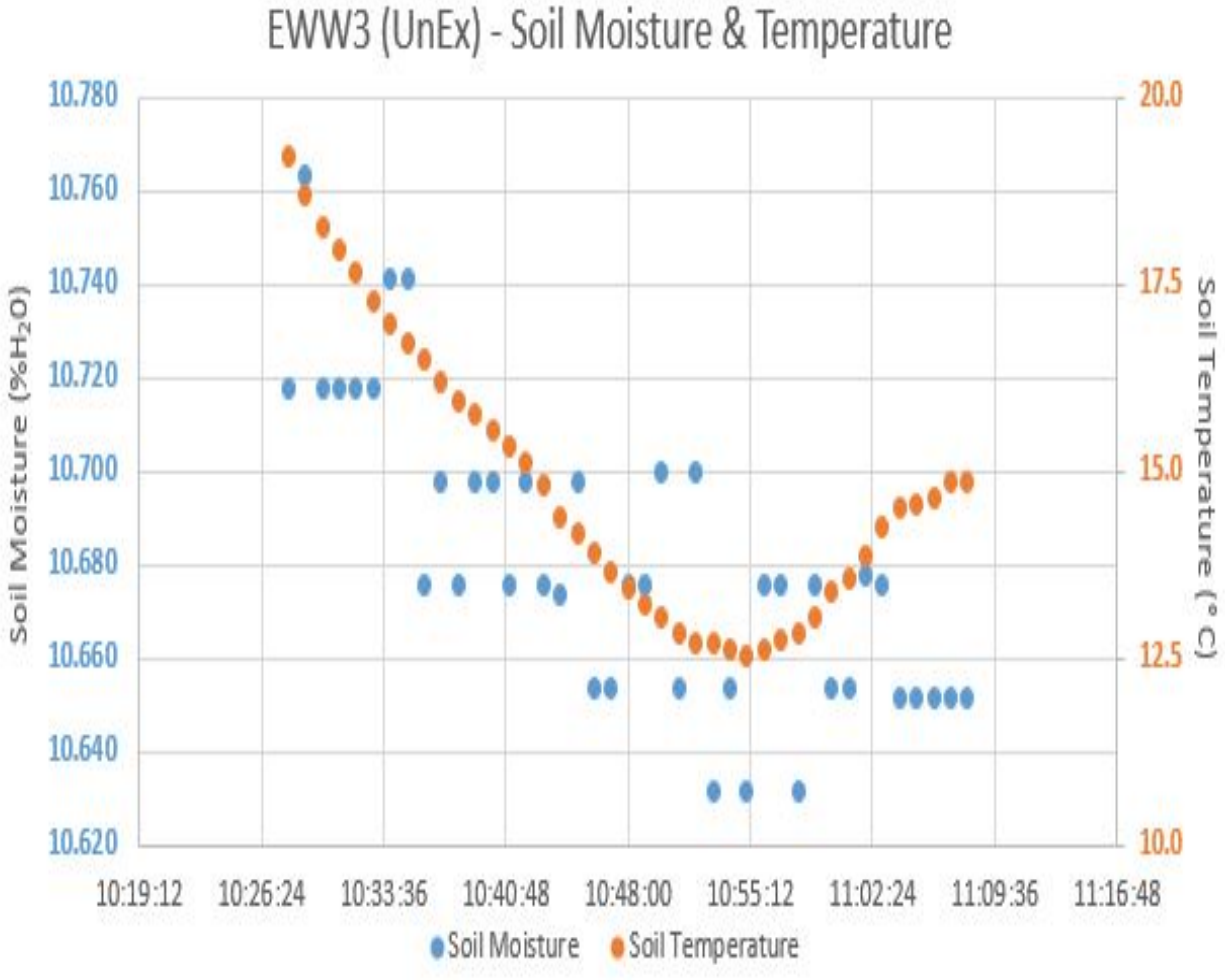

FIGURE A.4: Soil moisture and temperature data for EWW3.

Appendix B

Appendix: Pre- and Post-background Data

TABLE B.1: Summary of pre- and post-background concentrations and isotopic compositions at all sites. Uncertainty is presented as 2σ.

Location	PrePost Mean $[CH_4]$ (ppm)	PrePost Mean δ^{13}C-CH_4 (‰)	PrePost Mean $[CO_2]$ (ppm)	PrePost Mean δ^{13}C-CO_2 (‰)
WMCS	2.01 $\pm$0.01	-47 $\pm$5	425 $\pm$16	-11 $\pm$5
BHCS (DAY)	1.97 $\pm$0.01	-46 $\pm$5	449 $\pm$22	-11 $\pm$2
BHCS (NIGHT)	1.98 $\pm$0.02	-48 $\pm$5	455 $\pm$30	-11 $\pm$1
LC3S Oct2015	2.1 $\pm$0.3	-47 $\pm$5	417 $\pm$12	-9 $\pm$1
LC3S Feb2016 (UnEx)	1.92 $\pm$0.02	-46 $\pm$5	408 $\pm$3	-9 $\pm$2
LC3S Feb2016 (Ex)	1.92 $\pm$0.01	-46 $\pm$5	424 $\pm$35	-10 $\pm$2
EWW1 CS (UnEx)	1.91 $\pm$0.04	-47 $\pm$5	408 $\pm$15	-9 $\pm$1
EWW1 CS (Ex)	1.89 $\pm$0.01	-47 $\pm$5	430 $\pm$31	-10 $\pm$2
EWW1 (UnEx)	1.92 $\pm$0.07	-46 $\pm$5	403 $\pm$3	-9 $\pm$1
EWW1 (Ex)	2.0 $\pm$0.2	-46 $\pm$5	407 $\pm$13	-9 $\pm$1
EWW3 CS (UnEx)	2.08 $\pm$0.04	-46 $\pm$4	436 $\pm$56	-10 $\pm$2
EWW3 (UnEx)	1.97 $\pm$0.08	-46 $\pm$4	421 $\pm$28	-10 $\pm$2

Appendix C

Appendix: CO_2 Keeling Plots

The following graphs are CO_2 Keeling plots for the both seasons.

Summary of δ^{13}C-CO_2 compositions all sites.

TABLE C.1: Summary of δ^{13}-CO_2 compositions for sources measured at all control and test sites. Values within the parenthetical indicate the range of the 95% confidence interval.

Location	Unexcavated (‰)	Excavated (‰)
WMCS	-30.18 (-30.33, -30.04)	Not measured
BHCS (DAY)	-28.05 (-28.14, -27.95)	Not measured
BHCS (NIGHT)	-28.11 (-28.22, -27.95)	Not measured
LC3S Oct2015	-29.59 (-29.85, -29.34)	Not Measured
LC3S Feb2016	-24.37 (-24.80, -23.95)	-24.06 (-24.14, -23.98)
EWW1 CS	-22.65 (-22.90, 22.40)	-24.82 (-25.00, -24.82)
EWW1	-23.84 (-24.16, -23.51)	-17.64 (-17.89, -17.34)
EWW3 CS	-27.30 (-27.41, -27.69)	Not measured
EWW3	-27.93 (-28.17, -27.69)	Not measured

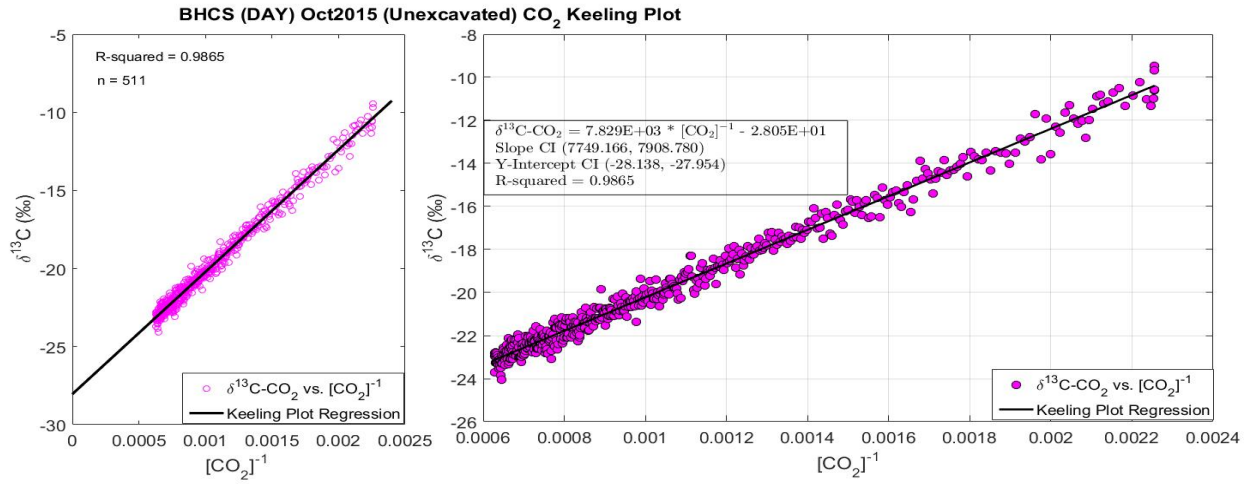

(A) BHCS (DAY)

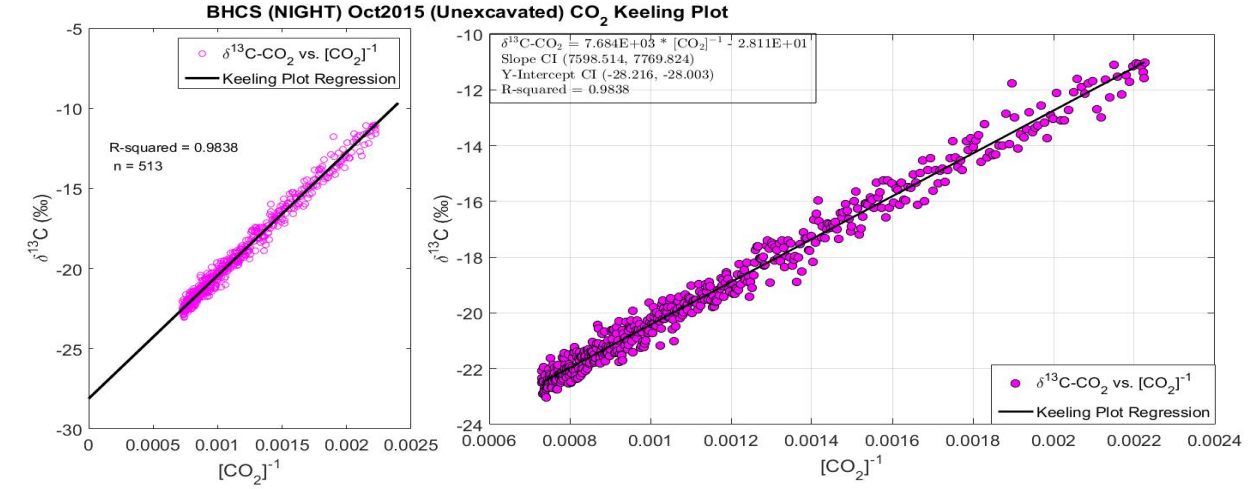

(B) BHCS (NIGHT)

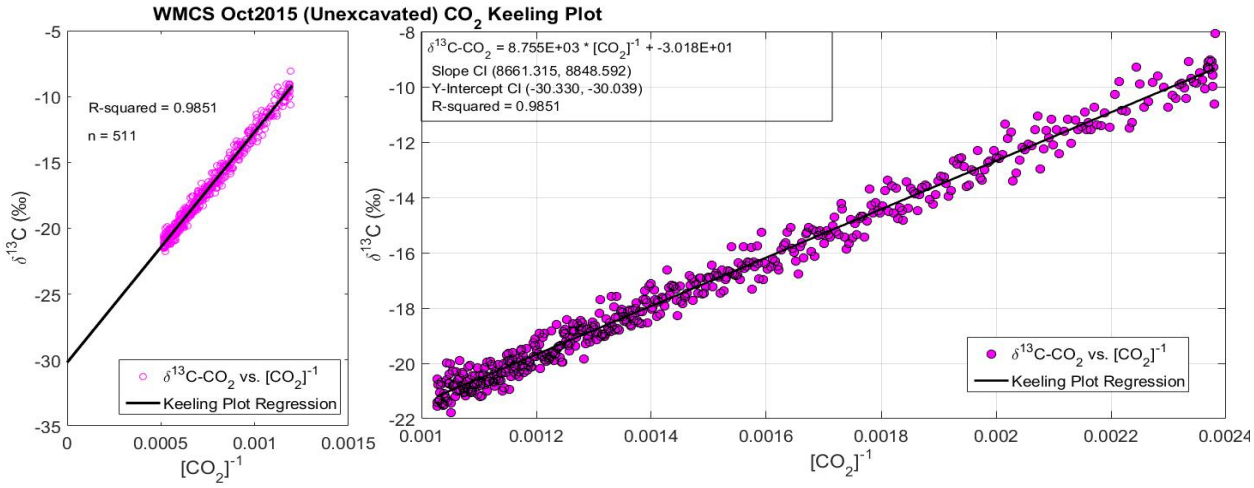

(C) WMCS

FIGURE C.1: Keeling plots for the control sites during the fall season (Oct 2015).

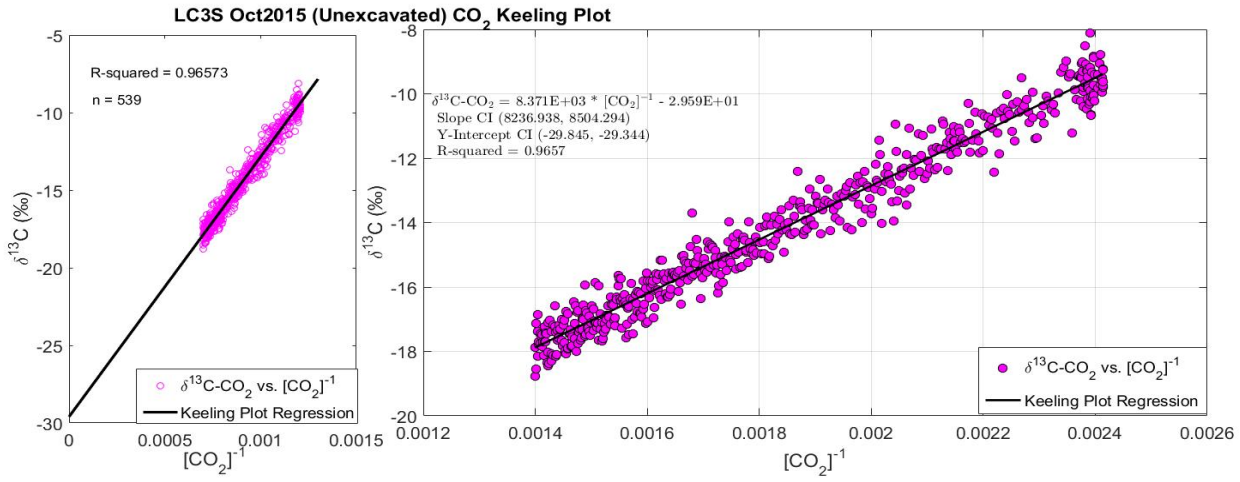

(A) LC3S Oct2015

FIGURE C.2: Keeling plots for the test site during the fall season (Oct 2015).

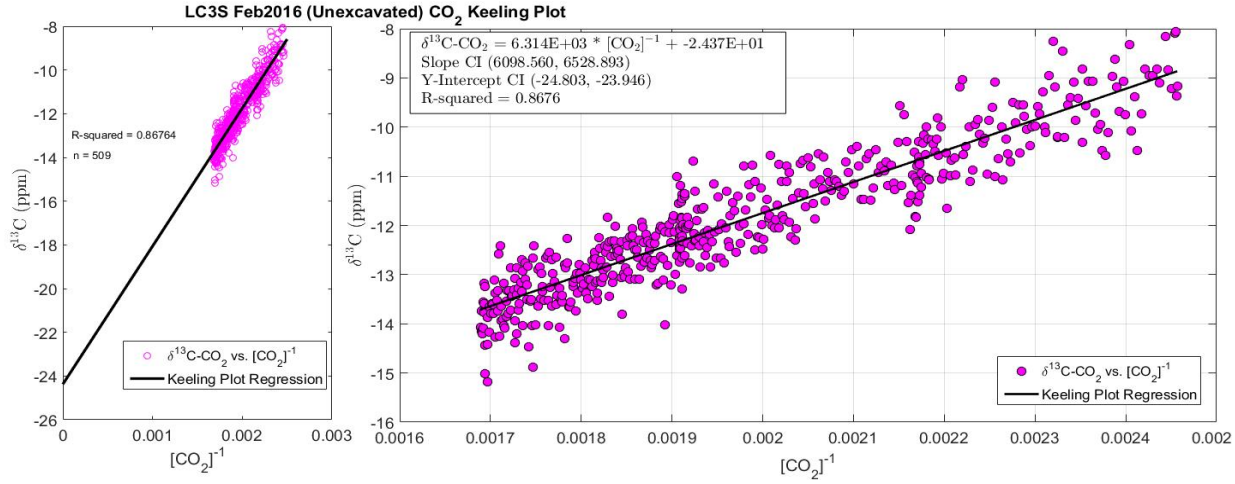

(A) Unexcavated

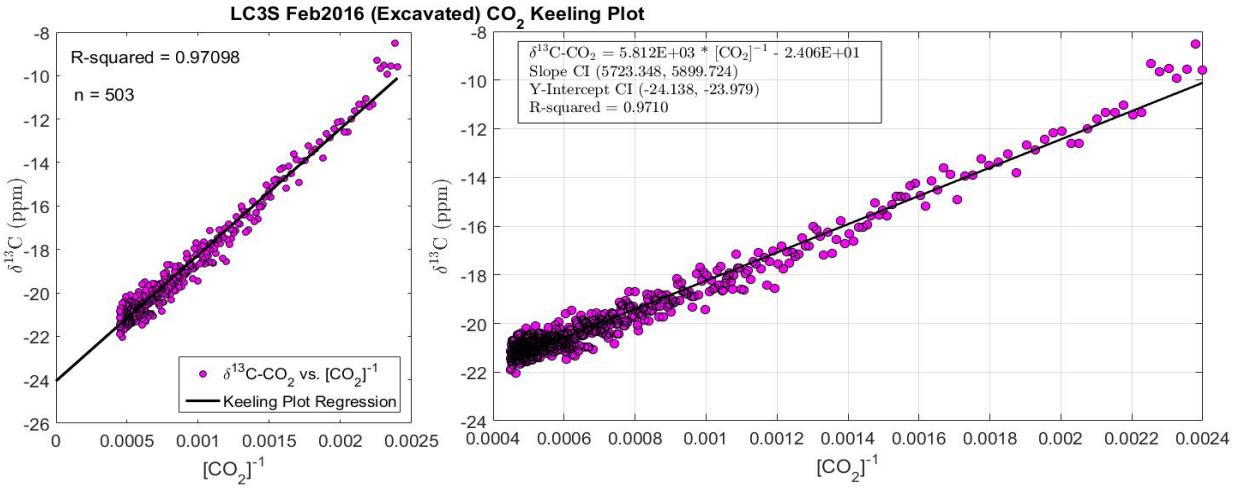

(B) Excavated

FIGURE C.3: CO_2 Keeling plots for the LC3S Feb 2016 site.

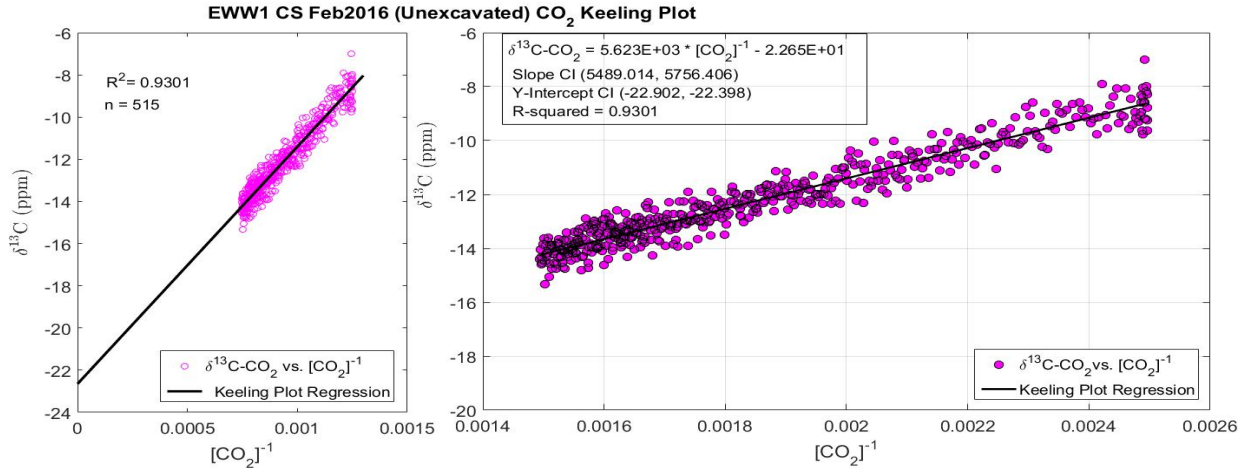

(A) Unexcavated

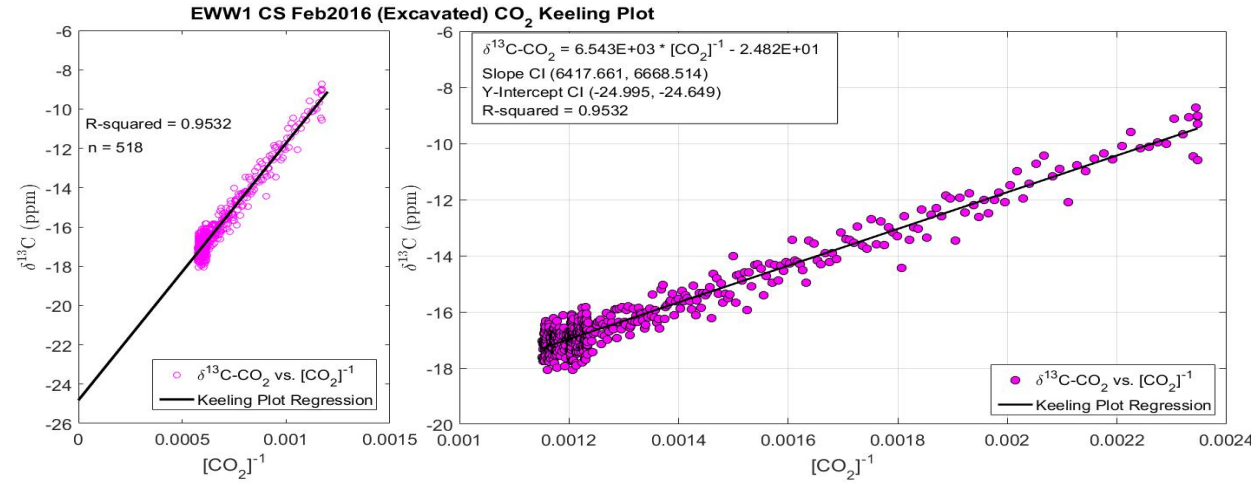

(B) Excavated

FIGURE C.4: CO_2 Keeling plots for the control site EWW1 CS.

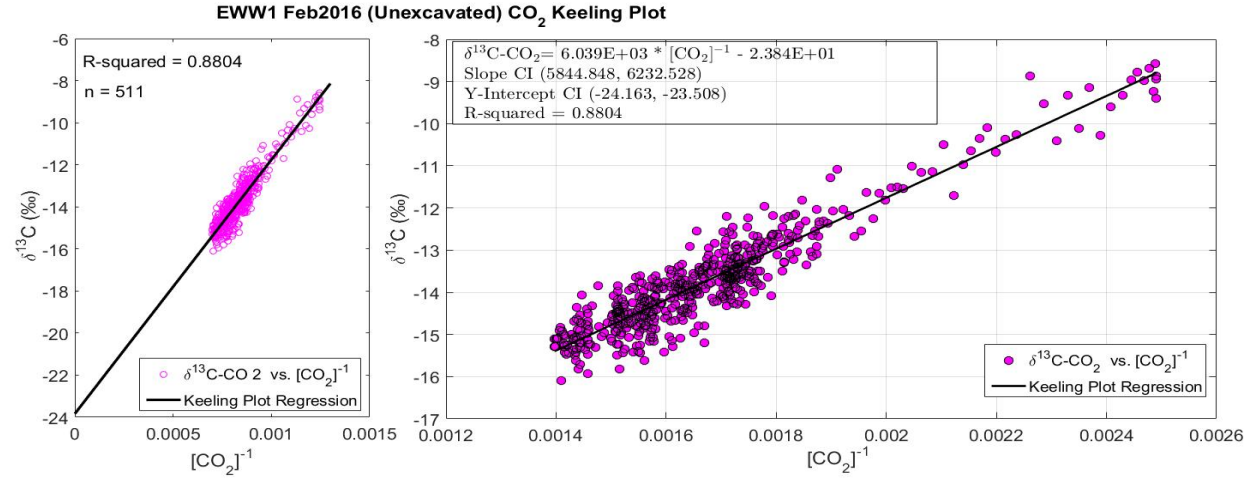

(A) Unexcavated

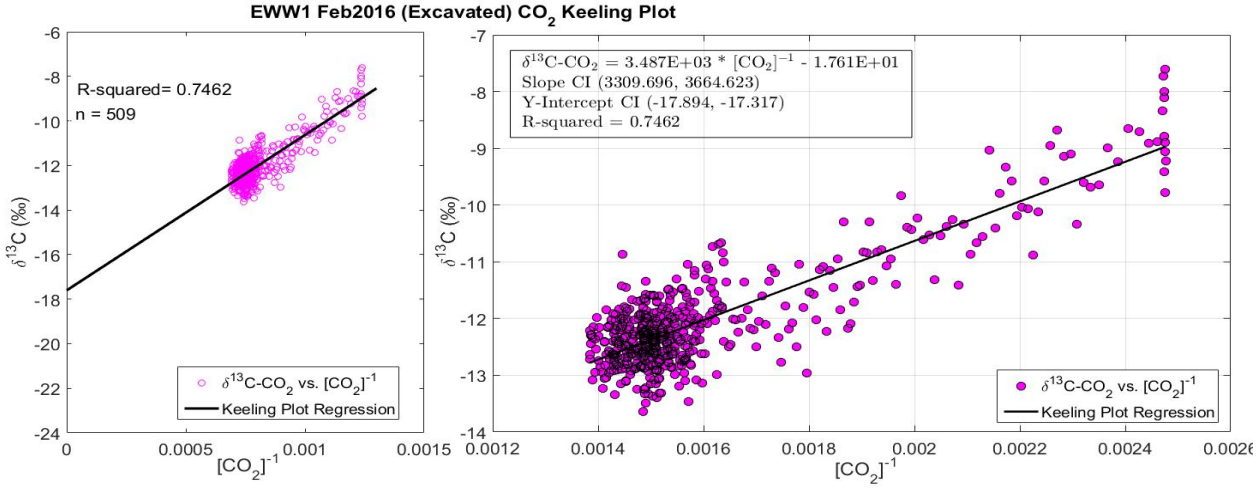

(B) Excavated

FIGURE C.5: CO_2 Keeling plots for the test site EWW1.

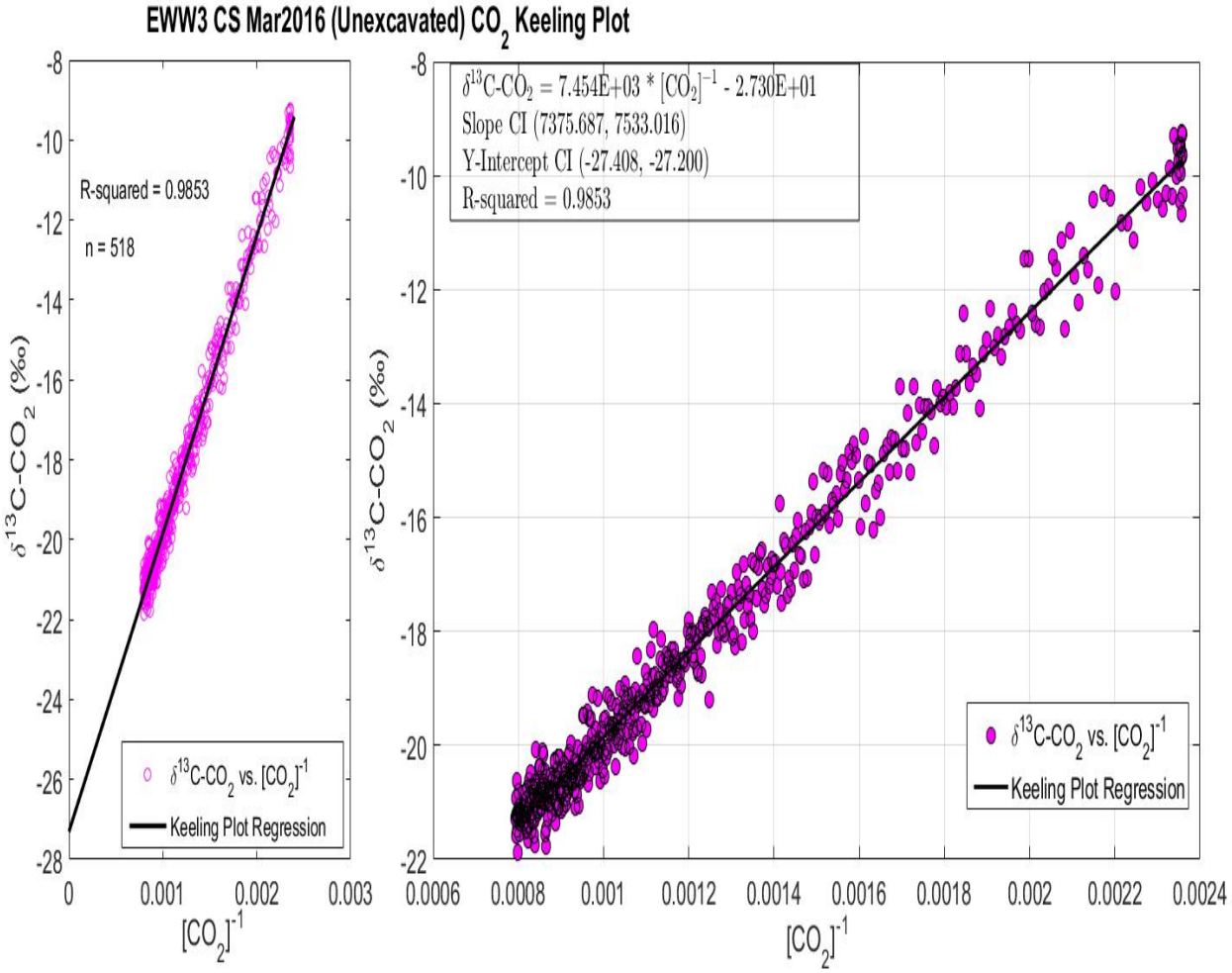

FIGURE C.6: CO_2 Keeling plots for the control site EWW3 CS.

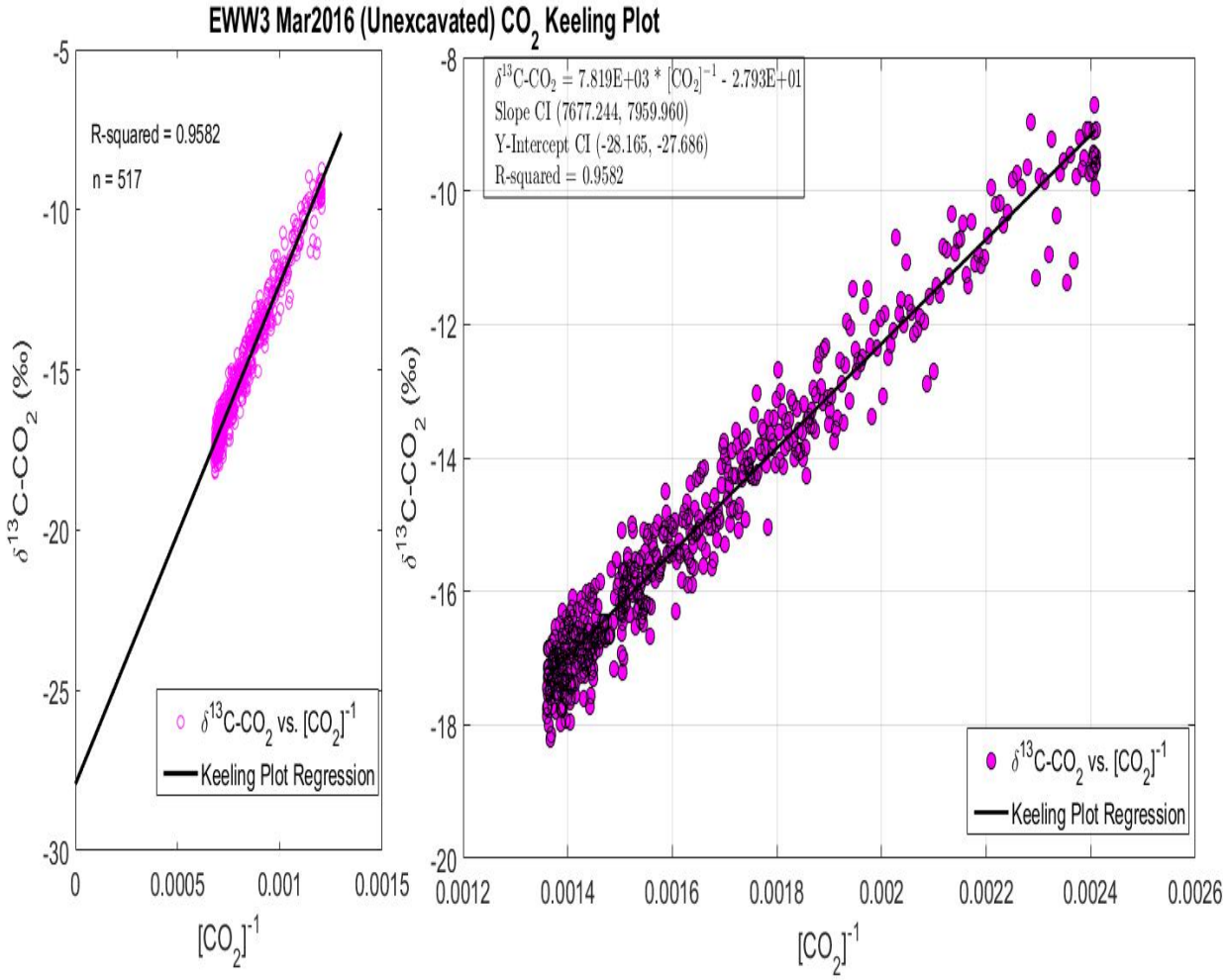

FIGURE C.7: CO_2 Keeling plots for the control site EWW3 CS.

Appendix D

Appendix: Stratigraphic Column

FIGURE D.1: Stratigraphic column for subsurface layers at eastern Tennessee region (Evenick and Hatcher, 2006).